Early universe cosmology and dark energy: from the Big Bang to the late expansion of the universe

Elisa Gouvêa Mauricio Ferreira

Department of Physics
McGill University
Montreal, Canada

June 2017

A thesis submitted to McGill University in partial fulfillment of the requirements for the degree of Doctor of Philosophy.

2017/06/25

Acknowledgments

First I would like to thank my supervisor Professor Robert Brandenberger for supervising, mentoring and supporting me during my Ph.D.. He taught me more than just physics but how to be a good scientist and educator. I also want to thank my co-workers, collaborators and friends Leila Graef, Hossein Bazrafshan Moghaddam, Guilherme Franzmann, Renato Costa, Rodrigo Cuzzinato, Ryo Namba, and specially Yi-fu Cai who was always there to discuss physics and collaborate. I would like to specially thank Jerome Quintin and Evan Mcdonough for their friendship, help, discussions, collaborations and for having shared this journey with me.

I also thank all my collaborators Professor Justin Khroury, Professor Elcio Abdalla, Professor Bin Wang, André Alencar da Costa, Fang Chen, the J-PAS collaboration and the BINGO collaboration.

I thank the Brazilian National Council for Scientific and Technological Development - CNPq (Science Without Borders) for the financial support during the completion of this degree. I also thank McGill university and the Department of Physics. Computations of this thesis were made on the supercomputer Guillimin from McGill University, managed by Calcul Qubec and Compute Canada. The operation of this supercomputer is funded by the Canada Foundation for Innovation (CFI), the ministre de l'conomie, de la science et de l'innovation du Qubec (MESI) and the Fonds de recherche du Qubec - Nature et technologies (FRQ-NT).

I want to thank and dedicate this to my family. To my parents and my brothers that have always supported me immensely and understood my absence in their lives knowing that I was pursuing my dream. Finally and foremost, I thank Wilson, my partner and best friend for the unconditional support and love.

Abstract

In this thesis we address two of the most outstanding problems in cosmology: the singularity problem and the late acceleration of the universe. In the first part, we address the singularity problem that appears in the context of bouncing cosmologies, and suggest a formalism based on the AdS/CFT correspondence to track the evolution of cosmological perturbations in the presence of a space-like singularity that appears in a specific realization of a deformed AdS space-time. Our construction sets the formalism for the evolution of a scalar field and the curvature perturbations on a regularized field theory living in the boundary of this space-time and shows that their momentum dependence is preserved, while a finite particle production occurs. In the second part, we show two works that give a contribution to the huge effort to unravel the nature of dark energy. In those, we focus in testing a model of dark energy where an interaction with dark matter is allowed. This dynamical model has impacts on the evolution of the parameters that describe our universe and we test these using the latest cosmological observations. We use data from the Cosmic Microwave Background, Baryon Acoustic Oscillations(BAO) and type Ia supernovae, and find good agreement with observations, putting constraints in the cosmological parameters. We address the recently found deviation from ΛCDM in high-redshifts found in measurements of the BAO of the Lyman-α forest from quasars. We show that Hubble parameter and angular distance at high-z for the interacting model have a better concordance with the ones obtained by the BOSS collaboration than the ΛCDM model, and that adding this data set improves the global fit of the model, although with low statistical significance.

Abrégé

Dans cette thèse, nous adressons deux des plus grands problèmes de la cosmologie : le problème de la singularité initiale et l'accélération tardive de l'univers. Dans la première partie, nous faisons face au problème de la singularité initiale dans le contexte des théories d'univers rebondissant et nous suggérons un formalisme basè sur la correspondance anti de Sitter/théorie conforme des champs (AdS/CFT) pour suivre l'évolution des perturbations cosmologiques avec la présence d'une singularité de genre espace qui apparaît dans une réalisation spécifique d'un espace-temps AdS déformé. Notre construction établie le formalisme pour l'évolution d'un champ scalaire et les perturbations de courbure dans une théorie régularisée des champs qui vie sur la frontiére de cet espace-temps et elle montre que leur dépendance de la quantité de mouvement est préservée alors qu'une production de particule limitée se produit. Dans la seconde partie, nous présentons deux travaux qui contribuent aux énormes efforts pour démystifier la nature de l'énergie noire. Dans ces articles, nous nous concentrons sur l'analyse d'un modèle d'nergie noire où une interaction avec la matière noire est permise. Ce modèle dynamique a des impacts sur l'évolution des paramètres qui décrivent notre univers et nous testons ceux-ci en utilisant les dernières observations cosmologiques. Nous utilisons des données provenant du fond diffus cosmologique, des oscillations acoustiques des baryons (BAO) et de supernovas de type Ia, et nous trouvons un bon accord avec les observations tout en mettant des contraintes sur les paramètres cosmologiques. Nous adressons la déviation du modèle Λ - matière noire froide (ΛCDM) à haut décalage vers le rouge trouvée récemment dans les mesures du BAO à partir de la forêt Lyman-α qui provient de quasars. Nous montrons que le paramètre d'Hubble et la distance angulaire à haut décalage vers le rouge pour le modèle d'interaction concorde mieux avec les valeurs obtenues par la collaboration BOSS en comparaison avec le modèle ΛCDM, et nous montrons que l'addition de cet ensemble de données améliore l'ajustement global du modèle, bien qu'avec une signification statistique faible.

Contents

List of Figures

List of Tables

Preface

This manuscript thesis contains four peer-reviewed and published articles that are original and consist of a distinct contributions to knowledge. These are presented in their original form, due to copyright, in Chapters 4, 5, 7 and 8. It is customary in the field of cosmology that the authors are listed in alphabetical order. For that reason, bellow we state the contribution of the author to each of the included works.

Contributions of the Author

Robert H. Brandenberger, Elisa G.M. Ferreira, Ian A. Morrison, Yi-Fu Cai, Sumit R. Das, Yi Wang, *Fluctuations in a cosmology with a spacelike singularity and their gauge theory dual description*, Phys. Rev. D 94 (2016) no.8, 083508.

This article is presented in Chapter 4. This paper is part of a large and ambitious research program to develop a new tool for cosmology. For that reason, it involved many researchers, and it represents the main topic of my Ph.D.. All the authors participated in the discussions, including during the three workshops organized to make progress on this research. I performed all of the calculations for this project.

Elisa G. M. Ferreira, Robert Brandenberger, *Holographic Curvature Perturbations in a Cosmology with a Space-Like Singularity*, JCAP 1607 (2016) no.07, 030.

This article is presented in Chapter 5 and is a continuation of the previous one, focusing on in cosmological observables. In this work, I performed the majority of the calculations and writing of the paper. The discussions and conclusions were made in collaboration with Professor Brandenberger who also checked the calculations and contributed to the writing of the manuscript.

André A. Costa, Xiao-Dong Xu, Bin Wang, Elisa G. M. Ferreira, E. Abdalla, *Testing the Interaction between Dark Energy and Dark Matter with Planck Data*, Phys. Rev. D89 (2014) no.10, 103531.

This work was the first of a long theoretical and numerical study of dark energy models, and it is presented in Chapter 7. The idea of this work was developed by me in collaboration with B. Wang and E. Abdalla. In this work I contributed in many different parts. I helped A.A.Costa in writing and implementing the numerical code used for the data analysis. My main participation was in the selection of models and parameters to be analysed, and the discussion of the results. I wrote the "Introduction" and the "Theoretical Setup" sections of the paper.

Elisa G. M. Ferreira, E. Abdalla, Jerome Quintin, Bin Wang, *New Evidence for Interacting Dark Energy from BOSS*, Phys. Rev. D95 (2017) no. 4, 043520.

This article is presented in Chapter 8. I initiated this project. I was responsible for the theoretical development, together with J. Quintin. I also ran the numerical code, developed in the previous work. Most of the analysis was done by me in collaboration with J. Quintin. I wrote around 85% of the paper, with the rest being written by J. Quintin. E. Abdalla and B. Wang contributed to the discussions.

Publications not included in this thesis

1. L.L. Graef, W.S. Hipolito-Ricaldi, Elisa G. M. Ferreira, Robert Brandenberger, *Dynamics of Cosmological Perturbations and Reheating in the Anamorphic Universe*, JCAP 1704 (2017) no. 04, 004.

2. W.S. Hipolito-Ricaldi, Robert Brandenberger, Elisa G. M. Ferreira, L.L. Graef, *Particle Production in Ekpyrotic Scenarios*, JCAP 1611 (2016) no.11, 024.

3. Yi-Fu Cai, Elisa G. M. Ferreira, Bin Hu, Jerome Quintin, *Searching for Features of a String Inspired Inflationary Model with Cosmological Observations*, Phys. Rev. D92 (2015) no.12, 121303.

4. Yi-Fu Cai, Fang Chen, Elisa G. M. Ferreira, Jerome Quintin, *A new model of axion monodromy inflation and its cosmological implications*, JCAP 1606 (2016) no.06, 027.

5. Hossein B. Moghaddam, Robert Brandenberger, Yi-Fu Cai, Elisa G. M. Ferreira, *Parametric Resonance of Entropy Perturbations in Massless Preheating* , Int. J. Mod. Phys. D24 (2015) 11, 1550082.

6. Elisa G.M. Ferreira, Robert Brandenberger, *The Trans-Planckian Problem in the Healthy Extension of Horava-Lifshitz Gravity*, Phys. Rev. D86 (2012) 043514.

7. A.B. Pavan, Elisa G.M. Ferreira, S. Micheletti, J.C.C. de Souza, E. Abdalla, *Exact cosmological solutions of models with an interacting dark sector*, Phys. Rev. D86 (2012) 103521.

8. C.E. Pellicer, Elisa G.M. Ferreira, Daniel C. Guariento, Andre A. Costa, Leila L. Graef, Andrea Coelho, Elcio Abdalla, *The role of Dark Matter interaction in galaxy clusters*, Mod. Phys. Lett. A27 (2012) 1250144.

Preprint Publications

- R. Battye *et al.* (including Elisa Ferreira), *Update on the BINGO 21cm intensity mapping experiment*, arXiv:1610.06826 [astro-ph.CO].

- J-PAS Collaboration (N. Benitez *et al.* [including Elisa Ferreira]), *J-PAS: The Javalambre-Physics of the Accelerated Universe Astrophysical Survey*, arXiv:1403.5237 [astro-ph.CO].

Chapter 1

Introduction

Cosmology is one of the fastest growing fields of physics. Very recently in the history of physics it has become a precision field of science and it continues to accumulate observational and theoretical successes. Those observations, together with the theory of general relativity and the cosmological principle, made possible to develop the standard cosmological model (SCM), a model that describes the geometry, evolution and composition of our universe that is expanding from nucleosynthesis, the epoch when the nuclei of light elements were formed, until today. Its observational pillars, the abundance of light elements, Hubble expansion and the Cosmic Microwave Background, describe a universe that is homogeneous and isotropic on large scales which is 13.9 billions of years old, and composed today of 4% baryonic matter, 0.01% radiation, 23% dark matter and 73% dark energy.

Recent cosmological observations confirm with great precision many of the hypothesis of this model, but also found some exciting deviations not described by its current form. This shows that in spite of its success, the SCM does not describe all the ingredients of our current universe. Cosmology faces a number of outstanding theoretical and fundamental challenges. From the Big Bang singularity, and problems with its initial condition, to the fact that 95% of what composes our universe is unknown, the problems faced require a new understanding of fundamental physics. From that it is clear that we need extensions to our current cosmological paradigm that involve the inclusion of a new description or even extensions of the physical laws we know. Of particular importance for this thesis are the singularity problem and the nature of dark energy that leads to the accelerated expansion of our universe. This thesis comprises a series of works that aim to address these two major

problems in cosmology.

One of the biggest problems in cosmology is the singularity problem. Singularities are a very general feature of many cosmological models, since they are unavoidable in the context of Einstein's gravity with standard matter. In this context, in an expanding universe the Penrose singularity theorem implies that initially the universe had an infinite energy density in a very small volume, which we call the Big Bang singularity. If try to extend our classical description to those regimes our current mathematical understanding and physical theories break down and cannot be used. Singularities appear in many cosmological models from the expanding SCM model to its extensions like the inflationary model [1–5], a period of accelerated expansion in the early universe, and bouncing models [6], where a period of contraction precedes the SCM expansion of the universe passing through a Big Bang/Big Crunch singularity. In the attempt to avoid the appearance of an initial singularity, one needs to either go beyond the theory of general relativity or else add matter in our universe that does not behave according to the standard (null) energy conditions. These approaches are somewhat *ad hoc* and reflect our attempt to extend our theories in the absence of a complete and fundamental quantum theory of gravity that attempts to describe the high energy and curvature regions of our universe.

In the absence of a quantum gravity theory to describe our universe, the singularity problem is hard to solve. We need new tools to be able to solve this problem. There have been many attempts in the literature to resolve the Big Bang/Big Crunch singularity, specially in the context of bouncing cosmologies. These use different techniques to effectively describe cosmology in the quantum regime using semi-classical techniques (see [7, 8] for some examples). Beyond the semi-classical approximation, string theory presents a concrete approach to quantum gravity where we can study quantum effects in cosmology. However, string theory is an unfinished theory and initially it did not present a non-perturbative description. In this context, the AdS/CFT correspondence [9] comes to the rescue, presenting a non-perturbative description of string theory.

The AdS/CFT is a conjecture relates a string theory with Anti-de-Sitter (AdS) boundary condition to quantum field theories living in the boundary of AdS and it is one of the most important advances in theoretical physics with applications in diverse areas. This conjecture provides an interesting avenue to solve the singularity problem since it offers the opportunity to treat the singularity in a weakly coupled and non-gravitational field theory, instead of in the strongly coupled, high curvature and quantum regime of gravity. There

have been many attempts in the literature to use this tool to describe the Big Bang/Big Crunch singularity [10–15]. We present here another attempt of that.

In cosmology, we are interested in providing a description of the evolution of the universe that yields observables that match the cosmological observations of the structure of our universe. The existence of a singularity in many bouncing models and the difficulty to describe mathematically these regions impact the predictability of those models. For that reason in our works we were interested in addressing the question of what happens to the cosmological perturbations generated in the contracting phase and that are expected to be the seeds for the formation of all the structures of our universe and must be described by current observations, after they pass the singularity. Our works intend to establish a formalism using the AdS/CFT correspondence to describe how the perturbations behave after passing through a cosmological singularity, accessing the imprints that the singularity might induce in the spectrum of those fluctuations as an important step for the understanding of the predictability of bouncing models. We propose a formalism for that in Chapter 4 (based on [16]) where we discuss fluctuations of a scalar field in a toy cosmology, a deformed AdS space-time. This is generalized to the discussion of curvature fluctuations that are related to observations, in Chapter 5 (based on [17]). These works are an attempt to access how good of a tool the AdS/CFT duality is for the purpose of resolving cosmological singularities and to give us first clues for consequences of cosmological singularities in cosmological perturbations. So, the construction presented here is a toy model of the early universe behaviour of a bouncing universe. The use of this construction is well motivated for many reasons. To start, the AdS/CFT correspondence is most well known and better demonstrated in its original context of a supergravity theory on AdS_5 space-time that is dual to a $\mathcal{N} = 4$ SYM theory on the boundary, where the theories on the bulk and boundary are determined. The correspondence is less understood in other contexts. Another motivation is that AdS space-time is commonly used as a prototype of a bouncing universe, aiding us in the description of a bouncing cosmology. Then, although we do not live in an AdS universe, and not in 5-dimensions, this prototype universe can help us understand if holography can be used to study the evolution of perturbations through space-like (cosmological) singularities.

The recent improvement in observational techniques available for the measurement of cosmological parameters shows us that the universe is composed in its majority by two unknown components: dark matter and dark energy. The first corresponds to 23% of the

total energy density of our universe and, because of its clustering properties, has an important role in the formation of the large scale structure of our universe. Dark energy is one most accepted explanantion for the apparent accelerated expansion of the late universe, discovered by the observation of distant Type Ia Supernovae by [18,19]. Although the influence of those components is measured gravitationally, their nature is still unknown, and this is one of the major problems in cosmology nowadays.

The simplest idea for the component responsible for this present acceleration is the cosmological constant. The standard cosmological model that includes this component plus cold dark matter. It is the ΛCDM and it is the preferred model given current observations [20]. However, the cosmological constant presents serious theoretical challenges. Since it is related to the energy of the vacuum, the value that is measured from cosmological observations coming from the current value of the Hubble parameter H_0 is different than the one calculated from field theory by many orders of magnitude. So, the cosmological constant suffers from serious fine tuning problems, not only from the fine tuning of its renormalized value but mainly from the radiative instabilities that leads to successive fine tunings. This, together with the coincidence problem, that states the coincidence that the densities of dark matter and dark energy are of the same order close to the present time even though those components have distinct evolutions, are known as the cosmological constant problems. These theoretical challenges give us motivation to search for alternatives explanations for the nature of dark energy. In particular, the search for a mechanism where dark energy is a dynamical quantity.

The dark sector can be richer than described in the ΛCDM model and a huge theoretical effort to explain the accelerated expansion resulted in a zoo of models with different mechanisms. These include (for a review see [21]) models inspired by inflationary models where a scalar field is included like quintessence, or modifications of General Relativity. Many proposed models also invoke an interaction between the chosen dark energy component and baryons, like the chameleon mechanism [22, 23], symmetron [24] and dilaton [25]; or with dark matter (for a classification of models see [26]), with models where the interaction is phenomenological [27–31] or even coming from field theory [32–35], Chaplygin gas, and many others. This list is far from complete and some of those models overlap. This shows how much freedom there is in the understanding of the dark universe.

Fortunately, we live in an era where an abundance of data from cosmological observations is or will be available with the exploration of the large scale structure of the universe

(LSS) [36] and of new windows of observations like 21cm cosmology [37]. There is currently a huge effort from the scientific community in order to measure the equation of state of dark energy and its possible time evolution, in order to understand the properties of this component, together with its influence on the cosmological parameters, and to possibly distinguish between some of the theoretical explanations available. In this thesis, we present attempts of constraining the properties of a model where dark energy interacts with dark matter to see how well they can describe the physics of our universe. We use a phenomenological model of this interaction with the intent of constrainig the parameters of dark energy and to compare how well this model fits the cosmological data in comparison to the standard ΛCDM model. In Chapter 8, based on [38], we test the effects of this model on the cosmological parameters using the most recent cosmological data available from the Cosmic Microwave Background (CMB), Baryon Acoustic Oscillations (BAO), Supernovaes and local measurements of the Hubble parameter. The data sets used above comprise mainly information from the early universe when the CMB was formed, and the very late local universe. If dark energy is dynamical or is coupled to dark matter, this effect would be more pronounced at earlier times, when the influence of dark energy is already strong but not today where its behaviour is very well measured to be close to the cosmological constant. For that, we need measurements that give us information about the properties of dark energy at different times, or redshifts. This investigation was made in Chapter 9, based on [39], where we used a new measurement of very distant quasars to evaluate a change in the cosmological parameters of the interacting dark energy model, and to compare this with a constant dark energy component from ΛCDM.

This thesis is organized as follows. Chapter 2 intends to present a review of cosmology and perturbation theory necessary for the understanding of the cosmology used in the following sections. The work is divided in two parts, that regard the two major questions studied in this thesis. Part I - Early Universe Cosmology, is dedicated to address the singularity problem that arises in the early evolution of the universe. We start this part with a very short review of the AdS/CFT correspondence, in Chapter 3, to aid the reader to understand the concepts presented in the following chapters. Chapter 4 presents the first article on the topic of fluctuations in a cosmology with space-like singularities. In Chapter 5 we present the second article on this theme, where we extend the conclusions from the first to cosmological observables.

Part II - Late Universe Cosmology, contains the studies of the nature of dark energy. Since this exploration is based on analysing the current cosmological observations, Chapter 6 is dedicated to a brief review the statistical methods of data analysis used in the following chapters. In Chapter 7 we analyse the phenomenological interacting dark energy model using the current precise cosmological observations. To study the dynamical nature of the dark energy component, this model is tested in Chapter 8 against the latest high redshift data available. We conclude the thesis in Chapter 9.

Chapter 2

Review of Cosmology

2.1 Homogeneous Universe

The background model that describes the evolution, structure and expansion of our universe is the SCM. This model is based on two theoretical pillars: Einstein's theory of General Relativity, which describes the dynamics of the universe, and the cosmological principle, the simplifying hypothesis that the universe is spatially homogeneous and isotropic on large scales; and three observational pillars: Hubble's law, which shows that the universe is expanding, the abundance pf light element, that confirms the hypothesis of primordial nucleosynthesis, and the cosmic microwave background, an isotropic black body radiation at a temperature of 3K that permeates all the universe.

In the SCM the dynamics of the universe is described by General Relativity. When combined with the cosmological principle symmetry, which means invariance under translations (homogeneity) and under rotations (isotropy), we have a solution for Einstein's equation, the Friedmann-Robertson-Walker (FRW) metric with line element:

$$ds^2 = dt^2 - a^2(t)\left[\frac{dr^2}{1-kr^2} + r^2\left(d\theta^2 + \sin^2\theta d\varphi^2\right)\right] \tag{2.1}$$

where t is the physical time and $(r,\, \theta,\, ,\varphi)$ are the comoving spatial polar coordinates, $a(t)$ is the scale factor which parametrizes the expansion of the universe or the radius of curvature of the space-time with curvature k, that can have the values $k = (-1, 0, +1)$ representing an hyperbolic, flat and spherical universe, respectively. It is also convenient to describe this

metric in conformal time η, defined by $d\eta = dt/a(t)$, where the FRW metric is takes the form of a a static Minkowski metric times $a^2(\eta)$, the conformal factor.

2.1.1 Kinematics

All the information that we have from observations of our universe comes from light that we receive from the universe. One of the biggest discoveries for cosmology, the verification that the universe is expanding by Hubble [40], was made by observing that the light emitted by galaxies had a deviation of its wavelength to the red region of the electromagnetic spectrum, know as redshift. The recessing velocity can be interpreted as an cosmological analogue of the Doppler effect and can be inferred through a redshift factor,$v = cz$, and can be inferred from the wavelength from the relation:

$$z = \frac{\lambda_{obs} - \lambda_{em}}{\lambda_{em}} = \frac{a\,(t_{obs})}{a\,(t_{em})} - 1\,. \tag{2.2}$$

where $\nu = c\lambda$. If $z > 0$ we call it a *redshift* and if $z < 0$ we have a *blueshift*. With that, Hubble could infer the recession velocities and find the empirical relation known as Hubble's law, $v = H_0\, l$, where l is the distance of the galaxies and H_0 is the Hubble's constant given by today's value of the Hubble parameter:

$$H(t) = \frac{\dot{a}(t)}{a(t)}\,. \tag{2.3}$$

The value of H_0 is measured with great precision today, but presents a tension in its values measured by CMB, $H_0 = 67.7 \pm 0.5$ [41], and by local observations from the Hubble Space Telescope, $H_0 = 73.8 \pm 2.4$ [42]. Two useful quantities related to $H(t)$ are the Hubble time, $t_H = H^{-1}$, and the Hubble radius, $r_H = cH^{-1}$.

Another important quantity of interest in cosmology are distances, which are important for observational measurements of the distant objects of our universe. In particular, we can define the angular diameter distance as $D_A = D/\delta\theta$, where D is a known physical size that can come from standard rulers, and $\delta\theta$ is the measured angular size. It can be related to the metric distance $d_m = S_k(\chi)$ obtained from the FRW metric line element: $ds^2 = dt^2 - a^2(t)\,(d\chi^2 + S_k(\chi)d\Omega^2)$, as $D_A = d_m(1+z)^{-1}$. It can also be related to the luminosity distance d_L, $d_A = d_L(1+z)^{-2}$, where the luminosity distance can be related to the comoving coordinate.

2.1.2 Dynamics

The kinematic description of the universe does not allow us to determine the behaviour of the scale factor. The dynamics if the universe is described by Einstein's equation of general relativity:

$$G_{\mu\nu} \equiv R_{\mu\nu} - \frac{1}{2} g_{\mu\nu} R = 8\pi G T_{\mu\nu} \,, \tag{2.4}$$

where the left side contains information about the geometry, encoded in the Einstein tensor $G_{\mu\nu}$, which expresses the curvature of the space-time by its components $R_{\mu\nu}$, the Ricci tensor, and R, the Ricci scalar. The right side of the equation is related to the matter content of the universe, described by the energy-momentum tensor $T_{\mu\nu}$. The left side can also contain a cosmological constant term Λ.

As we saw previously, we need to also impose the cosmological principle in the SCM. This implies that it is a good approximation to consider the universe to be filled by a perfect fluid (Weyl's postulate) [43]

$$T_{\mu\nu} = (\rho + p)\, u_\mu u_\nu - p g_{\mu\nu} \,, \tag{2.5}$$

where ρ is the energy density of the fluid, p it is the pressure and u_μ is the velocity four-vector of the fluid. In comoving coordinates, $u_\mu = (1, 0, 0, 0)$ and the energy-momentum tensor takes the form $T^\mu_\nu = diag\,(\rho,\, -p,\, -p,\, -p)$. As this fluid is homogeneous and isotropic, ρ and p are functions only of time. If the universe was composed of a scalar field, the energy momentum would take the form:

$$T^\mu_\nu = \partial_\mu \varphi \partial^\mu \varphi - \left[\frac{1}{2} \partial_\mu \varphi \partial^\mu \varphi - V(\varphi) \right] \delta^\mu_\nu \,, \tag{2.6}$$

where $u^\alpha \equiv \partial^\alpha \varphi / \sqrt{\partial_\mu \varphi \partial^\mu \varphi}$, $\rho \equiv \frac{1}{2} \partial_\mu \varphi \partial^\mu \varphi + V(\varphi)$, and $p \equiv \frac{1}{2} \partial_\mu \varphi \partial^\mu \varphi - V(\varphi)$, with $\varphi^{,\gamma} \varphi_{,\gamma} > 0$.

We can insert the definitions of the energy-momentum of the perfect fluid (2.5) , together the FRW metric (2.1) into Einstein's equation (2.4) resulting in the Friedmann equations:

$$\left(\frac{\dot{a}}{a} \right)^2 = \frac{8\pi G}{3} \rho - \frac{k}{a^2} \tag{2.7}$$

$$\frac{\ddot{a}}{a} = -\frac{4\pi G}{3} (\rho + 3p) \tag{2.8}$$

where here G is Newton's constant, and ρ and p represent the total energy density and pressure of all matter components of the universe. We can combine these equations by

taking the time derivative of (2.7) together with (2.8), which yields the continuity equation:

$$\dot{\rho} + 3H\left(\rho + p\right) = 0\,. \tag{2.9}$$

This equation expresses the covariant conservation $\Delta_\mu T^\mu_\nu = 0$, where Δ_μ is the covariant derivative. If the matter content was made of a scalar field, this conservation law yields the Klein-Gordon equation.

The Friedmann equation and continuity equations is a dependent system of equation that describes the dynamics of $a(t)$, $\rho(t)$ and $p(t)$. However, since these equations are not independent, to fully determine this system we need an extra equation. This equation characterizes the fluid that is present in the universe and relates the energy density and pressure by an equation of state ω:

$$p = \omega\rho\,. \tag{2.10}$$

Using this equation in the dynamical system we can see how each of the different matter components influences the evolution of the universe. We can parametrize most of the components of the universe by a constant equation of state with $\omega = 0$ for matter (baryonic or dark), $\omega = 1/3$ for radiation and $\omega = -1$ for a cosmological constant. This leads to the following dynamics:

$$\rho\left(t\right) = \begin{cases} \rho_0^m\, a^{-3} = \rho_0^m (1+z)^3\,, & \text{matter} \\ \rho_0^{rad} a^{-4} = \rho_0^{rad}(1+z)^4\,, & \text{radiation} \\ \rho_0^\Lambda\,, & \text{c.c.} \end{cases} \Rightarrow\; a\left(t\right) = \begin{cases} a_0^m t^{2/3}\,, & \text{matter} \\ a_0^{rad} t^{1/2}\,, & \text{radiation} \\ a_0^\Lambda e^{H_\Lambda t}\,, & \text{c.c.}\,. \end{cases} \tag{2.11}$$

where $H_\Lambda = \sqrt{8\pi G\rho_0^\Lambda/3}$ and c.c. stands for cosmological constant. Taking the second derivative of these solutions we can see that for matter and radiation the expansion of the universe decelerates, while for a cosmological constant it accelerates. If one had a component with a general $\omega = \omega(a)$, its evolution can be given by:

$$\rho = \rho_0\, e^{-\int 3(1+\omega)\frac{da}{a}} = \rho_0\, a(t)^{-3(1+\omega)}\,, \tag{2.12}$$

where in the last equality we assumed a constant equation of state. In this way we can describe a dark energy component, since $\omega < -1/3$ with a varying or constant equation of state, leads to a universe with accelerated expansion.

We can re-write the Friedmann equations using the density parameter, a parameter that can be related to the kinematic characteristics of the universe. As we mentioned, in the Friedmann equation, the quantity ρ is the total density given by the sum of the energy densities of each component in the universe. In this way, dividing both sides of the first Friedmann equation (with $\Lambda = 0$) by H^2, we have:

$$1 = \Omega_{total} - \frac{k}{a^2 H^2}\,, \tag{2.13}$$

where $\Omega_{total} = \sum_i \Omega_i$ is the relative total density, and $\Omega_i \equiv \rho_i/\rho_{crit}$ is the density parameter of the i^{th} component of the universe. The quantity:

$$\rho_{crit} = \frac{3H^2}{8\pi G}\,, \tag{2.14}$$

is the critical density. Writing the Friedmann equation in this way, we can see that the total density parameter can be written in terms of the curvature constant: if $\Omega_{total} > 1 \Leftrightarrow k = +1$ we have a closed universe, if $\Omega_{total} = 1 \Leftrightarrow k = 0$ we have a flat universe, and if $\Omega_{total} < 1 \Leftrightarrow k = +1$ we have an open universe. The universe today is close to flat, with $\Omega_0 \sim 1$ with 1% precision form measurements of the CMB by the WMAP satellite [44] combined with constraints from Sloan Digital Sky Survey and type-Ia supernovae.

The Friedmann equation can be written in terms of the density parameter:

$$\frac{H^2}{H_0^2} = \Omega_{m,0}\, a^{-3} + \Omega_{rad,0}\, a^{-4} + \Omega_{\Lambda,0}\,, \tag{2.15}$$

for an universe composed of matter (baryonic and cold dark matter), radiation (that can be photons and massless neutrinos) and a cosmological constant, where $\Omega_{total} = \Omega_m + \Omega_{rad} + \Omega_\Lambda = 1$.

2.1.3 Quick Review of the Thermal History of the Universe

In the previous sections we saw that each component of the universe leads to a different evolution of the universe. In this way we have to know the composition of the universe at each moment to be able to probe the history of its evolution.

From Hubble's law we can see that the universe is expanding. Going backwards in time, we can think that in its beginning, all the energy of the universe was contained in a

infinitesimally small volume, with infinite density and temperature, expanding and cooling from this point forward in time. This is why the SCM is also called the hot Big Bang model, where the Big Bang refers to this initial infinite density state or initial singularity. From this point on, the evolution of the universe depends on its matter content through the relations given in (2.11).

From the evolution of the densities of each component, we have a period of radiation domination when $z > z_{eq} \sim 10^4$, matter domination when $z_{eq} > z > z_\Lambda$, and the current accelerated expansion when dark energy dominates at $z < z_\Lambda$ The redshifts $z_{eq} = (\rho_{crit}\Omega_m)/(\rho^0_{rad}-1)$ correspond to the moment when the densities of matter and radiation is the same, and $z_\Lambda = (\Omega_\Lambda/\Omega_m)^{-1/3\omega} - 1$ when the densities of matter and dark energy are the same, for a constant $\omega < -1/3$. The value of z_Λ is an open problem in cosmology since dark energy's nature is unknown. This component cannot dominate the content of the universe too early in its history, impacting the formation of the large scale structures of the universe, so it started dominating at times close to today. This is known as the coincidence problem.

We describe here in a succinct way the thermal history of the universe, showing the different periods and non-equilibrium events that gave rise to the formation of the elements of the standard particle theory model and all the matter constituents of our universe today.

- *Contraction:* One of the possible models for the evolution of the universe is a universe that has a period of contraction previous to the current expansion era. The duration of this period is model dependent.

- *Planck era:* The Planck era comprises the period from the beginning of the universe until $\sim 10^{-43}$s with temperatures of order $T \sim 10^{32}$K $\sim 10^{19}$GeV. This period is not described by the SCM and in this period General Relativity is not valid and quantum effects are important.

- *Inflation:* This model was proposed as a possible solution to the problems of the SCM and consists of a period of accelerated expansion. If there is such a period in the evolution of our universe, it happenned from times ranging from Plancj times to 10^{-32}s.

- *Nucleosynthesis*: As the temperature of the universe cooled down and became of the order of $10^8 - 10^9$K, nuclear processes began to happen and formed the light elements that compose our universe. This happened between $1 - 500$s after the Big Bang and

forms from the already formed protons and neutrons, the hydrogen (H), deuterium (H^2), H^3 and helium (He).

- *Recombination and photon decoupling*: The universe is dominated by radiation since $z \gg 10^4$, and matter and radiation coexist in equilibrium. The light elements formed during nucleosynthesis are ionized, with the electrons and photons scattering freely. As the temperature cools down, these scattering become more rare and the free electrons start to bind into H and H^3. This period is called recombination and occurs from $z = 1400$ when the temperature is of order of $T \sim 3800$K until $z \sim 1100$ when $T \sim 3000$K, when the photons decouple from the radiation-matter plasma. This instant (which is actually a small period) is called last scattering surface and the photons that decouple at this instant free stream until today, given us the CMB, a picture of the universe around $z = 1100$.

- *Matter era*: After the decoupling of the photons, matter is the component that dominates in the universe, from $z = 10 - 2$. In this period the formation of the large scale structure occurs, with the formation of galaxies, stars and all the visible structures of our universe.

- *Dark Energy era*: Period of accelerated expansion in the late universe.

The SCM described in the previous sections has many problems. As we saw in this section some new mechanisms like inflation or bouncing cosmology and the introduction of a dark energy component appear as necessary extensions of this model in order to match the available cosmological observations.

2.2 Inhomogenous Universe

In the previous section we studied the homogeneous and isotropic background cosmology. However, in our current universe we observe galaxies, planets and other non-linear structures that show that the universe is not homogeneous bellow a certain scale. After the pioneering measurements from WMAP and Planck satellites, the detection of deviations from the background homogeneity, from small fluctuations in the temperature of the CMB that indicate perturbations in the energy density of the universe, of order of 10^{-5} were measured. We

review in this section the formalism necessary to treat these perturbation and its evolution in the linear regime, and to study their quantum origin in the context of (semi-classical) general relativity.

2.2.1 Cosmological Perturbations Theory in General Relativity

The growth of the initial perturbations was first described in the Newtonian limit, where structure are formed by gravitational instability. This study is important since it gives us an idea of the evolution of late time, super-Hubble perturbations. However, for a complete description if the perturbations in our universe, we need a decription in the context of general relativity and this is developed in this section (based on [45–47]). We are going to study small linear cosmological perturbations with respect to the background.

Classifying the Perturbation Modes

We start by perturbing the metric:

$$g_{\mu\nu} \to g^{(0)}_{\mu\nu} + \delta g_{\mu\nu} \,, \tag{2.16}$$

where $|\delta g_{\mu\nu}| \ll \left| g^{(0)}_{\mu\nu} \right|$, and the background metric is the flat FRW metric in conformal time with line element $ds^2_0 = g^{(0)}_{\mu\nu}(\eta)\, dx^\mu dx^\nu = a^2(\eta)\,(d\eta^2 - \delta_{ij} dx^i dx^j)$.

The metric is a symmetric tensor that has 10 perturbation degrees of freedom. We can decompose those perturbations into a irreducible set of modes: the scalar, vector and tensor modes. This SVT decomposition is useful since at linear level, the Einstein equation for each mode is decoupled from the others and we can treat the evolution of the scalars, vector and tensor perturbations separately.

So, we can describe the perturbation of each component of the metric. The δg_{00} can be described by one scalar function:

$$\delta g_{00}(\eta, \mathbf{x}) = 2a^2(\eta)\,\phi(\eta, \mathbf{x}) \,. \tag{2.17}$$

There are two irreducible ways of writing the non-diagonal component of the metric δg_{0i}, as the gradient of a scalar quantity and as a divergenceless vector:

$$\delta g_{0i}(\eta, \mathbf{x}) = 2a^2(\eta)\,(B_{,i} + S_i) \,, \tag{2.18}$$

where B is a scalar function and S_i is a vector with $S_{\ i}^{,i} = 0$ so the decomposition is irreducible and unique. The component δg_{ij} of the metric is a tensor and there are five irreducible ways to construct a tensor:

$$\delta g_{ij}(\eta, \mathbf{x}) = 2a^2(\eta)\left(2\psi\delta_{ij} + 2E_{,ij} + F_{i,\,j} + F_{j,\,i} + h_{ij}\right)(\eta, \mathbf{x}) \ , \tag{2.19}$$

where $\psi(\eta, \mathbf{x})$ and $E(\eta, \mathbf{x})$ are scalars that can determine a tensor in two different ways: by being multiplied by a tensor or by taking its Laplacian. The vector, $F_i(\eta, \mathbf{x})$, has to be divergenceless. And finaly, $h_{ij}(\eta, \mathbf{x})$ is a tensor that must be traceless $h_i^i = 0$ and transverse $h^i_{j,\,i} = 0$, so it cannot be decomposed into scalars and vectors.

Having determined the perturbations, we can re-arrange the metric perturbations dividing them into scalar, vector and tensor perturbations, with line element:

- *Scalar modes:* Described by 4 functions $\phi(\mathbf{x}, t)$, $\psi(\mathbf{x}, t)$, $B(\mathbf{x}, t)$, $E(\mathbf{x}, t)$:

$$ds^2 = a^2(\eta)\left\{(1+2\phi)\,d\eta^2 + 2B_{,i}d\eta dx^i + \left[(1-2\psi)\,\delta_{ij} - 2E_{,ij}\right]dx^i dx^j\right\} \ . \tag{2.20}$$

- *Vector modes:* It contains four degrees of freedom described by 2 vectors, $S_i(\mathbf{x}, t)$ and $F_i(\mathbf{x}, t)$.

$$ds^2 = a^2(\eta)\left[d\eta^2 + 2S_i d\eta dx^i - \left(\delta_{ij} - F_{i,j} - F_{j,i}\right)dx^i dx^j\right] \ . \tag{2.21}$$

- *Tensor modes:* Two tensor modes

$$ds^2 = a^2(\eta)\left[d\eta^2 - \left(\delta_{ij} - h_{ij}\right)dx^i dx^j\right] \ . \tag{2.22}$$

Gauge Transformations and Independent Variables

General relativity allows freedom in the choice of the coordinate system used. So it is important to know how the metric changes under those changes of coordinates in order that we can identify the modes that are physical from the ones that are a gauge artifact. For that, given an infinitesimal coordinate transformation:

$$x^\mu \to \tilde{x}^\mu = x^\mu + \xi^\mu \, , \tag{2.23}$$

where the ξ^μ has four components: ξ^0, that can generate scalar perturbations of the metric, and ξ^i, that can be decomposed in a irreducible ways into $\xi^i = \xi^i_\perp + \varsigma^{,i}$ where $\xi^i_\perp$ is a divergenceless vector that has two degrees of freedom that contribute to the vector perturbations, and ς a scalar function. Tensors are invariant under coordinate transformations and do not induce tensor perturbations.

The scalar and vector functions from the SVT decompositions of the metric transform under this change of coordinates. The scalar functions transform as:

$$\tilde{\phi} = \phi - \frac{1}{a}\left(a\xi^0\right)' , \qquad \tilde{B} = B + \varsigma' - \xi^0 , \tag{2.24}$$

$$\tilde{\psi} = \psi + \frac{a'}{a}\xi^0 , \qquad \tilde{E} = E + \varsigma . \tag{2.25}$$

while the vector transform as $\tilde{S}_i = S_i + \xi'_{\perp i}$ and $\tilde{F}_i = F_i + \xi_{\perp i}$. The tensor mode h_{ij} is invariant under gauge transformations. This shows us that the scalar and vector modes exhibit a gauge ambiguity with the appearance of fictitious perturbation modes that have no physical significance. One way to avoid this gauge redundancy is to adopt a gauge invariant description where we construct gauge invariant quantities independent of ξ^μ, the Bardeen variables:

Scalar modes:

$$\Phi \equiv \phi - \frac{1}{a}\left[a\left(B - E'\right)\right]' , \qquad \Psi \equiv \psi - \frac{a'}{a}\left(B - E'\right) . \tag{2.26}$$

Vector modes:

$$\bar{v}_i = S_i - F_i' . \tag{2.27}$$

Here we can see that the vector modes present four degrees of freedom, but only two of them characterize physical meaningful perturbations.

We can also solve the gauge redundancy problem by choosing and fixing a gauge where we are going to work. This amounts to impose conditions to fix the number of variables that are redundant. From the diffeomorphism invariance of general relativity, we need gauge away four degrees of freedom. The most used gauges in cosmology are the Newtonian, synchronous and spatially flat gauge, and they are defined by the choices, for the scalar modes only:

- *Newtonian or longitudinal gauge*: This gauge is given by the conditions:

$$B = 0\,, \qquad E = 0\,, \tag{2.28}$$

that gives the following line element for the perturbations:

$$ds^2 = a^2(\eta)\left[(1+2\phi)\,d\eta^2 - (1-2\psi)\,\delta_{ij}dx^i dx^j\right]\,. \tag{2.29}$$

In terms of the Bardeen variables:

$$\Phi = \phi\,, \qquad \Psi = \psi\,, \tag{2.30}$$

where ϕ and ψ are considered to be the generalized gravitational potential, giving the name to this gauge.

- *Synchronous gauge*: the synchronous gauge is the gauge where we choose the synchronous coordinates where $\delta g_{0\mu} = 0$. This implies that:

$$\phi = 0\,, \quad B = 0\,. \tag{2.31}$$

In this gauge there is still some arbitrarity in the 3-dimensional coordinate transformations. As the conformal temporal coordinate is fixed, we can say that in this coordinate system all the clocks in a given Hubble radius are synchonized, inspiring the name of this gauge.

- *Spatially flat gauge (or uniform curvature gauge) [?]*: This gauge is very convenient for cosmology because it simplifies the computation of the curvature perturbations, that are linked to the density perturbations that seeded the structures of our universe, for reasons that will become clear in the following sections. In this gauge, we have the condition:

$$\Phi = B = 0\,. \tag{2.32}$$

Linearized Einstein's equations

After defining the properties of the perturbations of the metric, we can now write their equations. For that we have expand the perturbed Einstein's equations in the linear regime

for small perturbations: $\delta G_{\mu\nu} = 8\pi G \delta T_{\mu\nu}$. At this level, the scalar, vector and tensor linearized equations are decoupled and we can study the evolution of each mode separately. Adopting the Newtonian gauge, we have the perturbed Einstein equation for each mode:

Scalar mode: Using the scalar perturbations of the metric in Newtonian gauge (2.29) we have,

$$\delta G^0_0 = \nabla^2\Psi - 3\mathcal{H}\left(\Psi^{'} + \mathcal{H}\Phi\right) = 4\pi G a^2 \delta T^0_0\,, \tag{2.33}$$

$$\delta G^0_i = \left(\Psi^{'} + \mathcal{H}\Phi\right)_{,i} = 4\pi G a^2 \delta T^0_i\,, \tag{2.34}$$

$$\begin{aligned}\delta G^i_j &= \left[\Psi^{''} + \mathcal{H}\left(2+\Phi\right)^{'} + \left(2\mathcal{H}^{'} + \mathcal{H}^2\right)\Phi + \frac{1}{2}\nabla^2\left(\Phi - \Psi\right)\right]\delta^i_j - \frac{1}{2}\left(\Phi-\Psi\right)^{,i}_{,j} \\ &= -4\pi G a^2 \delta T^i_j\,,\end{aligned} \tag{2.35}$$

where $\mathcal{H}$ is the comoving Hubble parameter.

Vector modes:

$$\delta G^0_i = 16\pi G a^2 \delta T^0_i\,, \tag{2.36}$$

$$\delta G^i_j = \left(\bar{v}_{i,j} + \bar{v}_{j,i}\right)^{'} + 2\mathcal{H}\left(\bar{v}_{i,j} + \bar{v}_{j,i}\right) = -16\pi G a^2 \delta T^i_{j(V)}\,, \tag{2.37}$$

where $\delta T^i_{j(V)}$ is the vector part of the perturbation of the energy-momentum tensor.

Tensor modes: from the tensor perturbations of the metric (2.22),

$$\delta G^i_j = \left(h^{''}_{ij} + 2\mathcal{H}h^{'}_{ij} - \nabla^2 h_{ij}\right) = 16\pi G a^2 \delta T^i_{j(T)}\,, \tag{2.38}$$

where $\delta T^i_{j(T)}$ is the tensor part of the energy-momentum perturbations, which usually is disregarded in cosmology.

In the absence of anisotropic stress, the space part of the perturbed energy-momentum tensor is expected to be also diagonal, as its background counterpart. For that, from the above equations, we need to have:

$$\Phi = \Psi\,. \tag{2.39}$$

This result is valid for any energy-momentum tensor with $\delta T^i_j \propto \delta^i_j$, i.e., when the matter content is described by a perfect fluid without anisotropic stress.

With that, we now need to describe the energy-momentum tensor. Here, we specialize in the case where the matter content is given by a scalar field. All the formalism presented here can also be described for a fluid-like energy-momentum tensor, as done in [46].

To evaluate the perturbations of the energy-momentum tensor that enter Einstein's equations, we need to perturb the scalar field:

$$\varphi\left(\eta,\,\mathbf{x}\right)\rightarrow\varphi\left(\eta\right)+\delta\varphi\left(\eta,\,\mathbf{x}\right)\,. \tag{2.40}$$

This perturbation is also affected by a infinitesimal coordinate transformation, with the scalar field transforming as $\delta\tilde{\varphi}=\delta\varphi+\varphi^{'}\xi^{0}$, which adds a scalar mode. Analogous to what was previously done, we can define a gauge invariant quantity for the scalar field:

$$\chi\equiv\delta\varphi+\left(B-E^{'}\right)\varphi^{'}\,. \tag{2.41}$$

With that, and knowing the form of the background energy-momentum tensor for the scalar field (2.6), we can write the perturbations of the energy-momentum tensor of the scalar field in the Newtonian gauge:

$$\delta T_{0}^{0}=-\varphi^{'}\chi^{'}-a^{2}V_{,\varphi}\chi+\Phi\varphi^{'}\,, \tag{2.42}$$

$$\delta T_{i}^{0}=-\partial_{i}\left(\varphi^{'}\chi\right)\,, \tag{2.43}$$

$$\delta T_{j}^{i}=-\left(\varphi^{'2}\Phi+a^{2}V_{,\varphi}\chi-\varphi^{'}\chi^{'}\right)\delta_{j}^{i}\,. \tag{2.44}$$

We can now write the linearized perturbed Einstein's equations for the scalar, vector and tensor modes. We begin with the scalar modes, where the equations for each component can be written as:

$$\nabla^{2}\Phi-3\mathcal{H}\left(\Phi^{'}+\mathcal{H}\Phi\right)=4\pi G\left(\varphi^{'}\chi^{'}+a^{2}V_{,\varphi}\chi-\Phi\varphi^{'}\right)\,, \tag{2.45}$$

$$\Phi^{'}+\mathcal{H}\Phi=4\pi G\,\varphi^{'}\chi\,, \tag{2.46}$$

$$\Phi^{''}+3\mathcal{H}\Phi^{'}+\left(\mathcal{H}^{'}+2\mathcal{H}^{2}\right)\Phi=4\pi G\left(\varphi^{'}\chi^{'}-\varphi^{'2}\Phi-a^{2}V_{,\varphi}\chi\right)\,. \tag{2.47}$$

As we can see, the scalar modes are the only ones that are coupled to the matter perturbations, and for that reason are the only one relevant for the formation of structure in the universe. This system of equation presents only two linearly independent equations.

Using the Klein-Gordon equation for this scalar field, we can arrange the equations, and re-write the perturbation equation as:

$$\Phi^{''} + 2\left(\mathcal{H} - \frac{\varphi^{''}}{\varphi^{'}}\right)\Phi^{'} - \nabla^2\Phi + 2\left(\mathcal{H}^{'} - \mathcal{H}\frac{\varphi^{''}}{\varphi^{'}}\right)\Phi = 0\,, \tag{2.48}$$

This equation for the scalar perturbations gives us the classical evolution of the cosmological perturbations. Since there is effectively only one propagating degree of freedom, we can define the variables:

$$u \equiv \frac{a}{\varphi^{'}}\Phi\,, \qquad \theta \equiv \mathcal{H}/a\varphi^{'}\,, \tag{2.49}$$

and the equation for the scalar perturbations is given by:

$$u^{''} - \nabla^2 u - \left(\frac{\theta^{''}}{\theta}\right)u = 0\,. \tag{2.50}$$

We can re-write this equation in momentum space as:

$$u^{''}_{\mathbf{k}} + \left(k^2 - \frac{\theta^{''}}{\theta}\right)u_{\mathbf{k}} = 0\,, \tag{2.51}$$

where $\mathbf{k} = a\mathbf{k}_{fis}$ is the comoving momentum. This equation is analogous to the equation of an harmonic oscillator with the term $\left(-\theta^{''}/\theta\right)$ acting as a time-dependent effect mass squared. The inverse of this effective mass represents the size of the comoving Hubble radius. This scale is important since it separates two regimes of behaviour of the evolution of the perturbation [45] the short wavelength perturbations, which are inside the Hubble radius ($k^2 > m^2_{eff}$) and that behave as harmonic oscillators in Minkowski space-time; and the long-wavelength perturbations which are outside the Hubble radius ($k^2 < m^2_{eff}$), and are the ones that feel the expansion of the universe. The long wavelength modes have a decaying and a growing solutions. In an expanding universe, the solution $u \sim \theta$ is the one that dominates. This means that the modes, after they leave the Hubble radius, are frozen with the wavelength of the size of the Hubble radius at the time they exited it, and remain like that until they re-enter the Hubble radius. The perturbations that we observe in the CMB re-entered the Hubble radius in the radiation epoch and encode the physics of the primordial mechanism that generated them, being either inflation or a bouncing cosmology.

In order to interpret the evolution of the long wavelength perturbations in a more convenient way, we construct different gauge invariant variables. We can define the comoving curvature perturbation [46, 48, 49]:

$$\mathcal{R} \equiv \Phi + \frac{2\mathcal{H}}{8\pi G}\frac{1}{\varphi'^2}\left(\Phi' + \mathcal{H}\Phi\right) . \tag{2.52}$$

It represents the gravitational potential on comoving surfaces with $\delta\phi = 0$ [**?**]. The equation for the perturbation in this variable is given by:

$$\mathcal{R}' = \frac{2\mathcal{H}}{8\pi G}\frac{1}{\varphi'^2}\nabla^2\Phi\,. \tag{2.53}$$

This variable is conserved for long wavelength perturbations, where $\nabla^2\Phi$ is negligible.

At this point we can see the advantage of the spatially flat gauge over the other gauges. Using this gauge, the comoving curvature perturbation is given by:

$$\mathcal{R} = \mathcal{H}\frac{1}{\varphi'}\xi\,. \tag{2.54}$$

and only depend on the perturbations of the scalar field and not on any perturbation of the metric.

Although the scalar modes are the most important ones for the formation of structure in the universe, it is important to see what happens to the vector and tensor modes.

The equations for the vector perturbations are given by:

$$\Delta\bar{v}_i = 8\pi G a^2\dot{\varphi}2\delta u_{\perp\, i}\,, \qquad \left(\bar{v}_{i,j} + \bar{v}_{j,i}\right)' + 2\mathcal{H}\left(\bar{v}_{i,j} + \bar{v}_{j,i}\right) = 0\,. \tag{2.55}$$

It is easy to see that the solution rapidly decays as the scalar factor increases, $\Phi_i \propto a^{-2}$. So, for these modes to be important cosmologically their initial values would have to be very large. They do not contribute to the formation of structures, describing rotational movements of the cosmic fluid.

The tensor modes are more interesting. Although they do not contribute to the formation of structures, they describe the gravitational waves, with the equation:

$$h_{ij}'' + 2\mathcal{H}h_{ij}' - \nabla^2 h_{ij} = 0\,. \tag{2.56}$$

Gravitational waves have two polarizations. We can expand h_{ij} in the following form:

$$h_{ij} = \frac{1}{a(\eta)} \int \frac{d^3k}{(2\pi)^3} \left[\mu_{\mathbf{k}}(\eta)\, \epsilon_{ij}(\mathbf{k})\, e^{i\mathbf{kx}} + \text{c.c.} \right] , \tag{2.57}$$

where ϵ_{ij} is the polarization tensor. Since those perturbations were defined as being transverse and traceless, the polarization tensor has to be symmetric, transverse $\epsilon_{ij} = \epsilon_{ji}$ and traceless $\epsilon^i_j = \epsilon_{ij}k^i = 0$ as well. With that, the equation has the form:

$$\mu^{''}_{\mathbf{k}} + \left(k^2 - \frac{a^{''}}{a} \right) \mu_{\mathbf{k}} = 0 . \tag{2.58}$$

which like the scalar case is analogous to a harmonic oscillator, but with different effective mass, $m^2_{gw} = -a^{''}/a$, meaning that they evolve only feeling the influence of the expansion and not the matter content.

2.2.2 Quantum Theory of Cosmological Perturbations

One of the central problems in cosmology is the primordial perturbations that seed the structures of the universe. All the models that try to describe the early universe, being this inflation, bounding cosmologies or even others, aim to address this question. To understand the generation of these primordial perturbations, we need to describe them using quantum theory. In this section we develop the quantum theory of cosmological perturbations where we quantize the first-order metric and matter perturbations about our expanding background [46]. This procedure leads to particle creation, generating the primordial perturbations.

We start from the Einstein-Hilbert action, coupled minimally to a matter action:

$$S = \frac{1}{16\pi G} \int d^4x \sqrt{-g} \left(R + 16\pi G \mathcal{L}_m \right) , \tag{2.59}$$

where $\mathcal{L}_m$ is the matter Lagrangian density. Our goal is to expand this action to second order, to obtain the linear equation for the perturbations, and study the quantization.

In order to do this, it is convenient to use the ADM formalism [50]. This formalism, developed by R. Arnowitt, S. Deser and C. W. Misner, presents a Hamiltonian formalism of General Relativity, and simplifies greatly the calculation of the second order action in a

canonical form. We start by writing the metric in the following form:

$$ds^2 = \left(\mathcal{N}^2 - \mathcal{N}_i\mathcal{N}^i\right) dt^2 - 2\mathcal{N}_i dx^i dt - g_{ij} dx^i dx^j \,, \tag{2.60}$$

where $\mathcal{N}$ is the lapse function and $\mathcal{N}_i$ the shift vector, and g_{ij} is the metric on the hypersurfaces of constant time. We can re-write the Einstein-Hilbert action with this metric and for a scalar field as the matter content,

$$\begin{aligned} S = \frac{1}{16\pi G} \int d^4x \sqrt{-g} [\mathcal{N} R^{(3)} + \mathcal{N} \left(K_{ij}K^{ij} - K^2\right) - 8\pi G \mathcal{N} \left(g^{ij}\partial_i\varphi\partial_j\varphi - 2V\left(\varphi\right)\right) \\ + 8\pi G \mathcal{N}^{-1} \left(\dot{\varphi} - \mathcal{N}^i\partial_i\varphi_i\right) \,, \end{aligned} \tag{2.61}$$

where $R^{(3)}$ is the Ricci scalar with respect to g_{ij} and $K_{ij} = \frac{1}{2}N^{-1}\left(\nabla_i N_j + \nabla_j N_i - \dot{g}_{ij}\right)$ is the extrinsic curvature tensor of the constant time hypersurfaces. Varying the action with respect to $\mathcal{N}$ and $\mathcal{N}_i$, yields the Hamiltonian and momentum constraints.

We want to identify the quantities of this formalism with the ones from the previous section. For this, we compare the metric (2.60) with (2.29), and find that in Newtonian gauge:

$$N^2 = (1 + 2\Phi) \,, \quad N_i = 0 \,, \quad g_{ij} = a^2 \left[\delta_{ij}\left(1 - 2\Psi\right) + F_{i,j} + F_{j,i} + 2h_{ij}\right] \,. \tag{2.62}$$

If we substitute these variables in the action (2.61), and take into account the constraints and the background equations, we can find the second order action with this formalism (see [46] for detailed calculations). The zeroth order expansion provides the background equations, while the first order expansion is identically equal to zero. With that, the terms of the second order expansion provide the second order action for the perturbations.

As mentioned above, we have only one propagating variable for each type of perturbation. The canonical variable of this second order action that describes each of those perturbations is given by the Mukhanov-Sasaki variables. For the scalar perturbations it is defined as:

$$v \equiv z\mathcal{R} \,, \tag{2.63}$$

with $z = 1/\theta = a\varphi^{'}/\mathcal{H}$. And for the tensor perturbations, the canonical variable is given by:

$$\mu_{ij} \equiv \sqrt{\frac{M_p^2}{4}} a h_{ij} \,. \tag{2.64}$$

where h_{ij} can be decomposed into its two polarizations:$h_{ij}\left(\eta, \mathbf{x}\right) = h_{+}\left(\eta, \mathbf{x}\right)\epsilon_{ij}^{+} + h_{\times}\left(\eta, \mathbf{x}\right)\epsilon_{ij}^{\times}$.

In terms of these canonical gauge invariant variables, the second order quadractic action for the scalar and tensor perturbations is:

$$S^{(2)} = \frac{1}{2}\int d\eta d^3x \left[\left(v^{'}\right)^2 - v_{,i}v_{,i} + \frac{z^{''}}{z}v^2\right] + \frac{1}{2}\int d\eta d^3x \sum_{\lambda=+,\times}\left[\left(\mu_{\lambda}^{'}\right)^2 - \mu_{\lambda,i}\mu_{\lambda,i} + \frac{a^{''}}{a}\mu_{\lambda}^2\right] . \tag{2.65}$$

where we see the time varying masses are as obtained before: $-\frac{z^{''}}{z}$ and $-\frac{a^{''}}{a}$. Going to momentum space, the equations of motion have a similar form then the found before:

$$v_{\mathbf{k}}^{''} + \left(k^2 - \frac{z^{''}}{z}\right)v_{\mathbf{k}} = 0\,, \quad \mu_{\mathbf{k}}^{''} + \left(k^2 - \frac{a^{''}}{a}\right)\mu_{\mathbf{k}} = 0\,. \tag{2.66}$$

We can also write the Hamiltonian for this system. For this, first we define the canonical conjugate momentum:

$$\Pi_v\left(\eta, \mathbf{x}\right) = \frac{\partial\mathcal{L}^{(2)}}{\partial v^{'}} = v^{'}\,, \qquad \Pi_\mu\left(\eta, \mathbf{x}\right) = \frac{\partial\mathcal{L}^{(2)}}{\partial\mu_{\lambda}^{'}} = \mu_{\lambda}^{'}\,, \tag{2.67}$$

which, by a Legendre transformation, leads to the Hamiltonian:

$$\begin{aligned} H &= \int d^3x \left(v^{'}\Pi_v + \mu_{\lambda}^{'}\Pi_\mu - \mathcal{L}^{(2)}\right) \\ &= \frac{1}{2}\int d^3x \left[\Pi_v^2 + v_{,i}v_{,i} - \frac{z^{''}}{z}v^2\right] + \frac{1}{2}\int d^3x \left[\Pi_\mu^2 + \mu_{\lambda,i}\mu_{\lambda,i} - \frac{a^{''}}{a}\mu_{\lambda}^2\right] . \end{aligned} \tag{2.68}$$

Quantization

With the quadratic action, we can proceed to the canonical quantization of this system. The second order action presented before reduces to the action of a real field with an external potential. In order to describe the procedure that can be used for both the scalar and the

tensor modes, we introduce the generalized variable $Q_l(\eta, \mathbf{x})$ that can be identified with either of the modes.

The action in this variable is given by:

$$S[Q_l] = \int d\eta d^3x \left[\left(Q_l'\right)^2 - Q_{l,i} Q_l^i + \frac{Z_l''}{Z_l} Q_l^2 \right]_{\mathcal{L}} , \tag{2.69}$$

with equation of motion $Q_l'' + \left(\nabla^2 - \frac{Z_l''}{Z_l}\right) Q_l = 0$, where Z_l is equal to z for the scalar mode and a for the gravity waves.

In the canonical quantization procedure, we promote these variable to operators $Q_l \to \hat{Q}_l$ and $\Pi_l \to \hat{\Pi}_l$, which must obey the commutation relations:

$$\left[\hat{Q}_l(\eta, \mathbf{x}), \hat{\Pi}_{l'}(\eta, \mathbf{y})\right] = i\delta_{ll'}\delta(\mathbf{x} - \mathbf{y}) , \tag{2.70}$$

$$\left[\hat{Q}_l(\eta, \mathbf{x}), \hat{Q}_{l'}(\eta, \mathbf{y})\right] = \left[\hat{\Pi}_l(\eta, \mathbf{x}), \hat{\Pi}_{l'}(\eta, \mathbf{y})\right] = 0 . \tag{2.71}$$

A general solution of the equation of motion can be written as the decomposition:

$$\hat{Q}_l(\eta, \mathbf{x}) = \int \frac{d^3k}{(2\pi)^{3/2}} \left[Q_{\mathbf{k},l}(\eta)\, \hat{a}_{\mathbf{k},l} \mathrm{e}^{-i\mathbf{kx}} + Q^*_{\mathbf{k},l}(\eta)\, \hat{a}^\dagger_{\mathbf{k},l} e^{i\mathbf{kx}} \right] , \tag{2.72}$$

where $\hat{a}_{\mathbf{k},l}$ and $\hat{a}^\dagger_{\mathbf{k},l}$ are the annihilation and creation operators, respectively, acting on the vacuum of the theory in the Fock representation. With the introduction of these operators, the status of operators passes from the fields to them. This procedure is known as second quantization. Those operators also obey the equal time commutation relations:

$$\left[\hat{a}_{\mathbf{k},l}, \hat{a}^\dagger_{\mathbf{k}',l'}\right] = \delta_{ll'}\delta\left(\mathbf{k} - \mathbf{k}'\right) , \qquad \left[\hat{a}_{\mathbf{k},l}, \hat{a}_{\mathbf{k}',l'}\right] = \left[\hat{a}^\dagger_{\mathbf{k},l}, \hat{a}^\dagger_{\mathbf{k}',l'}\right] = 0 . \tag{2.73}$$

which are valid only if the modes obey the normalization relation $Q'_{\mathbf{k},l} Q^*_{\mathbf{k},l} - Q^{*'}_{\mathbf{k},l} Q_{\mathbf{k},l} = 2i$, that represents the Wronskian of the classical solutions. This normalization allows us to fix the amplitude of $Q_{\mathbf{k},l}(\eta)$ that is compatible with Heisenberg's uncertainty principle.

The Hamiltonian for this system can be written in terms of the annihilation and creation operators as $\hat{H}_{\mathbf{k}} = \omega^2_{\mathbf{k},l}(\eta)\, \hat{a}^\dagger_{\mathbf{k}} \hat{a}_{\mathbf{k}}$, where $\omega_{\mathbf{k},l}(\eta) = k^2 - Z_l''/Z_l$.

We need to define the Fock space where these operators act. Since the Hamiltonian is quadractic and positive definite, there must exist the lowest energy state $|0\rangle$, where $H|0\rangle =$

$E_0 |0\rangle$, which leads to:

$$\hat{a}_{\mathbf{k},l} |0\rangle = 0 \, , \, \forall \mathbf{k} \, , \tag{2.74}$$

defining the vacuum state. We can act with the creation operator on the vacuum state generating the particle states. In the Heisenberg picture, the operators carry the time evolution, and these states define the Hilbert space.

Although this quantization procedure is very similar to the one for a free field, in the presence of an external field the invariance under space-time translations is broken and we cannot define a unique orthonormal basis. The quantization procedure now depends on the basis where the quantization was made and has a defined temporal direction. This effect leads to particle creation, since the vacuum defined for a time t_1 can be different from the vacuum defined at a time t_2. The vacuum of t_2 can be seen as a state with particles in comparison with the vacuum of t_1. Those states can be related by a Bogoliubov transformation in which one can calculate the number of created particles.

Power spectrum

In order to be able to compare the perturbations with observations, we need to evaluate the power spectrum. For that, first we compute the two point correlation function for the canonical variables:

$$\langle 0| \hat{Q}_l \left(\eta, \mathbf{x}\right) , \hat{Q}_l \left(\eta^{'}, \mathbf{y}\right) |0\rangle = \int \frac{d^3k}{\left(2\pi\right)^3} \underbrace{Q_{\mathbf{k},l} \left(\eta\right) Q^{*}_{\mathbf{k},l} \left(\eta^{'}\right)}_{G_{\mathbf{k},l}\left(\eta,\eta^{'}\right)} e^{-i\mathbf{k}(\mathbf{x}-\mathbf{y})} \, , \tag{2.75}$$

where $G_{\mathbf{k},l} \left(\eta, \eta^{'}\right)$ is the Green's function in momentum space. The power spectrum is defined from this equal times Green's function

$$\mathcal{P}_{Q_l} \left(k\right) = \frac{1}{2\pi^2} k^3 \lim_{\eta \to \eta_{hc}} G_{\mathbf{k}} \left(\eta, \eta\right) = \frac{1}{2\pi^2} k^3 \left|Q_{\mathbf{k},l} \left(\eta\right)\right|^2 |_{\eta=\eta_{hc}} \, . \tag{2.76}$$

For the scalar component this is written as:

$$P_{\mathcal{R}} = \frac{k^3}{2\pi^2} \left| \frac{v_{\mathbf{k}} \left(\eta\right)}{z} \right|^2 \, . \tag{2.77}$$

This quantity as seen by CMB observations should be approximately scale invariant. So,

for the chosen mechanism for the evolution of the early universe, the resultant dimensionless power spectrum for the generated cosmological perturbations must be close to scale invariant, which is commonly parametrized as:

$$\mathcal{P}_s \propto k^{n_s - 1} \,, \tag{2.78}$$

where n_s is the spectral index, with $n_s \sim 1$. The value of n_s is determined by observations, with its current value given by $n_s = 0.965 \pm 0.006$ [41].

Part I

Early Universe Cosmology

Chapter 3

The AdS/CFT Correspondence

The idea of holography, where the physics of a gravity theory in the bulk is encoded in non-gravitational theory on the boundary, originates from black-hole physics [51, 52]. In 1997, Maldacena [9], motivated by the physics of D-branes, found a concrete example of the holographic principle, the AdS/CFT correspondence. In its original form this is a correspondence between a type II-B string theory on a $AdS_5 \times S^5$ space-time to a $\mathcal{N} = 4$ super Yang-Mills (SYM) theory, which is conformally invariant, living in the boundary of this space-time. Here AdS_5 is the bulk space-time and refers to an Anti-de-Sitter space-time in five dimensions, and S^5 refers do the sphere in five dimensions.

The correspondence relates the bulk quantities R, the radius of the AdS space-time, and l_s, the string length, with the two dimensionless quantities in the SYM theory, the coupling g_{YM} and the rank of the gauge group N:

$$g_s = g_{YM}^2 \,, \qquad \left(\frac{R}{l_s}\right)^4 = 4\pi g_{YM}^2 N \,. \tag{3.1}$$

The regime where we understand string theory, the supergravity (SUGRA) limit, when $R > l_s$ is given when the 'tHooft coupling is large:

$$g_{YM}^2 N \gg 1 \,, \qquad \text{large}\, N \,, \tag{3.2}$$

and the gravity theory is weakly coupled (and stringy effects are not important). In this regime, the dual gauge theory is strongly coupled, which makes it very hard to describe.

An important aspect of the theory is that there is a match between the global unbroken

symmetries from both sides, namely the superconformal group $SU(2,2|4)$. This can be seen since the bosonic subgroup of the $\mathcal{N}=4$ SYM, $SU(2,2) \times SU(4)_R \sim SO(2,4) \times SO(6)_R$ is the isometry group of the $AdS_5 \times S^5$ space-time .

This conjecture has proved to be one if the most important recent developments in string theory that has applications in different domains of physics. Recently, there have been many uses in condensed matter physics, gravitational theories, quantum chromo-dynamics, nuclear theory, along with many other examples (for some examples see [53]). Although this construction has the status of a conjecture, since no formal proof is available, there is strong supporting evidence with the match of the symmetries on both sides of the theory, and the match of the spectra of supersymmetric modes [54]. Although still in a low level of accuracy, AdS/CFT also makes predictions that are in agreement with experiments, like for example the viscosity of the quark-gluon plasma formed in the aftermath of collisions between heavy atoms [55].

The low-energy limit presented above is called the weak version of the correspondence. In the strongest version, the correspondence is valid for any value of N and all regimes of coupling $g_s = g_{YM}^2$, although it is highly non-trivial to implement since in the bulk side we now have a full quantum type IIB string theory on $AdS_5 \times S^5$. This shows us that there can be regimes of the correspondence where the 'tHooft coupling can become small, and in this limit the finite gauge theory can be well understood, having a weakly coupled conformal theory on the boundary, the reverse case of the one presented above. However, in this limit, the bulk SUGRA breaks down since if the bulk curvature is of the order of the string scales, $R \sim l_s$, then stringy effects become important. In this sense one can use the gauge theory as a non-perturbative definition of the string theory with AdS boundary conditions. This suggests an interesting avenue to address the resolution of singularities, a subject that we explore in the following sections in the context of explaining how perturbations can evolve through a cosmological singularity. In our case, we are allowing the 'tHooft to change, but always keeping N large, to avoid the influence of non-planar diagrams in the weakly coupled CFT that are not suppressed if N is small and might influence the theory.

3.1 AdS space-time

The AdS_5 solution is embedded in a solution of a 10-dimensional type IIB supergravity theory and it is the geometry where the correspondence has its better defined example. In

this section we briefly describe the geometry of AdS space-time with Minkowski signature.

AdS_{d+1} space-time is the maximally symmetric solution o Einstein's field equation with a negative cosmological constant, $\Lambda = -d(d-1)/R^2$, where R is the AdS radius. It can be considered to be the Lorentzian hyperbolic space given by the equation:

$$-Y_{-1}^2 - Y_0^2 + Y_1^2 + ... + Y_d^2 = -R^2 \,. \tag{3.3}$$

The topology is that of a cylinder $S^1 \times \mathbb{R}$ times a sphere $S^2 d-1$, with boundary $S^1 \times S^{d-1}$.

We can describe AdS_d+1 in different coordinate systems. In global coordinates, AdS_d+1 has the metric:

$$ds^2 = R^2 \left[-\sec^2 \rho \, dt^2 + \sec^2 \rho \, d\rho^2 + \tan^2 \, d\Omega_{d-1}^2 \right] \,, \tag{3.4}$$

where $0 \leq \rho \leq \pi/2$ and $-\infty \leq t \leq \infty$. In this system the topology is globally a line times a d-dimensional disk. The boundary is the cylinder $S^{d-1} \times \mathbb{R}$ located at $\rho = \pi/2$.

We can also describe AdS_{d+1} in Poincaré coordinates, which cover only half the AdS_{d+1} space-time. In this coordinate system the metric can be written as:

$$ds^2 = \frac{R}{z} \left(dz^2 + -dt^2 + dx^2 \right) \,, \tag{3.5}$$

where $0 \leq z \leq \infty$. The boundary is at $z = 0$ and there is a horizon at $z = \infty$.

3.2 The Mapping

The original form of the conjecture did not provided details of the mapping between the bulk and boundary quantities. Witten [56], and Gubser, Klebanov and Polyakov [57] developed, for the Euclidean case (see [58] for the case with Lorentzian signature), a way to relate the states of the theories of the correspondence. Here, we show how to map a scalar field in AdS_5 to CFT operators [54, 59]. This description is important since, as said above, the duality is expected to hold dynamically, describing how a quantum gravity in AdS can be mapped into a CFT on its boundary. This is especially important in the case of the singularity resolution in Chapters 4 and 5, where the parameters describing both theories vary describing the correspondence in its different regimes.

The correspondence is described schematically as a relation between the generating functional of a $(d+1)$-dimensional gravity theory in the bulk and the partition function of a

d-dimensional CFT on the boundary $\mathcal{B}$ of the bulk space-time:

$$Z_{bulk}[\varphi_b] = \int_{\varphi\to\varphi_b} \mathcal{D}\varphi e^{-i\,S_{grav}[\varphi]} = \langle e^{\int_{\mathcal{B}} d^d x\,\varphi_b \mathcal{O}(x)}\rangle = Z_{CFT}[\varphi_b]\,, \tag{3.6}$$

where $S_{bulk}(\varphi)$ is the effective action of the bulk gravity theory, and φ_b is the near-boundary bulk field that acts as a source term for the operator $\mathcal{O}$ of the CFT theory. This is the most general version of the correspondence. A more practical and known form of this duality is when we consider the supergravity approximation. Having this, it is possible to compute any n-point correlation function given that we can calculate the path integral of the action of the gravity theory [1].

The path integral in the mapping depends on the behaviour of bulk fields as they asymptote to their boundary values. For that, we need to understand the dynamics of the fields in AdS_{d+1}[2]. We will study the simple case of a free massive scalar field in Lorentzian signature AdS$d+1$, $\varphi(z, x^\mu)$ where z is the radial AdS coordinate and $\mu = 0, ..., d$. The action of this field in AdS$d+1$ is:

$$S = \frac{1}{8\pi G}\int dz d^d x\sqrt{-g}\left(\frac{1}{2}g^{\mu\nu}\partial_\mu\varphi\partial_\nu\varphi + m^2\varphi^2\right)\,, \tag{3.7}$$

which leads to the Klein-Gordon equation:

$$\left(\Box + m^2\right)\varphi(z, x^\mu) = 0\,, \tag{3.8}$$

where $\Box = (1/\sqrt{-g})\partial_\mu\sqrt{-g}g^{\mu\nu}\partial_\nu$. Plugging in the Lorentzian AdS metric and using the ansatz with plane wave basis $\varphi(z, x^\mu) = \varphi_k(z)e^{ik_\mu x^\mu}$, and making a field redefinition $\phi_k(z) = z^{\frac{-d}{2}}\varphi_k(z)$, we have the equation of motion:

$$z^2\partial_z\phi_k(z) + z\partial_z\phi_k(z) - \left(m^2R^2 + \frac{d^2}{4} + k^2z^2\right)\phi_k(z) = 0\,. \tag{3.9}$$

Near the boundary of AdS, when $z = \to 0$, the solution asymptotes to $\varphi_k \sim z^\Delta$, where $\Delta\,(\Delta - d) = m^2R^2$, which has two roots leading to the asymptotic behaviour close to the

[1] The n-point correlation function is given by $\langle\mathcal{O}(x_0...\mathcal{O}(x_n)\rangle = \frac{\delta}{\delta j(x_0)}...\frac{\delta}{\delta j(x_n)}W|_{j(x)=0}$, where $W = \ln Z$ is the generating functional.

[2] In Euclidean signature AdS, there is a unique extension of the field to the boundary because of the absence of normalizable modes.

boundary:

$$\varphi(z, x^\mu) \sim \alpha_-(x^\mu)\, z^{\Delta_-} + \alpha_+(x^\mu)\, z^{\Delta_+}\,, \tag{3.10}$$

with

$$\Delta_\pm = (d/2) \pm \sqrt{\frac{d^2}{4} + m^2 R^2}\,. \tag{3.11}$$

The solution with Δ_+ is called normalizable and Δ_- non-normalizable. Normalizability is defined as finiteness with respect to the Klein-Gordon inner product:

$$(u_1, u_2) = i \int_\Sigma d^d x \sqrt{g} f^{tt} (u_1^* \partial_t u_2 - \partial_t u_1^* u_2)\,, \tag{3.12}$$

where u_1 and u_2 are solutions of the Klein-Gordon equation and Σ is a spacelike slice of AdS_{d+1}. Stability requires that the mass obeys the Breitenlohner-Freedman (BF) bound [60]:

$$m^2 \geq m_{BF} = -\frac{d^2}{4}\,, \tag{3.13}$$

We can see that tachyonic masses are allowed in AdS. This means that the asymptotic solution $\varphi \sim z^\Delta$ is normalizable when the field obeys the unitary bound $\Delta \geq (d-2)/2$.

The interpretation of these modes is the following. In order to have a well defined quantum field theory, one needs a complete set of normalizable modes, since these are used to build the Hilbert space in the bulk. So, these modes in the AdS/CFT correspondence are associated to CFT operators: $\varphi_{norm}(z, x) \leftrightarrow \mathcal{O}(x)$. Non-normalizable modes do not fluctuate, so they are not part of the Hilbert space. They are understood, in the AdS/CFT conjecture, to define the boundary values of the fields, which in turn are classical sources that modify the boundary theory:

$$\varphi_b(x) = \lim_{z \to 0} z^{\Delta - d} \varphi(z, x) \Rightarrow \int d^d x \varphi_b(x) \mathcal{O}(x)\,. \tag{3.14}$$

The expectation value of this modification is what defines the generating functional of the CFT.

These relations define the mapping between the gravity and boundary theory. The ambiguity in the choice of these modes amounts to a choice of boundary conditions that must be made in the Lorentzian signature correspondence. It is possible, then, to evaluate the

path integral of (3.6):

$$\langle e^{\int_{\mathcal{B}} d^d x\, \varphi_b \mathcal{O}(x)} \rangle = Z_{bulk}(\varphi_b) \to e^{-S_{cl}} \,. \tag{3.15}$$

The last relation is evaluated in the supergravity approximation, where we extremize with respect to the field given boundary condition, obtaining the classical action. Now, any n-point correlator can be calculated by a functional derivative of the supergravity action with respect to the boundary field.

We only described in detail scalar fields that are dual to operators in the CFT. However, the correspondence also applies to tensor fields. The most important duality that worth mentioning is the correspondence between the metric in the bulk (graviton) and the expectation value of the energy momentum tensor in the CFT theory.

Chapter 4

Fluctuations in a Cosmology with a Space-Like Singularity and their Gauge Theory Dual Description

4.1 Introduction

The AdS/CFT correspondence [9] is a most promising proposal for a non-perturbative definition of string theory. Thus, this correspondence should also have important consequences for early universe cosmology. In fact, over the years there have been several proposals which address the meaning of cosmological singularities in the dual field theory [10, 14, 61–63]. The general idea is the following: consider an asymptotically AdS space-time which is contracting towards a curvature singularity. According to the AdS/CFT dictionary, this may correspond to a dual conformal field theory which lives on the boundary which is in a nontrivial unstable state [61–63] or which has a time dependent coupling [10, 14] which becomes small when the bulk singularity is reached. While the bulk theory cannot be used to evolve further in time, it may be possible to track the time evolution in the dual field theory in a controlled fashion. It is then not unreasonable to assume that the dual field theory admits a continuation in time beyond the time $t_B = 0$ when the bulk singularity occurs.

There are several motivations for this investigation. One of the motivations comes from cosmology. Although the inflationary scenario [1–5] is the current paradigm of early universe cosmology and has been quite successful phenomenologically, it faces conceptual challenges.

In particular, a robust embedding of large field inflation into string theory has proven to be difficult (see e.g. [64–68]) [1] At the same time, it has been realized that there are alternative cosmological scenarios which are at the moment also in agreement with cosmological data. One of these is the "matter bounce" scenario (see [6] for a recent review), a bouncing scenario which begins with a matter-dominated phase of contraction during which the scales which we observe today with cosmological experiments exit the Hubble radius. It was shown in [71, 72] the if fluctuations begin in their Bunch-Davies vacuum at past infinity, that the growth of the fluctuations on super-Hubble scales converts the vacuum spectrum into a scale-invariant one for scales exiting the Hubble radius during the matter phase of contraction. Adding a small cosmological constant (of magnitude similar to the one observed today) leads to a small red tilt in the spectrum [73]. The observed spectrum of curvature fluctuations is indeed scale-invariant with a small red tilt (see [41] for the most recent data).

In the context of effective field theory and Einstein gravity, it is difficult to obtain a non-singular bouncing cosmology. One either needs to postulate that matter violates the "Null Energy Condition" (NEC) during the bounce, or one needs to go beyond Einstein gravity. Examples of the former are adding ghost condensate matter [74] or Galileon matter [75, 76], an example of the latter is Horava-Lifshitz gravity in the presence of non-vanishing spatial curvature [77]. However, it is doubtful whether any of these constructions actually can emerge from an ultraviolet complete theory such as string theory. Hence, it would be very interesting to investigate if the AdS/CFT correspondence leads to a consistent bouncing cosmology [2].

Regardless of the above motivation, it is clearly interesting to investigate what happens to classical spacelike singularities in a complete theory of gravity. In particular, does the holographic correspondence predict a time evolution beyond this "singularity" ? Despite a lot

[1] In "large field" inflation models, the field values are larger than the Planck scale during inflation. In large field inflation models, the inflationary slow-roll trajectory is a local attractor in initial condition space, a property not shared by small field inflation models (see [69] for a recent review). The "Weak Gravity Conjecture" [70] constrains a number of large field inflation models, but the applicability of this conjecture is still somewhat controversial.

[2] There are other approaches to string theory which indicate the possibility of obtaining non-singular bouncing cosmologies. One example is "string gas cosmology" [78] in which the universe begins in an emergent high temperature stringy Hagedorn phase, and in which the thermal string fluctuations in the Hagedorn phase lead to a scale-invariant spectrum of fluctuations with a small red tilt [79, 80]. Another example is the "S-brane bounce" of [81–83], in which an S-brane arising at an enhanced symmetry point in the early universe leads to the violation of the NEC which makes a non-singular bouncing cosmology possible.

of effort, it is not clear whether any of the AdS/CFT models which contain *true singularities* in the bulk admit a smooth time evolution in the dual theory. In the original model proposed in [62,63] which was based on earlier work of [61], there were some technical problems which indicated that the time evolution past the singularity was not under control [84], mainly due to the back-reaction of the fluctuations on the background space-time. There have been attempts to overcome these obstacles [85–87], but the final verdict is still out.

In the works of [10–12, 14, 15] a bulk dilaton field ϕ had a time dependent (or a null coordinate dependent) boundary condition so that e^{ϕ} becomes small at some time (or null time), while Einstein frame curvatures become large in the bulk, signifying a singularity. When the singularity is null, the dual theory appears to predict a smooth time evolution, and because of the absence of particle production one expects that the spacetime is smooth in the future. However for backgrounds with space-like singularities, as in [12] there is no clear conclusion. Even though the background supergravity solution is time symmetric, the issue relates to the effect of fluctuations. In the boundary field theory, the question becomes that of particle production. In [12] it was argued that in the case when the boundary theory coupling hits a zero, the time evolution of each individual momentum mode is in fact singular. However it was not clear what happens when one considers the full field theory. In a regulated version of the theory where the boundary coupling becomes small but does not hit a zero, time evolution is well defined. However, the energy due to particle production at times after the crunch would be large, and the spacetime will not bounce back to pure AdS even at very late times. On general grounds, one might expect that a black brane is formed [12] [3].

In this chapter, we turn to a different aspect of the kind of backgrounds with spacelike singularities studied in [10–12] as a result of a time dependent boundary condition for the bulk dilaton. The goal of our study is to include cosmological perturbations in this picture. This is important for at least two reasons. Firstly, it is important to study whether the background is stable against the addition of fluctuations. Secondly, most of the data which we would like to explain in cosmology concerns fluctuations (inhomogeneities in the distribution of galaxies and anisotropies in the temperature of the cosmic microwave background).

[3] There are AdS cosmologies in global AdS where the coupling enters a weak coupling region *slowly* where [13] argue that the time evolution is smooth. In this model, the Einstein frame curavatures are always small, but string frame curvatures become large. Even though the dual theory predicts a smooth evolution, the space-time beyond the crunch cannot be determined reliably, though the energetics imply that big black holes are not formed.

We will not explore further the important question whether there are apparently singular AdS cosmologies which lead to a bounce to a relatively empty space. Rather, we will study models of the same type as [10–12] which have Kasner singularitites. However we will keep e^{ϕ} finite (but small) at all times, rather than going to zero, by putting in a cutoff in time, ξ. More specifically, instead of the exact Kasner behavior near the singularity

$$e^{\phi}(t) = |t|^{\alpha}\,, \tag{4.1}$$

we will use

$$e^{\phi}(t) = |t|^{\alpha}\theta(|t|-\xi) + \frac{\cosh^2(M\xi)}{\cosh^2(Mt)}\xi^{\alpha}\theta(\xi-|t|)\,. \tag{4.2}$$

We do not know of exact solutions with such a cutoff dilaton : we *assume* that these can be constructed. In the presence of such a finite cutoff, the boundary gauge theory is well defined : our aim to study some aspects of this. In some sense, the spirit of our investigation is similar to that of [88–90] and [91, 92] (see also [93–96]) where signatures of a past Kasner singularities in the dual field theory were studied.

We want to determine how the *spectrum* of fluctuations evolves as the system passes through the "singularity". This question is independent of nature of the late time spacetime so long as there is a region of normal spacetime near the horizon, which is where the fluctuations are measured.

This question is particularly interesting if any of these models reliably predict a bounce since in this case connections with bouncing cosmologies studied by many cosmologists can be made. There are classes of scenarios where, starting from vacuum perturbations at early times in the contracting phase, a scale-invariant spectrum of fluctuations is generated before the bounce. This occurs both in matter bounce scenarios [71, 72] for scales which exit the Hubble radius in the matter-dominated phase of contraction, and also in Ekpyrotic models (in the presence of entropy fluctuations) [97–102]. To obtain a connection with observations, the spectrum after the bounce needs to be determined. It has been shown [103] that the form of the spectrum after the bounce can depend on details of the bounce, although in many toy models one finds that on large scales the spectrum is preserved (see e.g. the analysis of [104–108]). A result concerning the transfer of fluctuations in an ultraviolet complete theory is thus highly desired. However, this question is also of interest for the particular model which is analyzed in this chapter, which in all likelihood produces a black brane.

As is clear from previous work, the gauge theory is in a highly excited state as one approaches the region of weak 't Hooft coupling, possibly in a coherent state. In such a situation, we expect that we can learn a lot from the *classical limit* of the Yang-Mills theory. We therefore study the time evolution of small fluctuations around the background across the region of weak coupling. Such small fluctuations are related, by the AdS/CFT correspondence to bulk fluctuations. The kind of fluctuations we are interested in are those which are given by correlation functions on a fixed radial slice on AdS, close enough to the boundary. As we discussed, the space time in the future might contain black holes (branes). However so long as the space-time near the boundary is smooth and normal, we can use the AdS/CFT dictionary to translate boundary fluctuations to bulk fluctuations.

In this chapter we take a preliminary step towards computing the transfer of cosmological fluctuations from before the beginning to after the end of the high curvature bulk regime. We begin with a given spectrum of cosmological perturbations in the contracting phase of the bulk, while the bulk is still weakly coupled. At the time when the bulk becomes strongly coupled (and, correspondingly, the boundary conformal field theory becomes weakly coupled) we map the fluctuations onto fluctuations of the gauge fields in the boundary theory. We then evolve the fluctuations to the future in the weakly coupled region on the boundary. In our classical approximation, it is now straightforward to find the fate of these fluctuations at late times. The third step of our analysis is the reconstruction of bulk fluctuations from the boundary data to the future of the bulk singularity. Note that we are interested in fluctuations on scales of current cosmological interest. These scales are infrared modes from the point of view of the physics which we are considering. Specifically, the wavelength of the modes we are interested in is larger than the Hubble radius at the times between $-t_b$ and t_b when we evolve the fluctuations on the boundary.

Our main result is that the momentum dependence of classical fluctuations for momenta much smaller than the cutoff ($k\xi \ll 1$) does not change after crossing the weak 't Hooft coupling region, while their amplitudes change by $O(1)$ factors. This means that the spectrum of fluctuations of the dilaton field near the boundary also have this behavior. In particular, if we start out with a nearly scale invariant spectrum with a red tilt (as is the case for models of matter bounce), the spectrum right after the "bounce" will remain the same. While this result is shown for the bulk dilaton, we conjecture that the result we obtain will directly apply to the evolution of the gravitational wave spectrum, the reason being that a test scalar field in a cosmological background obeys the same equation of motion as that of

the amplitude of a particular polarization state of gravitational waves.

This chapter is organized as follows. In Section II, we review the proposed generalization of the AdS/CFT correspondence to a time-dependent background [10, 14]. Section III consider a bulk scalar field and its dual in the boundary gauge theory. As it turns out, the time-dependence of the background scalar field induces a time-dependence of the mass of the gauge field. In Section IV we study the evolution of the gauge field given the time-dependence of the coupling constants induced by the non-trivial scalar field in the bulk. Since we are interested in eventually computing linear fluctuations in the bulk, we will focus on linear perturbations of the boundary field. This leads to a dramatic simplification of the analysis. We can work in Fourier space. Each Fourier mode obeys an ordinary differential equation which is analogous to the equation which cosmological fluctuations in a time-dependent background obey in the context of standard General Relativistic perturbation theory. Hence, we can use the accumulated knowledge about the evolution of cosmological fluctuations in time-dependent backgrounds to solve for the evolution of the linear boundary gauge field perturbations through the time point $t = 0$ where the bulk theory becomes singular. Since the boundary theory is weakly coupled near the bulk singularity, the computations done in the context of the boundary theory remain under control. At large positive times (when the bulk theory becomes weakly coupled) we then reconstruct the bulk scalar field using boundary-to-bulk propagators. This is discussed in Section V where we also extract the power spectrum of the scalar field fluctuations at late times and relate it to the initial spectrum before the bulk singularity. We discuss and summarize our results in the final section.

4.2 Time-Dependent AdS Background and CFT Dual

The original Maldacena conjecture is a duality between a Type IIB string theory on $AdS_5 \times S_5$ and a conformal field theory, a supersymmetric Yang-Mills (SYM) $\mathcal{N} = 4$ large N $SU(N)$ gauge theory, living on the boundary of AdS_5 [9]. The two dimensionless quantities on the bulk side are R/l_s, where R stands for the AdS radius and l_s is the string length and the string coupling constant g_s. These are related to the two dimensionless quantities in the SYM theory, the Yang-Mills coupling g_{YM} and the rank of the gauge group N by

$$\frac{R^4}{l_s^4} = 4\pi g_{YM}^2 N \,, \qquad g_s = g_{YM}^2 \,. \tag{4.3}$$

The string coupling g_s is of course given by the bulk dilaton field φ

$$g_s = \exp\langle\varphi\rangle \,. \tag{4.4}$$

There are two particularly noteworthy aspects of this correspondence. Firstly, it relates a gravitational theory (the bulk theory) to a non-gravitational field theory on the boundary. From this point of view, the challenge of quantizing gravity suddenly takes on a completely new view. Secondly, the duality is a strong coupling - weak coupling duality. The bulk dilaton provides both a measure of the couplings in the bulk and in the boundary. However, it is precisely when the bulk theory becomes strongly coupled that the boundary theory becomes weakly coupled. In particular we can consider $N \gg 1$ so that bulk quantum effects are small, but $g_{YM}^2 N \ll 1$ so that the boundary theory is weakly coupled - this would correspond to bulk curvature scales of the order of string scale, signifiying that stringy effects become important in the bulk. This can be achieved, e.g. by having $g_s = g_{YM}^2 \ll 1/N$ for some fixed large N.

This suggests an interesting avenue to address the question of resolution of cosmological singularities. One possible way to do this is to consider a time dependent boundary condition of the bulk dilaton [10, 14]. By the standard AdS/CFT correspondence the dual field theory living on the boundary now has a time dependent coupling. A cosmological singularity corresponds to a divergence of the gravitational coupling and thus to a region where conventional approaches to quantizing gravity will fail. However, by the AdS/CFT correspondence the bulk theory is dual to a non-gravitational theory on the boundary, and the bulk singularity corresponds to a point in time when the boundary theory becomes weakly coupled. Thus, the usual principles of field theory quantization should be applicable, and one has to deal with a weakly coupled field theory which, however, is time dependent.

The first step is to consider the low energy limit of the bulk Type II string theory, namely Type II supergravity, and to focus on the bosonic sector of this theory. The second step is to allow for a time dependence in the bulk fields. The bulk fields involve the ten-dimensional metric, the dilaton φ and a five form F_5. The ansatz for such solutions is given by a non-trivial metric of the form

$$ds^2 = \frac{R^2}{z^2}\left[dz^2 + \tilde{g}_{\mu\nu}(x^\mu)dx^\mu dx^\nu\right] + R^2 d\Omega_5^2 \,, \tag{4.5}$$

where $d\Omega_5^2$ is the standard metric on a unit 5-sphere. The surface $z = 0$ is the boundary of the space-time. Note that the metric on a constant z slice is a function of the coordinates x^μ only. This also holds for the dilaton field $\varphi(x^\mu)$. Finally, the five form is given by

$$F_{(5)} = \omega_5 + \star_{10}\omega_5 \,. \tag{4.6}$$

As shown in [10], these bulk fields satisfy the full ten dimensional equations of motion provided

$$\tilde{R}_{\mu\nu} \;=\; \frac{1}{2}\partial_\mu\varphi\partial_\nu\varphi \,, \tag{4.7}$$

where $\tilde{R}_{\mu\nu}$ is the Ricci tensor of the metric $\tilde{g}_{\mu\nu}$, and where the dilaton φ obeys the Klein-Gordon equation

$$\partial_A\big(\sqrt{-g}g^{AB}\partial_B\varphi\big) \;=\; 0 \,. \tag{4.8}$$

In the above, g is the determinant of the full metric g_{AB}, and the indices A, B run over all five space-time dimensions.

$AdS_5 \times S_5$ is of course a special case of a space-time described by the metric (4.5). In this case, the metric $\tilde{g}_{\mu\nu} = \eta_{\mu\nu}$, the Minkowski metric, and the dilaton is constant. The radial coordinate z runs from $z = 0$ at the boundary to $z = \pm\infty$ at the Poincaré horizons.

Time-dependent deformations of this background were considered in [10–15]. Specifically, we shall consider a background of the form [12] obtained by introducing a time-dependent dilaton background and adjusting the metric of $\tilde{g}_{\mu\nu}$ such that the Einstein equation (4.7) and the Klein-Gordon equation (4.8) remain satisfied. We will mainly deal with a solution where the the boundary metric looks like that of a Friedmann universe

$$\tilde{g}_{\mu\nu}dx^\mu dx^\nu \;=\; -dT^2 + a^2(T)\delta_{ij}dx^i dx^j \;, \tag{4.9}$$

with T being the cosmic time and $a(T)$ the scale factor. The dilaton and scale factor were taken to be

$$a \sim |T|^{1/3} \;, \quad \varphi = \frac{2}{\sqrt{3}}\ln\frac{|T|}{R} \;. \tag{4.10}$$

This corresponds to an early contracting phase leading to a "Big Crunch" singularity at $T = 0$ followed by an expanding cosmology. In conformal time t, the four dimensional part

of the metric is

$$\tilde{g}_{\mu\nu}dx^\mu dx^\nu \;=\; 2|t|\big[-dt^2+\delta_{ij}dx^i dx^j\big], \tag{4.11}$$

while the dilaton is given by

$$\varphi=\sqrt{3}\ln\frac{|t|}{R}\;. \tag{4.12}$$

If the singularity can be resolved by mapping the dynamics to the boundary, we will have a stringy realization of a bouncing scenario, though one would not expect a perfect bounce. As mentioned in the introduction we do not know yet if this indeed happens.

The dilaton profile (4.12) leads to a diverging string coupling e^φ at early and late times : this would seem to require incorporation of bulk quantum corrections. However it turns out that one can obtain solutions which have bounded values of the coupling e^φ at all times, and whose behavior near the "singularity" is identical to the above. Such a solution is given by the metric [11]

$$ds^2=\frac{R^2}{z^2}\big[dz^2+|\sinh(2t)|\{-dt^2+\frac{dr^2}{1+r^2}+r^2d\Omega_2^2\}\big]\,, \tag{4.13}$$

and a dilaton

$$e^{\varphi(t)}=g_s|\tanh(t/R)|^{\sqrt{3}}\,. \tag{4.14}$$

Near $t=0$ the dilaton profile goes over to that in (4.12). The metric (4.13), whose four dimensional part is a FRW metric with constant negative curvature does not, however, become (4.11) as $t\to 0$. The difference between the two, however, become increasingly unimportant as $t\to 0$ where the bulk stress tensor is dominated by the time derivative of the dilaton rather than the spatial curvature.

A sketch of the space-time we are considering is given in Fig. 1. The vertical axis at $z=0$ is time, the horizontal axis at $t=0$ represents the AdS radial coordinate. The Poincaré horizons are at 45 degrees. While we will consider the solution (4.12) and (4.11) it is useful to think of this as embbeded in the solution (4.14) and (4.13) with a bounded dilaton. Then at early times the Yang Mills coupling is $g_{YM}^2=g_s$ and we will always consider $g_s\ll 1, N\gg 1$ with $(g_sN)\gg 1$. Thus the early time evolution is governed by the bulk supergravity equations. The time t_b is defined as the time when the 't Hooft coupling

of the boundary theory becomes $O(1)$, i.e.

$$t_b/R \sim (g_s N)^{-1/\sqrt{3}}\,. \tag{4.15}$$

Thus, in the region $t > -t_b$ and $t < t_b$ the bulk gravity theory is weakly coupled. For $-t_b < t < t_b$ the bulk curvatures grow large and stringy effects becomes important, while the boundary field theory is weakly coupled, although in the presence of a time dependent coupling.

Note that the solutions considered above have a non-trivial boundary value of the dilaton and a boundary metric which is conformal to flat space. However there are no subleading normalizable pieces of these bulk fields. From the dual field theory point of view, it thus appears that we have non-trivial time dependent sources, but a trivial response. This indicates that such cosmologies correspond to some non-trivial initial states. However the nature of this state in terms of the gauge theory variables is not known.

There is another feature of these solutions which deserves mention. The singularity at $t = 0$ extends from the boundary to the bifurcation point of the Poincare horizon at $z = \infty$. This means that there is in fact a singularity at any finite Poincare time which is infinitely far from the boundary. Presumably this feature has something to do with the nature of the initial state. However, as pointed out in [88–90], this bifurcation point singularity can be resolved by lifting the solution to one higher dimension and embedding the solution in a higher dimensional soliton solution.

In the following sections we are interested in evolving spectator massless bulk scalar field (which will be in fact taken to be the dilaton itself) perturbations from the past weakly coupled bulk region to the future weakly coupled bulk region by mapping the state onto the boundary at time $t = -t_b$, evolving on the boundary to positive times, and using boundary-to-bulk reconstruction techniques to recover fluctuations in the bulk.

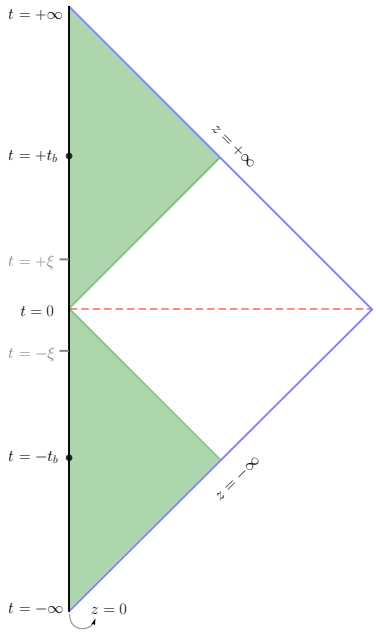

Fig. 4.1 Conformal diagram of the background space-time. The vertical axis at $z = 0$ is time t, the horizontal direction at $t = 0$ represents the coordinate z. The lines at 45 degrees are the Poincaré horizons at $z = \pm\infty$. If there were no deformation of AdS, the region drawn would correspond to the Poincare patch of AdS. We are considering a deformed space-time in which the bulk gravity is strongly coupled between $t = -t_b$ and $t = t_b$, and singular at $t = 0$. At the same time the boundary gauge theory becomes weakly coupled for t between $-t_b$ and t_b. Hence, after the time $-t_b$ the evolution on the boundary becomes tractable in perturbation theory. On the future side of the bulk singularity, the boundary theory remains tractable perturbatively until the time t_b when the the bulk theory becomes weakly coupled again at the cost of the boundary theory becoming strongly coupled. At that time we can reconstruct the bulk information (at least in the vicinity of the boundary) from boundary data (see e.g. [109–115]). As we will see, to study the evolution of the boundary fluctuations we need to impose a cutoff at $t = \pm\xi$.

4.3 The Bulk Theory of a Test Scalar in a Contracting Universe

To begin with, we consider a test scalar field of mass m living in the bulk space-time (in the following section we will take this test scalar field to be the dilaton itself). Its action takes

the form

$$S_\varphi \;=\; -\int d^5x\sqrt{-g}(g^{MN}\partial_M\varphi\partial_N\varphi + m^2\varphi^2)\;. \tag{4.16}$$

where g^{MN} is the metric of the five-dimensional deformed AdS space-time

$$ds_5^2 = \frac{R^2}{z^2}\left[dz^2 + \tilde{g}_{\mu\nu}(x^\mu)dx^\mu dx^\nu\right]\;, \tag{4.17}$$

with the four dimensional part $\tilde{g}_{\mu\nu}$ given by (4.9). Varying the action with respect to the scalar field yields the following equation of motion

$$\ddot{\varphi} + 3H\dot{\varphi} - a^{-2}\varphi_{,ii} + m^2\frac{R^2}{z^2}\varphi - \varphi_{,zz} + \frac{3}{z}\varphi_{,z} \;=\; 0\;, \tag{4.18}$$

where $H = \dot{a}/a$ is the Hubble parameter, and a dot denotes the derivative with respect to cosmic time T.

Since we are interested in the spectrum of fluctuations in the three spatially flat coordinates x^i, we first of all extract the x^i dependence by expanding in Fourier modes. The resulting differential equation is a partial differential equation in T and z, and we make a separation of variables ansatz to separate the T and z dependence. More specifically, we write

$$\varphi(T,z,x^i) \;=\; \mathcal{T}(T)Z(z)X(x^i)\,, \tag{4.19}$$

where the $X(x^i)$ are the spatial Fourier modes, i.e. solutions of

$$\nabla^2 X + k^2 X \;=\; 0\,, \tag{4.20}$$

with solutions which are positive or negative frequency oscillations in the three vector $\mathbf{x}$, where the rescaled temporal field

$$\tilde{\mathcal{T}}(t) \;\equiv\; a(t)\mathcal{T}(t)\,, \tag{4.21}$$

(with t being conformal time defined via $dT = adt$ obeys the equation

$$\tilde{\mathcal{T}}'' + \big(\omega^2a^2 + k^2 - \frac{a''}{a}\big)\tilde{\mathcal{T}} \;=\; 0\,, \tag{4.22}$$

(a prime denoting the derivative with respect to t) and the radial function $Z(z)$ obeys the equation

$$Z_{,zz} - \frac{3}{z} Z_{,z} + \big(\omega^2 - \frac{m^2 R^2}{z^2}\big) Z \, = \, 0 \, . \tag{4.23}$$

The separation constant ω plays the role of a temporal frequency. The solutions of the radial equation are Bessel functions

$$Z(z) \, = C_J z^2 J_\nu(\omega z) + C_Y z^2 Y_\nu(\omega z) \, , \tag{4.24}$$

with

$$\nu \, = \, \sqrt{4 + m^2 R^2} \, . \tag{4.25}$$

The temporal equation (4.22) takes on the familiar form of the coefficient function of a comoving Fourier mode of a massive scalar field (mass given by ω^2) in an expanding background space-time which undergoes cosmological squeezing (the final term on the left hand side of the equation). In the case $\omega^2 \, = \, 0$ it is also the equation of motion which gravitational waves in an expanding space obey [46,47]. In particular, in the case of infrared modes for which k^2 is negligible, then close to the singularity the mass term is negligible and the squeezing term dominates. In this chapter we will, however, not be evolving the fluctuations in the bulk until the singularity, but only to the point in time when the bulk theory ceases to be weakly coupled. Then, we will map them onto the boundary and evolve them with the boundary equations near the bulk singularity.

Our main result does not depend on the initial fluctuation spectrum. As a concrete example, however, we could e.g. take the initial spectrum to be scale invariant for modes whose wavelength is larger than the Hubble radius. During the phase of contraction the Hubble radius is decreasing in comoving coordinates (see Fig. 2). This is motivated by the fact that in several models of "bounce" cosmology (e.g. matter bounce of [71, 72] or Ekpyrotic [97] scenarios) an initial vacuum spectrum (see e.g. [116]) on sub-Hubble scales gets converted to a scale-invariant one once the scales exit the Hubble radius and undergo squeezing.

We will thus take the initial power spectrum

$$P(k) \, \equiv \, k^3 |(\delta\varphi)(k)|^2 \, , \tag{4.26}$$

on super-Hubble scales to have index $n = 0$ (where we are using the convention for the index used in the cosmology community for gravitational waves, namely $P(k) \sim k^n$).

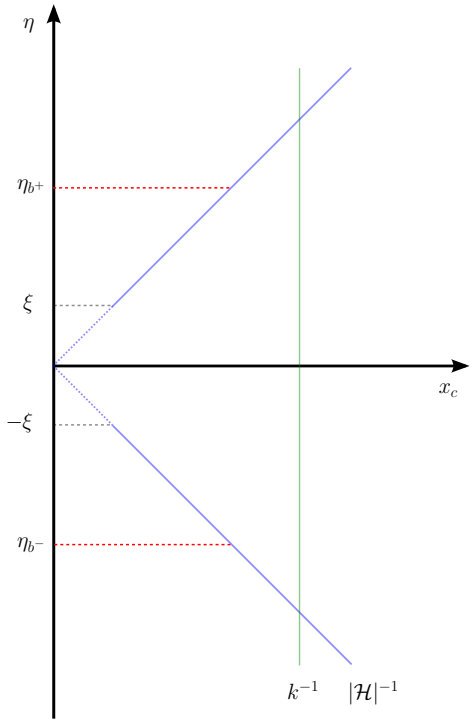

Fig. 4.2 Space-time sketch of the relevant times and length scales in our deformed AdS_5. The horizontal axis is comoving spatial coordinate (in direction perpendicular to the radial direction. The vertical direction is conformal time. τ_{B+} and τ_{B-} are the times when the coupling constant is 1, the times $\pm\xi$ occur when the bulk curvature reaches string scale. The vertical line represents the wavelength of a mode which we are interested in. Note that the length is larger than the Hubble radius at τ_{B+} and τ_{B-}. The blue lines at 45^o indicate the Hubble radius.

After discussing the bulk-to-boundary correspondence for the fluctuations we will determine the initial spectrum of perturbations of the boundary gauge fields which are induced by the inhomogeneities of the bulk field discussed above.

4.4 The Dual Boundary Theory

4.4.1 The Deformed Dual Boundary Theory

For a pure AdS bulk, the dual boundary theory is a $\mathcal{N} = 4$ SYM theory. According to the AdS/CFT correspondence, fields in the bulk are related to operators in the boundary theory. For example, the bulk metric $g_{\mu\nu}$ is dual to the boundary energy-momentum tensor $T_{\mu\nu}$. In this chapter we are interested in scalar field fluctuations in the bulk and their boundary evolution. Specifically, we will take this scalar field φ to be the dilaton φ. In this case, the bulk scalar field is dual to the trace of the square of the field strength tensor. For an exact AdS bulk, the boundary action is simply

$$S_{\rm YM} \,=\, -\frac{1}{4}\int d^4y \frac{1}{g^2_{\rm YM}} {\rm Tr}\left[F_{\mu\nu}F^{\mu\nu}\right] \,, \tag{4.27}$$

with

$$g^2_{\rm YM} \,=\, e^{\varphi} \,=\, g_s \,. \tag{4.28}$$

Here, we denote the boundary coordinates by y. We use a generalized AdS/CFT correspondence according to which the time-dependent dilaton in the bulk leads to a time-dependent gauge coupling of the boundary theory, i.e. (4.27) is generalized to be

$$S_{\rm YM} \,=\, -\frac{1}{4}\int d^4y e^{-\varphi(t)} {\rm Tr}\left[F_{\mu\nu}F^{\mu\nu}\right] \,. \tag{4.29}$$

The operator dual to the bulk dilaton is ${\rm Tr}F_{\mu\nu}F^{\mu\nu}$ at large N. This has been carefully derived in Appendix A of [12]. Note that we are always working at large N, but the 't Hooft coupling $g^2_{YM}N$ can become small.

The bulk solutions we are interested in have, in addition, a boundary metric which is non-trivial and time dependent. However in the slicing chosen in (4.5) and the time t chosen on the boundary at $z = 0$ as in (4.11), the metric on which the gauge theory lives is conformally flat. Since the boundary theory is the four dimensional SYM theory, the conformal factor decouples and the non-trivial effect is that of the time dependent dilaton [4].

What was said so far applies to an unperturbed theory. In the presence of perturbations the correspondence becomes more involved [117, 118]. Each supergravity perturbation has

[4] It is of course possible to choose other slicings, particularly those obtained by Penrose-Brown-Henneaux transformations in the bulk where the non-triviality of the metric plays a role. See e.g. [11].

two modes - one normalizable and the other not. The normalizable mode determines the expectation value of the boundary operator, the non-normalizable mode enters as the coupling of the operator in the boundary theory.

We are interested in evolving linearized bulk fluctuations. This means we will turn on normalizable bulk modes. Hence, we will be evolving the linear fluctuations in the gauge field A_μ on the boundary. The initial conditions for the gauge field fluctuations on the boundary are set by the dilaton perturbations via the linearized version of the correspondence

$$\varphi(y) \rightarrow \frac{1}{g^2_{\rm YM}} \langle {\rm Tr}[F^2(y)] \rangle \,, \tag{4.30}$$

where the normalizable dilaton fluctuation behaves in the standard fashion as

$$\varphi(z, y) \rightarrow z^4 \varphi(y) \,, \tag{4.31}$$

as one approaches the boundary $z = 0$.

The effects of linear dilaton fluctuations on the evolution of the gauge field fluctuations would be a second order effect in the amplitude of fluctuations. Hence, at linear level in perturbation theory there is no such coupling and the only effect of the dilaton on the gauge field fluctuations is via the dilaton-dependence of the gauge coupling constant at background level.

Given a spectrum of dilaton fluctuations at early times in the bulk, we will evolve them in the bulk until bulk perturbation theory breaks down at time $-t_b$. At that point, we compute the boundary values of the dilaton fluctuations and use them to determine the initial values of the gauge field fluctuations δA_{mu} at that time.

4.4.2 Evolution of the Boundary Fluctuations Before the Singularity

As we have mentioned, the dilaton field evolves as a function of cosmic time and initially takes a large value, and thus the Yang Mills coupling is also very large initially which implies that the boundary theory is strongly coupled in the far past. (It is useful to think in terms of the solutions (4.13) and (4.14) with bounded dilaton profiles). At these early times, the dynamics of the whole space-time can be studied making use of the bulk theory since the gravity sector is weakly coupled. As the universe contracts, the value of e^φ decreases and the corresponding 't Hooft coupling of the field theory becomes $O(1)$ at the time $-t_b$ given

by (4.15). This is the time where the gravity approximation begins to fail.

As the bulk space further contracts, the boundary theory becomes weakly coupled as $g^2_{\rm YM}N < 1$. When $t = 0$ and $\varphi \to -\infty$, the bulk singularity point is reached. While it may appear that the boundary gauge theory is now free, as shown in [12], each momentum mode of the gauge theory displays a singular behavior. We therefore work with the modified dilaton profile (4.2) with $\alpha = \sqrt{3}$ so that this is a genuine bulk solution for $|t| > \xi$.

We will make a gauge choice

$$A_0 = 0\,, \tag{4.32}$$

and also impose an additional constraint

$$\partial^i A_i = 0\,. \tag{4.33}$$

The Gauss Law constraint is then automatically solved [12].

The form of the action (4.29) suggests a field redefinition (for an analysis in terms of the original variables see Appendix A)

$$A_\mu \to \tilde{A}_\mu \equiv e^{-\varphi/2} A_\mu\,. \tag{4.34}$$

This has two effects. The first is that it introduces a "mass" term for the redefined field. With a dilaton which depends only on time, the effective mass square is given by

$$M^2_{\rm YM} \,=\, \frac{\ddot{\varphi}}{2} - \frac{\dot{\varphi}^2}{4}\,. \tag{4.35}$$

The second effect is to bring in a factor of $e^{\varphi/2}$ in front of the cubic interaction term and a factor of e^{φ} in front of the quartic interaction . This might suggest that as $t \to 0$ the nonlinear terms become small and can be ignored. However, as shown in [12] this is incorrect. If one substitutes a general solution of the linearized equations of motion (see below) into the action one finds that the fields $\tilde{A}_\mu$ blow up as $t \to 0$ in such a way that the original field A_μ becomes $O(1)$. Therefore, for arbitrary amplitudes the nonlinear terms cannot be ignored.

However we are interested in the time evolution of *small* fluctuations of the gauge field. The nonlinear terms are then suppressed because the amplitudes are small. In the following we will deal with the linear theory. Effects of nonlinearities will be explored in a future work.

Then the leading terms in the equation of motion for $\tilde{A}_i$ give

$$-\partial_\mu \partial^\mu \tilde{A}_i + M_{\rm YM}^2 \tilde{A}_i \, = \, 0 \, . \tag{4.36}$$

In the background (4.2) M_{YM}^2 becomes

$$M_{YM}^2(t) = \begin{cases} -\frac{\alpha(\alpha+2)}{4t^2} \, , & \text{if } |t| > \xi \\ -\frac{\alpha(\alpha+2)}{4\xi^2} \, , & \text{if } |t| < \xi \, . \end{cases} \tag{4.37}$$

Note that the coefficients in the mass term diverge as $t \to 0$ if $\xi = 0$. This is why the evolution of the fluctuations is non-trivial in spite of the fact that the boundary gauge theory becomes weakly coupled at this time. Note that in terms of the original variables A_μ there is no divergence. But a branch cut in the solutions remains. Working with the rescaled variables has the advantage that the equation of motion is similar to that of a simple quantum mechanics problem in a non-trivial potential, and we can use our knowledge about quantum mechanical scattering problems to find good ways to solve the equation.

In linear theory, each Fourier mode will evolve independently. In fact, we are interested in following modes which early in the contracting phase have a wavelength smaller than the Hubble radius and then exit the Hubble radius at some point in time (i.e. the Hubble radius decreases such that the wavelength becomes larger). Thus, we Fourier transform the gauge field

$$\tilde{A}_\nu(\xi^\mu) \, = \, \int_{-\infty}^{\infty} d^3\vec{k} \; c_A(\vec{k}) \tilde{A}_k(t) \epsilon_\nu e^{i\vec{k}\cdot\vec{\xi}} \, , \tag{4.38}$$

where ϵ_ν is the polarization unit vector. The Fourier mode $A_{\vec{k}}$ then obeys the following equation of motion:

$$\ddot{\tilde{A}}_k + (k^2 + M_{\rm YM}^2)\tilde{A}_k \, = \, 0 \, , \tag{4.39}$$

which is a harmonic oscillator equation with time-dependent mass. Upon quantization, the Fourier mode can be written as a combination of creation and annihilation operators, and the time-dependence of the mass leads to squeezing of the wave function in the same way that infrared modes of cosmological perturbations and gravitational waves are squeezed on super-Hubble scales in a dynamical cosmological background.

The general solution of a Fourier mode of the gauge field can be written in terms of Bessel functions:

$$\tilde{A}_k(t) \;=\; \begin{cases} (-t)^{\frac{1}{2}}\left[\mathcal{D}_J^-(k)J_{\nu_g}(-kt)+\mathcal{D}_Y^-(k)Y_{\nu_g}(-kt)\right]\,, & \text{if} \quad t\le -\xi, \\ \mathcal{A}\,\exp[\beta t]+\mathcal{B}\,\exp[-\beta t]\,, & \text{if} \quad -\xi\le t\le \xi, \\ t^{\frac{1}{2}}\left[\mathcal{D}_J^+(k)J_{\nu_g}(kt)+\mathcal{D}_Y^+(k)Y_{\nu_g}(kt)\right]\,, & \text{if} \quad t\ge \xi\,, \end{cases}$$

with the index

$$\nu_g \;=\; \frac{1+\alpha}{2} \qquad \alpha=\sqrt{3}\,, \tag{4.40}$$

and

$$\beta \equiv \sqrt{\frac{\alpha(\alpha+2)}{\xi^2}-k^2}\,. \tag{4.41}$$

For $t<\xi$ the solution of the above mode equation involves two coefficients $\mathcal{D}_J^-$ and $\mathcal{D}_Y^-$ which can be determined by matching the bulk solution and the boundary operator at the surface of $-t_b$. We are interested in modes which start out in the vacuum state early during the phase of contraction, i.e. in their Bunch-Davies [116] state.

On sub-Hubble scales (large values of kt) both modes are oscillating. For small values of kt the modes have very different asymptotics. If $\mathcal{D}_Y^-=0$ around the moment $-t_b$ then the asymptotic form of the solution is

$$\tilde{A}_k(t) \;\sim\; \mathcal{D}_J^-\frac{|t|^{\frac{1}{2}}}{\Gamma_{1+\nu_g}}\left(\frac{|kt|}{2}\right)^{\nu_g}\,, \tag{4.42}$$

i.e. it is in general a decaying mode as $t\to 0$. The second mode scales as

$$\tilde{A}_k(t) \;\sim\; -\mathcal{D}_Y^-\frac{\Gamma_{\nu_g}}{\pi}|t|^{\frac{1}{2}}\left(\frac{2}{|kt|}\right)^{\nu_g}\,, \tag{4.43}$$

which is a growing mode which in fact diverges as $t\to 0$. This is a reflection of the fact that the mass term diverges. The physical solution will be dominated by the growing mode unless $\mathcal{D}_Y$ vanishes. But it will not vanish in the general case. In particular, if we were to match the solutions to a Bunch-Davies vacuum, then we would expect the magnitude of both coefficients $D_{J,Y}^-$ in (4.4.2) to be of the same order.

4.4.3 Determination of the Spectrum of the Boundary Fluctuations at $-t_b$

A key step in our analysis is to extract the spectrum of the boundary gauge field from that of the bulk dilaton. The coefficients $\mathcal{D}_J$ and $\mathcal{D}_Y$ are determined via (4.30) by taking the limit of the dilaton fluctuations at the boundary. We make this identification at the time $-t_b$ when the coupling constant vanishes. At first sight, we are faced with a puzzle: the right-hand side of (4.30) is quadratic in the gauge field, the left-hand side is linear in the dilaton. It is thus non-trivial to infer the gauge field fluctuations from the bulk dilaton. The approach we will take is to look for a power law form of the gauge field Fourier modes $A_\mu(k)$ which yields the spectrum of the bulk dilaton fluctuations we are starting with.

Recall that we are interested in perturbations on cosmological scales which are in the far infrared and for which spatial gradient terms can be neglected. Thus, the dominant term for the infrared modes in $\mathrm{Tr}[F^2(\xi)]$ is the term $\dot{A}_i^2$. Inserting the Fourier expansion of $A_i(x)$ yields

$$\dot{A}_i^2 \;=\; \int d^3k_1 d^3k_2 \dot{A}_i(k_1)\dot{A}_i(k_2) e^{i(k_1+k_2)x} V \,, \tag{4.44}$$

where V is the normalization volume used to define the Fourier transform.

In writing (4.44) we have ignored the nonlinear terms which are contained in $Tr(F^2)$. This is because we are interested in the spectrum of small fluctuations so that the nonlinear terms are suppressed by powers of the amplitude.

We introduce new momenta

$$\begin{aligned} k_1 &= \frac{1}{2}(k+k') \,, \\ k_2 &= \frac{1}{2}(k-k') \,. \end{aligned} \tag{4.45}$$

We write down the Fourier expansion of the dilaton field φ, and insert into (4.30) and (4.31) to identify Fourier coefficients. This leads to

$$\varphi(k) \;=\; \frac{1}{4}\int d^3k' \dot{A}_i\left(\frac{k+k'}{2}\right)\dot{A}_i\left(\frac{k-k'}{2}\right) V^{1/2} \,, \tag{4.46}$$

where φ is defined in (4.31).

One way to find a consistent $A_i(k)$ to give rise to a power law bulk spectrum $\varphi(k) \sim k^{-\gamma}$ is as follows. We can divide this integral into a region R_1 with $k' < k$ and a region R_2 with

$k' > k$. In the integral over region R_1 we can set $k' = 0$ to find the approximate result

$$k^3 \dot{A}_\mu^2(k) \sim k^{-\gamma}, \tag{4.47}$$

and hence (making use of the fact that on super-Hubble scales $\dot{A} \sim HA$)

$$A_i(k) \sim k^{-\frac{\gamma+3}{2}}. \tag{4.48}$$

It is straightforward to check that this is a consistent solution for any $\gamma > 0$. Substituting (4.48) into (4.46) we get

$$\varphi(k) \sim \int d^3k'(k^2 - (k')^2)^{-(\gamma+3)} = k^{-\gamma} \int d^4q(1-q^2)^{-\frac{\gamma+3}{2}}. \tag{4.49}$$

The integral over q is convergent when $\gamma > 0$. In particular, for a scale invariant spectrum $\gamma = 3/2$.

A non-zero value of A_i would lead to nonzero values for operators involving higher powers of the field strength. In this chapter, however, we are interested in *small fluctuations*. This means that the effect of operators like $\mathrm{Tr}F^n$ are suppressed.

For cosmological scales we are interested in, the modes are outside of the Hubble radius at the time $-t_b$. Hence, we can use the small argument limit of the Bessel functions. We will assume that at $t = -t_b$ both modes have the same amplitude. Let us denote the total amplitude of $A(k)$ (we are dropping the index i) by $2\tilde{A}$ (which is k-dependent). Then we find the following values of the coefficients D_Y^- and D_J^- before the bounce

$$\begin{aligned} D_Y^- &= \tilde{A}|-t_b|^{-1/2}\left(\frac{|-kt_b|}{2}\right)^{\nu_g}, \\ D_J^- &= \tilde{A}|-t_b|^{-1/2}\left(\frac{|-kt_b|}{2}\right)^{-\nu_g}. \end{aligned} \tag{4.50}$$

At this point we know the equation of motion and the initial conditions for the boundary gauge field at the time $-t_b$ when the boundary theory becomes weakly coupled and when we begin the evolution of the fluctuations on the boundary. The evolution can be followed by determining the coefficients $\mathcal{A}, \mathcal{B}, \mathcal{D}_J^+, \mathcal{D}_Y^+$ by standard matching of the function $\tilde{A}_k(t)$ and its time derivative at $t = \pm\xi$, as detailed in the next section.

4.4.4 Evolution of Boundary Fluctuations through the Singularity

It is useful to discuss matching of solutions of the general form

$$\tilde{A}_k(t) = \begin{cases} A_-(k)F_1(t) + B_-(k)G_1(t)\,, & \text{if} \quad t \le -\xi, \\ \mathcal{A}\,\exp[\beta t] + \mathcal{B}\,\exp[-\beta t]\,, & \text{if} \quad -\xi \le t \le \xi, \\ A_+(k)F_2(t) + B_+(k)G_2(t)\,, & \text{if} \quad t \ge \xi. \end{cases}$$

Matching $\tilde{A}$ and its time derivative across $t = \pm\xi$ then leads to

$$\begin{aligned} A_+ &= \frac{1}{\Delta}\{\cosh(2\beta\xi)[F_1(-\xi)\dot{G}_2(\xi) - \dot{F}_1(-\xi)G_2(\xi)] \\ &+ \sinh(2\beta\xi)[\frac{1}{\beta}\dot{F}_1(-\xi)\dot{G}_2(\xi) - \beta F_1(-\xi)G_2(\xi)]\}A_- \\ &\quad + \frac{1}{\Delta}\{\cosh(2\beta\xi)[G_1(-\xi)\dot{G}_2(\xi) - \dot{G}_1(-\xi)G_2(\xi)] \\ &+ \sinh(2\beta\xi)[\frac{1}{\beta}\dot{G}_2(\xi)\dot{G}_1(-\xi) - \beta G_1(-\xi)G_2(\xi)]\}B_-\,, \end{aligned} \tag{4.51}$$

$$\begin{aligned} B_+ &= \frac{1}{\Delta}\{\cosh(2\beta\xi)[F_2(\xi)\dot{F}_1(-\xi) - \dot{F}_2(\xi)F_1(-\xi)] \\ &+ \sinh(2\beta\xi)[-\frac{1}{\beta}\dot{F}_1(-\xi)\dot{F}_2(\xi) + \beta F_1(-\xi)F_2(\xi)]\}A_- \\ &\quad + \frac{1}{\Delta}\{\cosh(2\beta\xi)[F_2(\xi)\dot{G}_1(-\xi) - \dot{F}_2(\xi)G_1(-\xi)] \\ &+ \sinh(2\beta\xi)[-\frac{1}{\beta}\dot{F}_2(\xi)\dot{G}_1(-\xi) + \beta G_1(-\xi)F_2(\xi)]\}B_-\,, \end{aligned} \tag{4.52}$$

where we have defined

$$\Delta \equiv F_2(\xi)\dot{G}_2(\xi) - G_2(\xi)\dot{F}_2(\xi)\,. \tag{4.53}$$

To specialize to the case of interest we need to substitute

$$\begin{aligned} F_1(t) &\equiv (-t)^{1/2}J_{\nu_g}(-kt)\,, & F_2(t) &\equiv (t)^{1/2}J_{\nu_g}(kt)\,, \\ G_1(t) &\equiv (-t)^{1/2}Y_{\nu_g}(-kt)\,, & G_2(t) &\equiv (t)^{1/2}Y_{\nu_g}(kt)\,, \\ A_\pm &= \mathcal{D}_J^\pm\,, & B_\pm &= \mathcal{D}_Y^\pm\,. \end{aligned} \tag{4.54}$$

Since we are always interested in wavenumbers small compared to the various time scales t_b and ξ, we can replace the Bessel functions by their small argument values for $k\xi \ll 1$. This yields

$$\begin{aligned}
2\nu\mathcal{D}_J^+ &= \Big[-\cosh(2\beta\xi) + \sinh(2\beta\xi)\Big(\frac{1}{4\beta\xi}(1-4\nu_g^2)+\beta\xi\Big)\Big]\mathcal{D}_J^- \\
&+ \big(\frac{2}{k\xi}\big)^{2\nu_g}\Big[\cosh(2\beta\xi)(2\nu_g-1)+\sinh(2\beta\xi)\Big(\beta\xi+\frac{1}{4\beta\xi}(1-2\nu_g)^2\Big)\Big]\mathcal{D}_Y^- \,, \\
2\nu\mathcal{D}_Y^+ &= \big(\frac{k\xi}{2}\big)^{2\nu_g}\Big[\cosh(2\beta\xi)(2\nu_g+1)-\sinh(2\beta\xi)\Big(\frac{1}{4\beta\xi}(1+2\nu_g)^2+\beta\xi\Big)\Big]\mathcal{D}_J^- \\
&+ \Big[\cosh(2\beta\xi)+\sinh(2\beta\xi)\Big(\beta\xi+\frac{1}{4\beta\xi}(1-4\nu_g^2\Big)\Big]\mathcal{D}_Y^- \,. \qquad (4.55)
\end{aligned}$$

We now substitute the initial conditions, (4.50) to calculate $\tilde{A}_k(t)$ at time $t = t_b$. The result is

$$\begin{aligned}
\tilde{A}_k(t_b) &= \frac{\tilde{A}(k)}{2\nu_g}\Big[2\sinh(2\beta\xi)\Big(\beta\xi+\frac{1}{4\beta\xi}(1-4\nu_g^2)\Big) \\
&+ \Big(\cosh(2\beta\xi)(2\nu_g+1)-\sinh(2\beta\xi)\big(\beta\xi+\frac{1}{4\beta\xi}(1+2\nu_g)^2\big)\Big)\Big(\frac{\xi}{t_b}\Big)^{2\nu_g} \\
&+ \Big(\cosh(2\beta\xi)(2\nu_g-1)+\sinh(2\beta\xi)\big(\beta\xi+\frac{1}{4\beta\xi}(1-2\nu_g)^2\big)\Big)\Big(\frac{t_b}{\xi}\Big)^{2\nu_g}\Big] \,. \qquad (4.56)
\end{aligned}$$

The significant point about (4.56) is that in the $k\xi \ll 1$ limit, the expression inside the square bracket becomes independent of the momentum k. This is because $\beta = \left(\frac{\alpha(\alpha+2)}{4\xi^2} - k^2\right)^{1/2}$, leading to $\beta\xi \approx \frac{1}{2}\sqrt{\alpha(\alpha+2)}$. The sole momentum dependence comes from the overall factor $\tilde{A}(k)$ which is the amplitude at $t = -t_b$. This means that the spectrum of $\tilde{A}_k$ is the same as $t = -t_b$ and $t = t_b$. The amplitude is however amplified, since for $t_b \gg \xi$ we get

$$\begin{aligned}
\tilde{A}_k(t_b) &\approx \frac{1}{4\nu_g}\Big[\cosh(2\beta\xi)(2\nu_g-1)+\sinh(2\beta\xi)\Big(\beta\xi+\frac{1}{4\beta\xi}(1-2\nu_g)^2\Big)\Big]\Big(\frac{t_b}{\xi}\Big)^{2\nu_g}\tilde{A}_k(-t_b) \\
&\sim \Big(\frac{t_b}{\xi}\Big)^{2\nu_g}\tilde{A}_k(-t_b) \,. \qquad (4.57)
\end{aligned}$$

The amplification is due to squeezing of the perturbation modes while their wavelength is larger than the Hubble result.

This result holds for arbitrary functional form of $\tilde{A}(k)$. In particular, when $\tilde{A}(k)$ is a power law and given by a scale invariant spectrum at $t = -t_b$ the spectral index does not change at $t = t_b$.

This is our main result. In the next section we will argue that this result in the boundary theory implies that the spectrum of cosmological fluctuations on a constant z slice in the bulk is also unchanged as the system goes through $t = 0$.

4.4.5 The General Result

From the above analysis it is now clear that the final result does not really depend on the details of the time dependence of the boundary coupling. This conclusion agrees with what was found when studying non-singular bulk cosmological models (see e.g. [6] for a recent review). Consider the equation for the gauge field perturbation (4.36) with a function $M_{YM}^2(t)$ which is smooth and bounded everywhere. Whenever the equation (4.39) has a regular solution for $k = 0$, it is clear that $\tilde{A}_i$ and its time dervative at $t = t_b$ is related to those at $t = -t_b$ by a Bogoliubov transformation

$$\begin{bmatrix} \tilde{A}_i(k, t_b) \\ \dot{\tilde{A}}_i(k, t_b) \end{bmatrix} = \begin{bmatrix} M_{11} & M_{12} \\ M_{21} & M_{22} \end{bmatrix} \begin{bmatrix} \tilde{A}_i(k, -t_b) \\ \dot{\tilde{A}}_i(k, -t_b) \end{bmatrix},$$

where the matrix M_{ij} depends on the potential, but not on k. Therefore if the initial conditions are such that

$$\tilde{A}_i(k, -t_b) \sim \dot{\tilde{A}}_i(k, -t_b) \sim B(k)\,, \tag{4.58}$$

it follows that

$$\tilde{A}_i(k, t_b) \sim \dot{\tilde{A}}_i(k, t_b) \sim B(k)\,, \tag{4.59}$$

up to factors which do not depend on k. The specific power law enhancement factor in (4.57) is a feature of the fact that the coupling constant is a power law away from the region of small coupling.

Therefore the momentum dependence of the fields in the future is the same as that in the past for all momenta small compared to all other scales in the problem.

4.5 Reconstruction of the Bulk from the Boundary Data

Given the amplitude and spectrum of the gauge field fluctuations after the singularity, we can reconstruct the late time spectrum of the bulk dilaton after the bounce. We evolve the boundary data until the time $+t_b$ when the 't Hooft coupling becomes unity.

As we emphasized above, the nature of the entire spacetime at positive times in the presence of these fluctuations is not known and might contain a black brane in the bulk. We will, however, assume that there is a region near the boundary where the curvatures are small enough to enable us to use the AdS/CFT dictionary. In particular we will assume that the bulk dilaton field at a point $(z, \vec{x}, t)$ for small enough z can be reconstructed from the dual boundary operator $\mathcal{O}$ using a bulk boundary map of the form

$$\varphi(z, \vec{x}, t) \; = \; \int dt' d^3x' K(\vec{x}', t'|z, \vec{x}, t)\mathcal{O}(\vec{x}', t') \, , \tag{4.60}$$

where the kernel $K(x', t'|z, x, t)$ (where (t', x') are boundary coordinates and (t, x, z) are the bulk coordinates) is non-vanishing only for points within the AdS causal wedge (see Fig. 3) of compact support. Due to the translation symmetry of the background, we assume that the kernel K depends only on the relative spatial separation $|\vec{x}' - \vec{x}|$.

The idea of the reconstruction is depicted in Figure 3: we consider a wedge sticking into the bulk with base on the boundary. The wedge is centered at the time t_b We need the boundary points of the wedge to all have time coordinate $t' > \xi$ - otherwise the wedge will intersect the singular part of the bulk. This will limit the distance from the boundary to which we can reconstruct the bulk.

As we will see, we will in fact never need the explicit form of the boundary-to-bulk propagator in order to extract the spectrum of bulk dilaton fluctuations. The only property of this propagator which will be used is that it is non-vanishing only within the wedge shown in Figure 3. In particular as $z \to 0$, one recovers the correspondence (4.31).

Now we turn to the extraction of the power spectrum of the bulk field φ in the future of the reconstruction time t_b. Our starting point is equation (4.60) which gives the bulk field in terms of the known boundary data. To extract the spectrum of fluctuations, we need to take the Fourier transform of $\varphi(z, x, t)$ in the spatial hyperplane perpendicular to the AdS

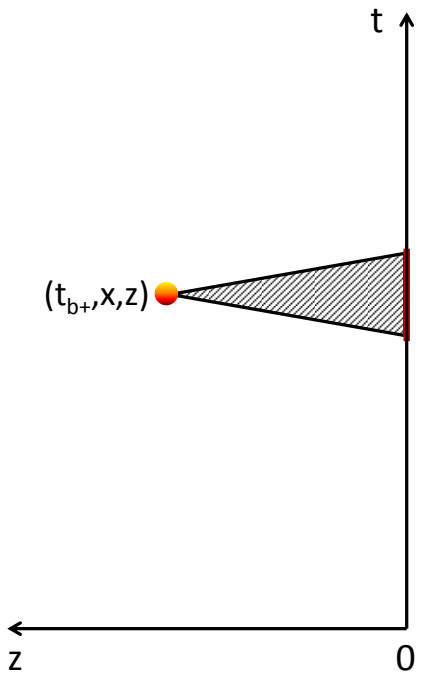

Fig. 4.3 Sketch of the reconstruction process for bulk operators in the future of the singularity. The vertical axis is time, the horizontal axis indicates the radial coordinate z. The solid line is the boundary.The bulk field at a point with coordinates (t_b^+, x, z) is given by integrating the boundary data against the boundary-to-bulk propagator. The integration involves data in the shaded region only. The solid curves connecting the bulk point to the boundary are null geodesics.

radial coordinate axis z:

$$\tilde{\varphi}(z,k,t) \;=\; V^{-1/2}\int d^3x\varphi(z,x,t)e^{ik\cdot x}\,, \tag{4.61}$$

where the tilde symbol indicates the Fourier transform.

We now insert the reconstruction formula (4.60) into the above. Introducing the new coordinates

$$\begin{aligned} \mathbf{x}' &= \mathbf{x}+\mathbf{y}'\,, \\ t' &= t+s\,. \end{aligned} \tag{4.62}$$

the result becomes

$$\tilde{\varphi}(z,k,t) \,=\, V^{-1/2} \int ds d^3y' K(y',s|z,t) e^{-i\mathbf{k}\mathbf{y}'} \int d^3x e^{i\mathbf{k}(\mathbf{x}+\mathbf{y}')} \mathcal{O}(x+y',t+s)\,. \tag{4.63}$$

The final integral simply gives the Fourier mode of the boundary operator:

$$\tilde{\varphi}(z,k,t) \,=\, \int ds d^3y' K(y',t+s|z,t) e^{-i\mathbf{k}\mathbf{y}'} \mathcal{O}(k,t+s)\,. \tag{4.64}$$

We are interested in values of k which are small compared to both the inverse Hubble radius and the AdS radius. Assuming that the propagator K has support within the AdS causal wedge (see Figure 3) of the bulk point, then for all values of the boundary coordinate $\mathbf{y}'$ for which K does not vanish we have $\mathbf{k}\mathbf{y}' \ll 1$, and one has approximately

$$\tilde{\varphi}(z,k,t) \,\simeq\, \int ds d^3y' K(y',s|z,t) \mathcal{O}(k,t+s)\,. \tag{4.65}$$

The k- dependence of the bulk fluctuation is therefore completely determined by the k-dependence of the expectation value of the operator $\mathcal{O}$, which - in our framework - is in turn determined by the k- dependence of the gauge field fluctuations $A_k(t)$. We have seen that the spectral index of the latter does not change when we cross the "singularity". The time integral in (4.65) has an extent which is roughly of the same order as z. Therefore for z small enough, the k dependence of $\tilde{\varphi}(z,k,t)$ is basically given by the k-dependence of the gauge field fluctuations. Hence, we find that the spectral index of fluctuations close enough to the boundary does not change when matching across the "singular" region (singular in quotation marks because we have cut off the actual singularity). On the other hand, the amplitude of the spectrum changes by a factor $\mathcal{F}$ given by

$$\mathcal{F} \,=\, \left(\frac{t_b}{\xi}\right)^{2\nu_g}\,. \tag{4.66}$$

In particular, the bulk spectrum on a small z slice is chosen to be scale invariant, i.e. $\varphi(k) \sim k^{-3/2}$ the spectrum continues to be scale invariant.

4.6 Conclusion and Discussion

In this chapter we have studied the evolution of linearized test field fluctuations in a deformed AdS/CFT cosmology. The deformed AdS background which is the basis of our study is obtained by introducing a nontrivial time-dependence for the dilaton and choosing the metric such that the bulk supergravity equations of motion are satisfied. The background begins with a contracting phase which approaches a bulk singularity at time $t = 0$. As the singularity is approached, the background becomes highly curved. At the time $-t_b < 0$ the gravitational theory becomes strongly coupled. However, the dual gauge theory which lives on the boundary becomes weakly coupled. After the singularity, the bulk expands, and after some time $t_b > 0$ the bulk theory once again becomes weakly coupled.

Our goal is to compare the spectrum of fluctuations of the bulk field in the far past ($t < -t_b$) and in the far future ($t > t_b$). Specifically, we consider fluctuations in the dilaton field. We evolve the fluctuations in the bulk until $t = -t_b$, map them onto the boundary at that time, infer the spectrum of the boundary gauge field fluctuations at this time and then evolve the boundary gauge field fluctuations forward in time, past the singularity, until the time $t = t_b$. At that time, we reconstruct the bulk dilaton field using boundary-to-bulk propagators which are nonvanishing only in a 'AdS causal wedge wedge, and compute the spectrum of the fluctuations.

Since the boundary fluctuations blow up at the time $t = 0$ in spite of the fact that the boundary theory is weakly coupled, we need to smooth out the singularity. We, therefore, modify the dilaton between $-\xi < t < \xi$, where ξ is a cutoff scale and then match the boundary fluctuations in a standard fashion.

Our main result is that the spectral index of the dilaton fluctuations near the boundary is the same in the far past and the far future. While we do not have the tools to map out the future space-time, we believe that our result will have important implications for pre big-bang scenarios of cosmology.

Chapter 5

Holographic Curvature Perturbations in a Cosmology with a Space-Like Singularity

5.1 Introduction

In spite of its many successes, early universe cosmology faces a number of outstanding theoretical and fundamental challenges. One of the most fundamental questions that remain to be answered in cosmology is the singularity problem. Singularities appear in many cosmological models and are unavoidable in some contexts like Einstein gravity with matter fields that do not violate the null energy condition (NEC). Both Standard Big Bang cosmology and the inflationary universe scenario [1–5, 119, 120] realized in the context of scalar field matter coupled to classical General Relativity are examples where an initial Big Bang singularity is present (see the classic paper [121] for the proof that an initial singularity appears in Standard Big Bang cosmology and [122] for an extension to inflationary cosmology). Bouncing cosmologies, alternative scenarios for the evolution of the universe where a contraction period precedes the expansion of the universe, also have singularities at the bounce point, at least if they are realized within the realm of Einstein or dilaton gravity coupled to matter obeying the NEC. One can avoid Big Bang/Big Crunch singularities by postulating matter which violates the NEC (see e.g. [6, 74–76, 107, 123] for some specific models, and [6] for a review), or by going beyond Einstein gravity (e.g. by choosing gravita-

tional Lagrangians with specifically chosen higher derivative terms [124, 125], by considering the Horava-Lifshitz gravitational action [77], or by assuming certain nonlocal gravitational Lagrangians [126, 127]). However, there are doubts as to whether these constructions can be embedded in a consistent quantum theory of gravity [128]. A consistent understanding of singularity resolution can presumably only be studied in such an ultraviolet complete theory, superstring theory being the prime example.

In this context the AdS/CFT correspondence could come to use. This correspondence [9] is a proposal for a non-perturbative treatment of string theory and states that the dynamics of a bulk Anti-de Sitter (AdS) space-time that includes gravity is encoded in the boundary of this space-time, where a conformal field theory (CFT) with no gravity lives. This conjecture has been used in many different fields of physics, from black hole physics to condensed matter, with great success (for a review e.g. [129]). It has already been proposed in the literature that the AdS/CFT correspondence could be used to resolve cosmological singularities [61–63, 84–86], specially in the context of singular bouncing models such as the Pre-Big-Bang [130] and Ekpyrotic [97] scenarios.

Bouncing cosmologies have recently been studied extensively as possible alternatives to cosmological inflation for producing the fluctuations which we are currently mapping out with observations. If the equation of state of matter in the contracting phase has $w > -1/3$, where w is the ratio of pressure to energy density, then scales exit the Hubble radius during contraction. Hence, it is possible to have a causal generation mechanism for fluctuations in the same way as in inflationary cosmology, where scales exit the Hubble radius in an expanding phase if the equation of state of matter obeys $w < -1/3$. As was pointed out in [71, 72], if the equation of state of matter during the time interval when scales which are measured now in cosmological observations exit the Hubble radius has the equation of state $w = 0$ (i.e. a matter-dominated equation of state), then initial vacuum perturbations originating on sub-Hubble scales acquire a scale-invariant spectrum [1], the kind of spectrum which fits observations well [2]. A scale-invariant spectrum of fluctuations can also be obtained in the Pre-Big-Bang [131, 132] and in the Ekpyrotic [98–102] scenarios, making use of entropy modes. The major problem in these analyses is that the fluctuations have to be matched from the contracting phase to the expanding phase across a singularity (for singular

[1] Note that the curvature fluctuations grow on super-Hubble scales in a contracting universe [71, 72], whereas they are constant in an expanding universe if the fluctuations are purely adiabatic.

[2] A slight red tilt of the spectrum emerges if the effects of a dark energy component are included [73].

bouncing cosmologies) or in the region of high curvature (in nonsingular models in which new physics provides a nonsingular bounce) where the physics is not under control. This is the second place where the AdS/CFT correspondence could become useful: the boundary theory becomes weakly coupled precisely where the bulk theory becomes strongly coupled, and hence we can expect that the evolution of the fluctuations on the boundary will be better behaved.

We here consider a time-dependent deformation of AdS [10–13] (see also [14, 15]) which yields a contracting phase with increasing curvature leading to a bulk singularity at a time which we call $t = 0$. The evolution for $t > 0$ is the mirror inverse of what happens for $t < 0$. This means that the bulk is expanding with decreasing curvature. The challenge for our work hence is to explore if the AdS/CFT correspondence can be used to determine the cosmological perturbations in the expanding phase starting with some initial cosmological perturbations in the contracting phase. In the case of a singular bouncing bulk cosmology this question cannot be answered from the point of view of the bulk evolution of those perturbations, and in a non-singular bouncing setup the evolution in the bulk cannot be reliably computed in a perturbative approach. For example, there are ambiguities if one wants to apply the matching condition approach [133, 134] to connect early time to late time fluctuations (see e.g. [103]). The goal of our work is to avoid these difficulties in the bulk evolution in the strongly coupled region by mapping the dynamics onto the boundary theory which is weakly coupled near $t = 0$. The AdS/CFT correspondence presents an unique opportunity to understand the effects of a bulk singularity on cosmological observables. Specifically, we are interested in computing the amplitude and slope of the spectrum of cosmological perturbations after the bounce given the spectrum before the bounce.

In [16] the authors studied the evolution of matter scalar field perturbations using the AdS/CFT correspondence in a deformed AdS_5 spacetime, where a spacelike singularity is present. This background spacetime is a time dependent background studied before in [10–13] where the dilaton bulk field has a time dependence which as $t \to 0$ produces a curvature singularity. The bulk theory is weakly coupled for $|t| > t_b$ and strongly coupled for smaller values of $|t|$. In the context of this background the authors studied dilaton perturbations on a hypersurface perpendicular to the AdS radial coordinate, starting with a scale invariant spectrum on super-Hubble scales at early times $t < -t_b$. When bulk gravity becomes strongly coupled at $t = -t_b$, the perturbations were mapped to the boundary theory, a $\mathcal{N} = 4$ Super Yang-Mills (SYM) theory, and the fluctuations of the corresponding boundary fields were

then evolved from $t = -t_b$ to $t = t_b$. This SYM model has a time-dependent coupling constant that goes to zero at the same time as the singularity occurs in the bulk. However, in spite of the fact that the boundary theory becomes free at $t = 0$, it was found that infinite particle production occurs between $t = -t_b$ and $t = 0$. Thus, it was necessary to introduce a cutoff: the coupling constant was kept finite but small in a short period of time $|t| < \xi$ around the singularity, where $\xi \ll t_b$. This made it possible to evolve the fluctuations unambiguously past the time $t = 0$ where the bulk singularity occurs until the late time $t = t_b$ after the singularity when the bulk theory becomes weakly coupled again. After that, for the infrared modes that are of cosmological interest (and whose wavelength is much larger than the Hubble radius already at the time $t = -t_b$), the bulk scalar field perturbations were reconstructed. It was found that the late time scalar field perturbations have a scale invariant spectrum, showing that the spectral index does not change while passing through the region of the highly curved (and maybe even singular) bulk. On the other hand, the amplitude of the scalar field perturbation spectrum is amplified - a consequence of the squeezing of the perturbation modes on super-Hubble scales in the contracting phase.

The evolution of scalar matter perturbations is interesting since it offers us a good guide as to the evolution of gravitational waves [3]. However, of more interest in cosmology is the spectrum of the scalar metric perturbations, since those lead to the adiabatic density perturbations responsible for structure formation in the universe. The goal of the present chapter is to extend the analysis of [16] to the case of cosmological perturbations.

Scalar cosmological perturbations are more complicated to analyze than matter scalar field fluctuations. They are made up of a combination of metric and matter inhomogeneities which take different forms in different coordinate systems. In the case of purely adiabatic perturbations [4] the information about the inhomogeneities is most conveniently encoded in the quantity $\mathcal{R}$, the curvature perturbation in comoving gauge (the gauge in which the matter field fluctuation vanishes [48]), a quantity that remains constant in time outside the Hubble radius [49, 136–140].

According to the AdS/CFT dictionary, the metric perturbation $\delta g_{\mu\nu}$ has as its dual

[3] The squeezing of the amplitude of gravitational waves on super-Hubble scales is governed by the same equation as the squeezing of matter scalar field fluctuations, whereas the scalar metric fluctuations are in general squeezed by a different factor - see e.g. [135] for a short review, and [46] for a more comprehensive survey of the theory of cosmological perturbations.

[4] For a single matter field the perturbations on super-Hubble scales are automatically adiabatic. In the case of multiple matter fields the adiabaticity condition means that the relative energy density fluctuations in each matter field are the same.

operator in the CFT the expectation value of the boundary energy momentum tensor. In order to reconstruct the curvature perturbations (which are a combination of the metric and the matter fluctuations) in the future of the space-time singularity, one needs to know the full evolution of the boundary operators corresponding to both the bulk matter scalar field and the metric perturbations.

We argue in this chapter that there exists a gauge choice that can simplify this problem. We generalize the spatially flat gauge to the 5-dimensional case. This gauge allows us to describe the curvature perturbations as a function only of the perturbations of the scalar field that represents the matter in our space-time. We do this by using the gauge freedom to gauge away the metric perturbation degrees of freedom which leaves us with only the scalar field perturbations. Because of this choice of gauge we only need to know how the scalar field perturbations behave at late times. This allows us to perform the same analysis as in [16], and to evolve the perturbations of a scalar field using the boundary theory in a singular deformed AdS_5 space-time. With this gauge choice, the analysis of scalar field fluctuations is all we need to be able to reconstruct the curvature perturbations in the future of the space-time singularity.

This chapter is organized as follows. Section II contains a summary of the dynamics of the deformed AdS bulk space-time containing a spacelike singularity. In Section III we discuss the cosmological perturbations in this deformed AdS_5 space-time and present the generalized spatially flat gauge. Section IV shows the main result, namely how to obtain the curvature perturbation at late times evolving from an initial bulk perturbation using the AdS/CFT correspondence. We find that the spectral index is not changed when comparing the spectrum at late and early times, but that there is an increase in amplitude resulting from the squeezing of the Fourier mode wave functions.

5.2 Bulk Dynamics

We are interested in studying cosmological backgrounds in the context of the AdS/CFT correspondence. Some time-dependent backgrounds in string theory were studied in [10–13] where the bulk solution can be thought as a time-dependent deformation of $AdS_5 \times S^5$ with a corresponding $\mathcal{N} = 4$ supersymetric Yang-Mills (SYM) theory containing a time dependent gauge coupling constant as a dual theory.

This background bulk solution can be described by the line element

$$\begin{aligned} ds^2 &= \frac{\ell^2}{z^2}\left(dz^2 + \tilde{g}_{ab}dx^a dx^b\right) \\ &= \frac{\ell^2}{z^2}\left[dz^2 + \frac{2|t|}{3\ell}\left(-dt^2 + \delta_{ij}dx^i dx^j\right)\right], \qquad t \gtrless 0,\ z \in (0, +\infty), \end{aligned} \tag{5.1}$$

where t is conformal time and z the AdS radial dimension, plus a $d\Omega_5^2$ term representing the S^5 factor. In the second line we are choosing a special Kasner type solution. Note that t denotes conformal time.The dilaton profile is given by

$$\phi(x) = \phi(t) = \sqrt{3}\ln\left(\frac{|t|}{\ell}\right), \quad \Rightarrow \quad e^{\phi(x)} = \left(\frac{|t|}{\ell}\right)^{\sqrt{3}}, \tag{5.2}$$

with ℓ being the AdS scale. Throughout this chapter we use conventions that Greek letters $\mu, \nu, \ldots$ run over all of the five space-time indices $0, \ldots 4$, Latin indices from the beginning of the alphabet $a, b, \ldots$ run over the indices $0, \ldots, 3$ corresponding to the four-dimensional space-time perpendicular to the AdS radial direction, and Latin letters $i, j, \ldots$ run over the spatial indices $1, 2, 3$.

This solution can be embedded in a solution of a 10-dimensional type IIB supergravity theory provided that the metric and the dilaton satisfy the equations of motion

$$\partial_\mu\left(\sqrt{-\tilde{g}}\tilde{g}^{\mu\nu}\partial_\nu\phi(x)\right) = 0, \quad R_{ab}[\tilde{g}] = \frac{1}{2}\nabla_a\Phi\nabla_b\phi(x). \tag{5.3}$$

The bosonic sector of this embedding includes a RR 5-form flux which supports the S^5 tensor factor of the space-time. The S^5 factor will not play a role in the following and we will thus not track it further.

The element (5.1) is easily recognized to be a deformation of the line element of pure AdS in Poicaré coordinates, where the AdS coordinate runs from $z = 0$ at the boundary to $z = \infty$ at the Poincaré horizon. In pure AdS the induced metric on constant-z hypersurfaces is the Minkowski metric. In our solution the induced metric is instead composed of two copies of a Friedmann-Robertson-Walker (FRW) metric, as seen in (5.1), one for $t < 0$ describing a collapsing geometry, and another for $t > 0$ describing an expanding geometry. The solution contains a spacelike singularity, "Big Crunch" singularity, at $t = 0$. It is also singular as $z \to \infty$ at any fixed $t \neq 0$. A sketch of the part of space-time covered by our coordinates

is shown in Figure 5.1. Due to the singularities, the spacetime cannot be Cauchy-extended beyond the Poincaré horizons which bound the coordinate chart. The string coupling is given by $g_s = e^{\phi(x)}$ and goes to zero at the singularity. If the singularity can be resolved by mapping the dynamics to the boundary, we will have a stringy realization of a boucing scenario.

We are assuming the the bulk universe initially begins in an AdS vacuum at some early moment t_i and the background is given by a weakly coupled supergravity theory. At the moment $-t_b$, the bulk gravity becomes strongly coupled, but at the same time the boundary gauge theory become weakly coupled. Hence, after the time $-t_b$ the evolution on the boundary becomes tractable in perturbation theory. On the future side of the bulk singularity, the boundary theory remains tractable perturbatively until the time t_b when the the bulk theory becomes weakly coupled again at the cost of the boundary theory becoming strongly coupled. At that time we can reconstruct the bulk information (at least in the vicinity of the boundary) from boundary data (see e.g. [109–112]).

We will take our space-time to be the hypersurface of some constant AdS radial coordinate z. We will be interested in considering linear fluctuations of matter and scalar metric degrees of freedom on this surface at some initial time $t \ll -t_b$, and computing the corresponding fluctuations on the same constant z surface in the future of the singularity, once the bulk theory once again becomes weakly coupled, i.e. at $t = t_b$.

To resolve the singularity in the background (5.1, 5.2) and study the evolution of perturbations to the future of $t = -t_b$ we will map the problem onto the boundary using the AdS/CFT dictionary. We can see that the boundary of this 5 dimensional solution is conformally flat and has a second order pole as $z \to 0$. So, in order to do holography we must specify a conformal frame, *i.e.* we must provide a defining function $\Omega(x)$ which behaves like $O(z^2)$ as $z \to 0$, and which in turn selects the induced boundary metric $h_{ab}(x)$ via

$$ds^2_{bndry} := h_{ab}(x)dx^a dx^b = \lim_{z\to 0} \Omega^2(x)\gamma_{ab}(x)dx^a dx^b \,, \tag{5.4}$$

where γ_{ij} is the metric of a maximally symmetric three-dimensional hypersurface (the metric of Euclidean three space, of the three sphere or the three-dimensional hypersphere). The above is an asymptotic solution in Fefferman-Graham form [141, 142] that represents the

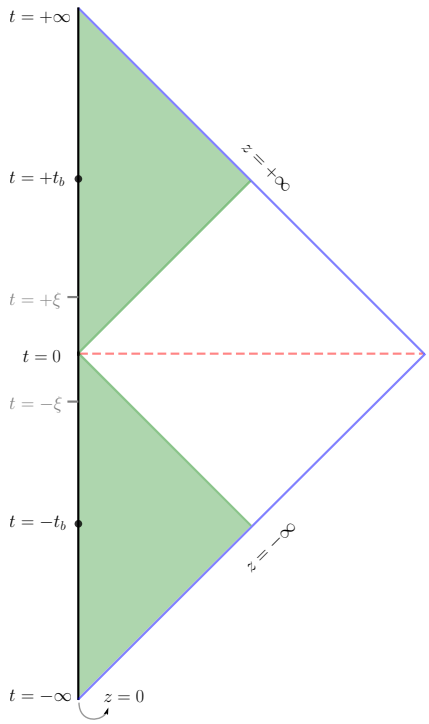

Fig. 5.1 Conformal diagram of the background space-time. The spacelike singularities is shown in red. The vertical axis is time t, the horizontal direction represents the coordinate z (with the boundary on the left side). If there were no deformation of AdS, the region drawn would correspond to the Poincare patch of AdS. The green regions may be covered by Fefferman-Graham [141, 142] charts with Minkowski boundary metrics.

conformal structure. There are two natural choices for $\Omega(x)$. First, if we select

$$\Omega_{\mathrm{FRW}}(x) = \frac{z}{\ell}, \tag{5.5}$$

then the boundary limit is particularly simple and the conformal boundary has metric $h_{ab}(x) = \gamma_{ab}(x)$. We refer to this as the FRW frame. A second choice is

$$\Omega_{\mathrm{M}}(x) = \left(\frac{3z^2}{2\ell|t|}\right)^{1/2}. \tag{5.6}$$

With this choice the boundary metric is flat. We refer to this as the Minkowski frame.

It is important to realize that $\Omega_M(x)$ is singular as $t \to 0$, and as a result the conformal transformation implied by $\Omega_M(x)$ is singular. One of our basic assumptions is that this conformal transformation is nevertheless a symmetry of the CFT.

Let us now turn to the CFT description of our solution. In this time-dependent background, the dual boundary theory is a $\mathcal{N} = 4$ SYM theory with a source. Following the usual dictionary [143], the AdS-Neumann part of $\phi(x)$ sets the value of the Yang-Mills coupling via

$$g^2_{YM}(x) = \lim_{z\to 0} e^{\phi(x)} \,. \tag{5.7}$$

In the Minkowski frame, this theory lives in flat space. Note that when the non-normalizable part of $\phi(x)$ varies with time, as in our example, the SYM theory in the boundary is sourced by a coupling that is time-dependent. So, the time dependent dilaton in the bulk corresponds to a time-dependent Yang-Mills coupling on the boundary. This coupling goes to zero as $t \to 0$ and the CFT becomes free.

5.3 Cosmological Perturbations in the Deformed AdS_5

We want to compute the cosmological perturbations from the space-time described above. In [16], we perturbed only the scalar field, namely, the dilaton. However, to fully describe the cosmological perturbations, we need to include the perturbations of the metric. For this, we need to perturb this deformed AdS_5 metric (see e.g. [144–146] for general discussions of cosmological fluctuations in brane world like five dimensional space-times).

Our starting point is the perturbed five-dimensional space-time metric

$$g_{MN} \;=\; g^{(0)}_{MN} \;+\; \delta g_{MN} \,, \tag{5.8}$$

where the first term on the right hand side denotes the background metric which depends only on t and z, and the second the linear fluctuations (which depend on all five space-time coordinates).

We can make a field redefinition in order to write the background metric in the following way:

$$ds^2 \;=\; d\bar{z}^2 + \tilde{g}_{ab} d\bar{x}^a d\bar{x}^b \,, \tag{5.9}$$

where $\bar{z} = (l/z)z$ and $\bar{x}^\mu = (l/z)x^\mu$. In some papers in the literature this is called a Gaussian

normal coordinate system, and it is equivalent to restrict the coefficient in front of the z-part of the metric to be unity. In the following we will drop the tilde signs on the coordinates.

After including linear fluctuations, the metric can be written, performing the usual scalar-vector-tensor decomposition with respect to spatial rotations on the constant z spatial hypersurface, as (see e.g. [46, 135])

$$ds^2 \;=\; -dz^2(1+C_0)+C_a dx^a dz+a^2(t)\left[(1+2\Phi)\,dt^2-2B_i d\bar{x}^i dt-(\delta_{ij}+h_{ij})\right]dx^i dx^j\,, \quad (5.10)$$

where, as we recall, t is the conformal time, and Φ, B_i and h_{ij} are functions of all space-time variables. The linear quantities C_0 and C_a are new metric fluctuations associated with the presence of the radial AdS direction. We can further decompose the $3-$vector B_i into a scalar and a divergenceless part and the rank-2 symmetric tensor h_{ij} into scalar, vector and tensor parts:

$$\begin{aligned} B_i &= \partial_i B+\hat{B}_i \qquad (5.11)\\ h_{ij} &= 2\Psi\delta_{ij}+2\left(\partial_i\partial_j-\frac{1}{3}\delta_{ij}\nabla^2\right)E+\left(\partial_i\hat{E}_j+\partial_j\hat{E}_i\right)+2\hat{E}_{ij}\,, \end{aligned}$$

where this decomposition is irreducible since the hatted quantities are divergenceless, $\partial^i\hat{E}_i$ and $\partial^i\hat{E}_{ij}=0$, and the tensor part is traceless, $\hat{E}^i_i=0$. Note that the tensor $\hat{E}_{ij}$ corresponds to gravitational waves, $\hat{B}_i$ and $\hat{E}_j$ to vector perturbations, and the remaining functions Φ, Ψ, B and E to the scalar metric perturbations. This perturbed metric and the variables are analogous to the fluctuations in a usual 4-dimensional cosmology when restricted to constant z slices. However, one needs to remember that the quantities calculated also depend of the coordinate z. In the following we will neglect vector perturbations and gravitational waves.

Together with the metric perturbations, we need to perturb the energy-momentum tensor of the 5-dimensional bulk. The matter content in our case is the dilaton field. This can be perturbed as follows, as in [16]

$$\bar{\phi}\,(z,\mathbf{x},t) \;=\; \phi\,(z,\mathbf{x},t)+\delta\phi\,(z,\mathbf{x},t)\;, \quad (5.12)$$

where ϕ represents the background dilaton field and $\delta\phi$ its linear perturbation.

General relativity allows for a freedom in the choice of the coordinate system. At the

linearized level the space of coordinate transformation is five-dimensional, allowing us to impose five gauge conditions in order to remove residual gauge degrees of freedom. As is done in the four space-time dimensional theory of cosmological perturbations we use two of these gauge freedoms to simplify the scalar sector of the metric. One choice is *longitudinal* gauge in which one sets $B = E = 0$. Two gauge degrees of freedom are vector from the point of view of the constant z hypersurfaces and can be used to reduce the number of vector modes, and the remaining gauge degree of freedom involves the z direction and could be used to set $C_0 = 0$. Making these choices, the scalar cosmological fluctuations involve the variables Φ, Ψ and $\delta\phi$ (plus the variables C_a which will not be important for us). An alternative choice is to pick the *spatially flat gauge* (*uniform curvature gauge*) in which the curvature on the constant time (and z) hypersurfaces is constant in space. In the absence of anisotropic stress Φ and Ψ coincide, and the Einstein constraint equation related the other two variables [5]. Hence, on a fixed t and z hypersurface, the information about scalar cosmological perturbations is encoded in terms of a single function.

Our goal will be to compute the evolution of the $3+1$ dimensional curvature fluctuation variable $\mathcal{R}$, which in the absence of entropy fluctuations is conserved on super-Hubble scales and thus encodes the relevant information about the scalar cosmological perturbations. It is hence the useful variable to track on super-Hubble scales, the scales we are interested in in this work (and also the ones which are of interest in inflationary cosmology).

We choose to work in uniform curvature gauge [6]. In this gauge, the variable $\mathcal{R}$ is on super-Hubble scales given by

$$\mathcal{R} = -\frac{\mathcal{H}}{\phi'}\delta\phi\,. \tag{5.13}$$

in terms of the scalar field fluctuation $\delta\phi$. The coefficient relating $\mathcal{R}$ and $\delta\phi$ is given by the comoving Hubble constant and by the background scalar field. Note that a prime indicated the derivative with respect to conformal time.

The variance for $\mathcal{R}$ in this gauge is given by the variance of $\delta\phi$. For each Fourier mode

[5] An easy way to see this is by noting that a matter perturbation $\delta\phi$ inevitably leads to a metric fluctuation of scalar type.

[6] Note that some gauges can become singular. For example, for scalar field matter the comoving gauge becomes singular when the scalar field comes to rest. The uniform curvature gauge may also break down in the time interval $-\xi < t < \xi$. We are, however, never following the evolution of the bulk metric fluctuations in this interval, and hence we do not have to worry about a possible breakdown of this gauge.

we have

$$\langle|\mathcal{R}_k|^2\rangle \;=\; \left(\frac{\mathcal{H}}{\phi'}\right)^2 \langle|\delta\phi_k|^2\rangle\,. \tag{5.14}$$

5.4 Holographic Curvature Perturbation at Late Times

The goal of the section is to calculate the conserved curvature perturbation in our deformed spacetime at late times. With the general spatially flat gauge developed above, we are able to write the curvature perturbation in terms of the perturbations of the scalar field and its background value. This is important in our setup, since it avoids one having to understand how the metric perturbations evolve holographically in this singular spacetime.

In our previous work [16], we showed a prescription for obtaining the bulk perturbation of a scalar field $\delta\phi$, the dilaton in our case, at late times $t > t_b$ in the weakly coupled region of the expanding period, given initial conditions for the perturbations of the scalar field in the bulk in the weakly coupled contracting phase. We were interested to understand how the presence of the singularity affects the initial scalar field perturbations. In particular, we investigated if the power spectrum given in the bulk at past times is changed after the singularity. We showed that the final spectrum of $\delta\phi_k$ remains scale invariant, given it was scale invariant in the past.

We now show how to use the results of our previous work to compute the quantity that is of interest in cosmology, the curvature perturbation. As we saw in the previous section, then when working in the *uniform spatial curvature gauge* we only need the power spectrum of the scalar field to obtain the power spectrum $P_{\mathcal{R}}$ of the curvature perturbations

$$P_{\mathcal{R}} \;=\; \left(\frac{\mathcal{H}}{\phi'}\right)^2 P_{\delta\phi} = \frac{1}{2\pi^2}k^3\left(\frac{\mathcal{H}}{\phi'}\right)^2 |\delta\phi_k\,(z,t)\,|^2\,. \tag{5.15}$$

Thus, if we have the solution of the bulk scalar field in the future of the singularity, $\delta\phi_k(+t_b)$, we are able to obtain the power spectrum of the curvature perturbation from the above relation.

As was shown in [16], the bulk scalar field fluctuations in the future of the singulariy can be locally reconstructed from the boundary data via [109, 110]

$$\delta\phi\,(t,x,z) \;=\; \int dt'd^3yK\,(t',y|t,x,z)\,\mathcal{O}\,(t',y)\;, \tag{5.16}$$

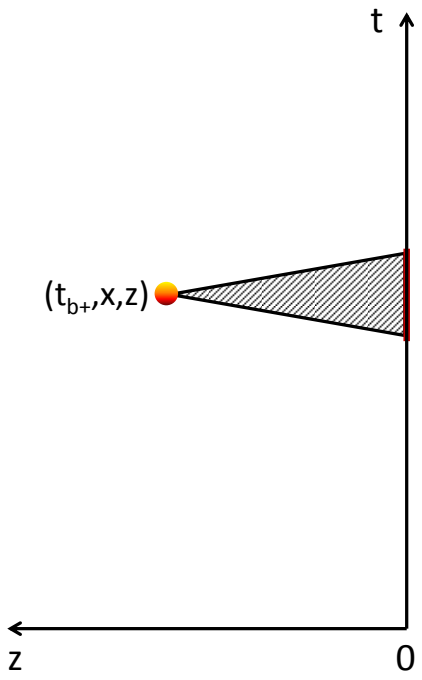

Fig. 5.2 Sketch of the reconstruction process for bulk operators in the future of the singularity. The vertical axis is time, the horizontal axis indicates the radial coordinate z. The solid line is the boundary.The bulk field at a point with coordinates (t_b^+, x, z) is given by integrating the boundary data against the boundary-to-bulk propagator. The integration involves data in the shaded region only. The solid curves connecting the bulk point to the boundary are null geodesics.

where the kernel $K\left(t', y|t, x, z\right)$ is the bulk-to-boundary propagator (or "smearing function"). The important property of this smearing function is that its support is confined to the "AdS causal wedge", *i.e.* to points with $|\delta t| \equiv t' - t < z$ (see Fig. 2). The exact form of the smearing function will not be important for our analysis.This construction is similar to a boundary value problem (see also [112–115]). This means that $\delta\phi\left(t, x, z\right)$ corresponds to a local operator $\mathcal{O}\left(y, t'\right)$ in the CFT, with a map defined by the smearing function.

We can make a translation in the time and space coordinates: $t' = t + s$ and $y = x + y'$. The smearing function is invariant under translations of the x coordinates. In pure AdS it would also be invariant under time translations. In the case of our deformed AdS, the kernel has an explicit time-dependence. The important point is that the kernel has support within the AdS causal wedge. Hence, as long as we consider values of z not too far from the

boundary, the region of support of the kernel for the time $t = t_b$ is far away from the space-time singularity, and the kernel is hence well defined. The fact that the kernel is independent of the three dimensional spatial coordinates x on the fixed z surface implies that the kernel does not effect the shape of the power spectrum.

Our interest is to be able to find the spectrum of the perturbations in the future. For that, we need to work with the Fourier transform of (5.16). This is given by:

$$\begin{aligned} \delta\phi_k(z,t) &= \int ds d^3y' e^{-iky'} K(t+s, y'|z,t)\, \mathcal{O}(k, t+s)\,, \\ &\simeq \int ds \underbrace{\int d^3y' K(s+t, y'|z,t)}_{M(t,s,z)} \mathcal{O}(k, t+s) \end{aligned} \tag{5.17}$$

where in the last line we considered only the IR limit, the one of interest for cosmological perturbations. We can see from this equation that $\mathcal{O}(k, t+s)$ has the same k-dependence as $\delta\phi_k$, with the amplitude smeared and calculated at a translated time.

We do not need to know the exact form of the kernel for our deformed AdS_5. All we need to assume is the existence of such a smoothing function with a causal structure similar to the one for pure AdS (obtained in [109, 110]). The differences between the smearing functions in pure AdS in and our deformed space-time would appear in the time-mode solutions used in the construction of K, since here we have a FRW spacetime on the boundary instead of Minkowski, leading to a different normalization for $K(s, y'|z)$. The important property of the smearing function is that it has support on the causal wedge of AdS, and selects only data on the boundary that is space-like separated with $\mathbf{ky'} << 1$, given by the values of $\mathbf{y'}$ where the smearing function does not vanish. It is very important in our case that the only data necessary for the reconstruction of the bulk field is local, since the presence of the singularity makes part of the data in the past inaccessible in the future of the deformed AdS Poincare chart. We can see that from the green regions of Figure 5.1.

We can then write the power spectrum of the uniform curvature perturbation with respect to the boundary data. From equation (5.15), and knowing that for our bulk $\mathcal{H} = a'/a$, where a prime denotes the derivative with respect to conformal time, and where in our case

$$a(t) = \frac{2}{3}\frac{|t|}{l}\,, \tag{5.18}$$

we have

$$P_{\mathcal{R}}(k,t) = \frac{1}{(2\pi l)^2} k^3 |\delta\phi_k(z,t)|^2 = \frac{1}{(2\pi l)^2} k^3 \left| \int ds M(s,z) \mathcal{O}(k,t+s) \right|^2 . \tag{5.19}$$

Thus, the power spectrum of $\mathcal{R}$ has the same slope as that of the boundary operator $\mathcal{O}$. This boundary operator given in this equation is known from the AdS/CFT correspondence: The scalar field in the bulk corresponds to the expectation value of the trace of the square of the field strength of a conformal field theory living on the boundary:

$$\mathcal{O} = \langle \mathrm{tr} F^2 \rangle . \tag{5.20}$$

This is the same operator whose evolution was studied in our previous paper [16], and in the following we will just briefly summarize the analysis which relates the late time spectrum of $\mathcal{O}$ with the initial spectrum of $\delta\phi$.

In our case, the boundary conformal field theory is a $\mathcal{N} = 4$ Super Yang Mills (SYM) theory in $3+1$-dimensions with a Yang-Mills coupling that varies in time, inherited from the time-dependent dilaton from the bulk. Given this theory, we can evaluate the operator, since

$$F_{\mu\nu} = 2\partial_{[\mu} A_{\nu]} - i [A_\mu, A_\nu] . \tag{5.21}$$

We ignore the term with the commutator since this is subdominant in our analysis. We adopt Coulomb gauge ($\partial_i A^i = 0$) and set $A_0 = 0$. Then the Fourier transform of the field strength tensor reduces to

$$\mathrm{Tr}[F^2(k,t)] = 2\dot{A}_k^2 - 2(k_j A_{k_i})^2 + 2k_i A_{k_j} k^j A^{k_i} , \tag{5.22}$$

where summation over the index k is implied. We are only interested in the infrared (IR) modes, where k is small, so we can drop the last two term of the previous expression and thus obtain the approximate relation

$$\mathrm{Tr}[F^2(k,t)] = 2\dot{A}_k^2 , \tag{5.23}$$

where once again summation over k is implied.

The fundamental field of this theory is the vector field A_μ, and it can be evolved in time, given its equation of motion in the boundary. So, the field $A_\mu(+t_b)$, necessary to calculate the operator $\mathcal{O}(x, t_b)$ can be evolved from a initial vector field through $t = 0$, the time when the singularity happens. This time also corresponds to the place where the YM coupling vanishes and the theory becomes free.

Since the gauge theory becomes free, it could have been expected that the gauge field fluctuations pass through $t = 0$ without any problem. However, as discussed in [16] this is not the case. In terms of the original Fourier space modes $A(k, t)$ there is a branch cut in the evolution equations, and in terms of the canonically normalized field corresponding to $A(k, t)$ there is in fact a divergence. This divergence corresponds to the blowup of particle production which is expected from the point of view of the bulk theory, where the fluctuation modes obtain infinite squeezing at $t = 0$. Hence, it is not surprising that at the level of fluctuations the boundary theory at this point becomes sick and infinite particle production occurs. This does not allow us to evolve the field passed $t = 0$. In order to be able to perform the evolution, we imposed a regularization of the YM coupling, making it constant during a period $[-\xi, \xi]$, where ξ is smaller than t_b, and matching the solutions (and their first derivatives) in the periods $t < -\xi$, $-\xi < t < \xi$ and $t > \xi$.

We perform this matching in the boundary theory since in the bulk, at times $\xi = \sqrt{\alpha'}$, where α' is the string scale, the Ricci scalar reaches the string scale and the bulk supergravity description breaks down. So, matching on the boundary can be performed at time ξ, much closer to the singularity, where the bulk theory is already in the strong limit. Since the theory in the boundary has no gravity, this matching is under much better control and goes closer to the singularity than what could be done by working in the bulk if we want to make sure that the perturbative expansion is justified.

With that, we can relate the solution of the field A_μ from early to late times past the singularity, first re-scaling the gauge field by $\tilde{A}_k(t) = e^{\phi/2} A_k(t)$ to obtain a canonically

normalized field [7]. The analysis of [16] yielded the result

$$\tilde{A}_k(t) = |t|^{\frac{1}{2}} \left[D_J^+ J_{\nu_g}(|kt|) + D_Y^+ Y_{\nu_g}(|kt|) \right] , \tag{5.24}$$

where $\nu_g = (1+\sqrt{3})/2$, and where the mode coefficients D_J^+ and D_Y^+ are related to the ones D_J^- and D_Y^- before the singularity by:

$$D_J^+ = \frac{1}{2\nu_g} D_Y^- + 2^{-2\nu_g} \left(1 + \frac{1}{2\nu_g}\right) (k\xi)^{2\nu_g} D_J^- , \tag{5.25}$$

$$D_Y^+ = -\frac{1}{2\nu_g} D_J^- + 2^{2\nu_g} \left(1 - \frac{1}{2\nu_g}\right) (k\xi)^{-2\nu_g} D_Y^- . \tag{5.26}$$

At late times, at time $t = t_b$, when we map the results from the boundary to the bulk, the gauge field is then given by:

$$\tilde{A}_k(t_b) \simeq \left(\frac{t_b}{\xi}\right)^{2\nu_g} \tilde{A}(-t_b) , \tag{5.27}$$

which means that the k-dependence of the field remains the same after passing through the singularity, changing only its amplitude that is enhanced by the factor

$$\mathcal{F}(t) \, = \, (t_b/\xi)^{2\nu_g} \ . \tag{5.28}$$

So, given an initial condition in the gauge field $A_k(-t_b)$, we can time evolve this field until time t_b in the future of the singularity, and then calculate the operator $\mathrm{Tr}\,[F^2(k,t')]$ and obtain the power spectrum.

This initial value for the gauge field in the boundary theory can be inferred from the initial scalar field in the bulk. As done in our previous work, we choose a particular scaling of the Fourier modes of the boundary gauge field such that the operator $\mathcal{O}$ has the same amplitude and scaling as what is induced from the bulk scalar field fluctuations which we

[7] Note that $\tilde{A}$ diverges as $t \to 0$. This divergence will lead to divergent particle production of charged fields which couple in the usual way to $\tilde{A}$, but not to those which couple in the usual way to A. The cutoff which we introduce to control the divergent growth of the fluctuations of $\tilde{A}$ will also control the divergent growth of the fluctuations of charged fields which couple to $\tilde{A}$.

are starting out with. From (5.20) and (5.23) we have

$$m_{pl}^4 \delta\phi^{in}(k) \,=\, \frac{1}{2}\int_0^k d^3k' \dot{A}^{in}\left(\frac{k+k'}{2}\right)\dot{A}^{in}\left(\frac{k-k'}{2}\right)V^{1/2} \,=\, \mathrm{Tr}\left[F^2(-t_b)\right]_k \,=\, \mathcal{O}\left(k,-t_b\right)\,, \tag{5.29}$$

where V is a normalization volume introduced in the definition of the Fourier transform (such that the Fourier modes of A have the mass dimension of a harmonic oscillator, *i.e.* $-1/2$). This integral can be performed in two regions, R_1 where $k < k'$, and R_2 where $k > k'$. In region R_1 we can set $k' = 0$ and get, approximately

$$m_{pl}^4 \delta\phi^{in}(k) \,\sim\, k^3 \dot{A}_k^2 V^{1/2}\,. \tag{5.30}$$

In the case when the initial bulk scalar field has a scale invariant power spectrum, $\delta\phi \propto k^{-3/2}$, the gauge field at $t = -t_b$, the time of matching onto the boundary in the past, has $A_k^{in}(t) = A_k(-t_b) \sim k^{-9/4}$. Assuming this scaling for the gauge Fourier modes, it can easily be seen that Region R_2 gives gives a contribution comparable to (5.30). With the initial conditions given by (5.29) and the growth of the gauge modes given by (5.27) we can write the boundary data in the future, encoded in the operator:

$$\mathcal{O}\left(k,t\right) \,=\, \frac{(4\nu_g)^2}{\xi^{4\nu_g}} t^{2(2\nu_g)}\frac{1}{2}\int_0^k d^3k' \dot{A}\left(\frac{k+k'}{2},-t_b\right)\dot{A}\left(\frac{k-k'}{2},-t_b\right)V^{1/2} = \mathrm{Tr}\left[F^2(-t_b)\right]_k\,. \tag{5.31}$$

Now we have all the ingredients to obtain the power spectrum of curvature perturbations past the singularity, given an initial bulk scalar field perturbation in the past:

$$\begin{aligned} P_{\mathcal{R}} &= \frac{k^3}{(2\pi)^2}\left|\int ds M(s,z)\mathrm{Tr}\left[F^2(t_b)\right]_k\right|^2\,, \\ &= \frac{(4\nu_g)^4}{(2\pi)^2\,\xi^{8\nu_g}}\,k^3\,t^{4(2\nu_g)}\left|\int ds M(s,z)\frac{1}{2}\int_0^k d^3k' \dot{A}\left(\frac{k+k'}{2},-t_b\right)\dot{A}\left(\frac{k-k'}{2},-t_b\right)V^{1/2}\right|^2\,. \end{aligned} \tag{5.32}$$

Integrating over region R_1, and taking $k' = 0$, we have

$$P_{\mathcal{R}} = \frac{(4\nu_g)^4}{(2\pi)^2 \xi^{8\nu_g}} k^3 t^{4(2\nu_g)} \left| \int ds M(s,z)\, k^3 \dot{A}^2(k, -t_b) \right|^2 ,$$
$$= \frac{(4\nu_g)^4}{(2\pi)^2 \xi^{8\nu_g}} k^3 t^{4(2\nu_g)} \left| \int ds M(s,z) m_{pl}^4 \delta\phi^{in}(-t_b) \right|^2 . \quad (5.33)$$

For the case presented in [16] when we have a scale invariant spectrum for the bulk scalar field in the past, with $\delta\phi^{in} \propto k^{-3/2}$, this implies that $\dot{A}(k, -t_b) \propto k^{-9/4}$. Plugging this expression into (5.33) we see that at $t = t_b$ in the future:

$$P_{\mathcal{R}} \simeq \frac{(4\nu_g)^4}{(2\pi l)^2 \xi^{8\nu_g}} t_b^{4(2\nu_g)} \big[\int ds M(s,z) \big]^2 m_{pl}^8 . \quad (5.34)$$

The power spectrum for the curvature perturbations is scale invariant. This means that the index of the power spectrum of the curvature flluctuations is not changed after passing through the singularity. So, if we start in the contracting phase with a scale invariant power spectrum of curvature fluctuations before the singularity, then the final curvature perturbations will also be scale invariant, carrying at late times an enhancement factor in the amplitude, related to particle production occurring on super-Hubble scales close to the bulk singularity.

5.5 Conclusions and Discussion

We have used the AdS/CFT correspondence to propagate cosmological fluctuations from the contracting phase to the expanding phase of a time-dependent deformation of an AdS bulk space-time which has a curvature singularity at a time $t = 0$. The bulk space-time is weakly coupled for $|t| > t_b$, and strongly coupled for $|t| < t_b$. Since the CFT on the boundary becomes weakly coupled for $|t| < t_b$, we map the bulk perturbations onto the boundary at the transition time $t = -t_b$, evolve the fluctuations in the conformal field theory until $t = t_b$, and then reconstruct the bulk perturbations.

We have shown that there is a gauge choice for the bulk space-time coordinates in which the information about cosmological fluctuations can be encoded in terms of the dilaton perturbations. This is the frame we use to map the inhomogeneities onto the boundary. We

use the same choice of coordinates to reconstruct the bulk for in the future of the strongly coupled bulk region, i.e. for $t > t_b$.

For the background with a bulk curvature singularity, particle production in the boundary theory diverges at $t = 0$. Hence, to obtain a well-defined evolution, we need to regulate the boundary theory (and thus also the bulk theory) in some time interval $|t| < \xi$, where $\xi \ll t_b$. In the regulated theory, it is then possible to unambiguously compute the evolution of the linearlized cosmological perturbations. We find that, as in the case of dilaton fluctuations in [16], the spectral index of infrared perturbations is the same before entering and after exiting the region of large space-time curvature. The amplitude of the spectrum, on the other hand, changes by a factor which depends on the ratio of t_b and ξ. These results agree with what is obtained in some models of nonsingular bounces in which rather ad hoc new physics is used to obtain the bounce (see e.g. [144–146]). What is satisfying in our approach is that the bounce is obtained using fundamental ingredients from superstring theory.

One may ask what impact the regulation of the boundary theory in the time interval $-\xi < t < \xi$ has on the bulk theory. It will not correspond to a solution of the supergravity equations. However, we do not view this as a problem since in the time interval $-\xi < t < \xi$ we are in the very high bulk curvature region where the supergravity action is not a good approximation for the underlying string theory. As interesting question which we do not address in this chapter is what additional bulk objects should appear if we want to obtain the modified bulk theory. By mapping the physics problem we are interested in onto the boundary we avoid having to tackle this difficult problem. In fact, the main advantage of mapping the evolution of metric fluctuations through a high curvature bulk region onto the boundary is that in the bulk high curvature region the boundary theory is weakly coupled and hence the evolution of the fluctuations is under much better control.

Note that there are other ways to obtain a bouncing cosmology from superstring theory. One recent example makes use of the T-duality symmetry in the Euclidean time direction to obtain a so-called S-brane bounce [81–83, 147]. Another approach is in [148]. It is also possible that as a consequence of the Hagedorn spectrum of string states [149] coupled with the T-duality symmetry in compact spatial directions one obtains an early emergent Hagedorn phase [78], in which case thermal fluctuations of a gas of strings would be the source of the observed cosmological perturbations [79]. These different approaches lead to signatures which are distinguishable (and also distinguishable from conventional inflationary cosmology) in cosmological observations, in particular because of different predictions of the

tilt of the gravitational wave spectrum [150–152], the running of the spectrum [153] and the amplitude and shape of the three point function of the curvature fluctuation [154, 155].

Part II

Late Universe Cosmology

Chapter 6

Methods of Data Analysis

In this part of the thesis we are going to study a model that explains the late evolution of our universe, the interacting dark energy model, testing it using the most recent cosmological observations. This chapter introduces the statistical methods used to perform the data analysis in Chapters 7 and 8. We also describe the likelihoods of each of the probes used in the experiments considered.

6.1 Maximum Likelihood Method

In this section we give a quick review (based on [156–159]) of the most common and used estimation method: the maximum likelihood method that aims to obtain the most likely parameters of a model that explains a given statistical observation.

We start by defining the likelihood as the probability density of a given data set $\{x_i\} = \{x_1, x_2, \cdots, x_N\}$ to be explained by a set of parameters $\vec{a}$:

$$\mathcal{L}\left(x_i|\vec{a}\right) = \prod_{i=1}^{N} f\left(x_i|\vec{a}\right) , \tag{6.1}$$

where each data has a conditional probability density (pdf), $f\left(x_i, \vec{a}\right)$, which defines the probability of the measured value x_i within an interval given by the uncertainty of this measurement, to be given by the set of parameters $\vec{a}$: $P = \int_{x_1}^{x_2} pdf(x_i|\vec{a})dx$. The likelihood can be seen as the joint density probability of N independent measurements, given by the product of each of them, for an independent sets of data.

The maximum likelihood method is used to estimate the parameters $\vec{a}$ given the measurements x_i, by finding the estimators of the parameter $\hat{a}(x_i)$ that maximizes the likelihood. These estimators are the parameters that present the best fit to the likelihood and are the solution to the system:

$$\frac{\partial \mathcal{L}\left(x_i|a_j\right)}{\partial a_j} = 0\,, \qquad j = 1, ..., m\,. \tag{6.2}$$

With this likelihood and using Bayes' theorem, we can define:

$$p\left(a_j|x_i,\right) = \frac{\mathcal{L}\left(x_i|\vec{a}\right)\, p\left(a_j\right)}{p\left(x_i\right)}\,, \tag{6.3}$$

where $p\left(a_j|x_i,\, M\right)$ is the posterior probability of the parameter, and it gives the answer we want: the probability that the parameter a_i coming from the theory can be explained by the data x_i. The density $p\left(a_j\right)$ is called prior probability and it contains the information about our knowledge of the parameters before the experiment. This is usually known from theory or from previous experiments, and one can choose flat priors or Gaussian priors (or even more sophisticated choices). One needs to be very careful, since a wrong choice of prior might lead to wrong posterior and a wrong result. $p\left(x_i\right)$ is the evidence, the *pdf* of the data. The evidence is seen as the condition for imposing the normalization of the posterior probability.

Having the posterior distribution, one can extract a lot of information about the parameters of the model given the data. First, we can obtain the estimator for the parameters by maximizing the posterior:

$$\frac{p\left(a_j|x_i,\right)}{\partial a_j} = 0\,, \qquad j = 1, ..., m\,. \tag{6.4}$$

One can also find the probability of a chosen parameter a_j by integrating over the other parameters, a procedure we call marginalizing:

$$p(a_j) = \int \cdots \int p(a_j|x_i)\, da_1, \cdots da_{j-1} \cdot da_{j+1} \cdots da_N\,. \tag{6.5}$$

Another piece of useful information that we can infer for the parameters is their confidence region, defined by:

$$\int_{R(\alpha)} p\left(a_j|x_i,\right) d^m a = \alpha\,, \tag{6.6}$$

where α is a number $0 < \alpha < 1$ that can be linked to the probability of the parameters to be within that region. The most used $\alpha = 0.683,\ 0.954,\ 0.997$ that correspond to the 1σ, 2σ and 3σ confidence levels. The procedure is to find $R(\alpha)$ for the level of confidence chosen.

All these calculations are simplified significantly if the *pdf*'s are Gaussian. In this case, maximizing the likelihood is equivalent to the problem of minimizing the χ^2, that is given by the exponent of the exponential of the Gaussian distribution. This procedure is the known least square method.

Not all the data are or can be approximated by a Gaussian and the use of the maximum likelihood method becomes complicated. However, the central limit theorem assures that if we have N events, where each one has a pdf and finite variance, then in the limit when $N \to \infty$ (or very large), the sum tends to a Gaussian distribution. This result is very important in cosmology not only because it simplifies the analysis but since the linear perturbations are expected to be Gaussian. Deviations from gaussianity bring an opportunity to explore new physics in the early and late universe.

6.2 Data Sets

In this section we describe the data and likelihood of each of the data sets used in our analysis: CMB temperature anisotropies, BAO, type Ia Supernovae and local measurements of H_0. For the measurement of the Lyman-α forest from high-redshift quasars, although a likelihood was provided by the BOSS collaboration, we constructed our own.

First, we will show how the primordial power spectrum generated by an early universe mechanism for the generation of the primordial perturbations connects to the observations done in the CMB and late universe.

6.2.1 Connecting Observations to the Primordial Perturbations

As we saw in Section 3.2, for any mechanism that generates the primordial perturbations in the early universe (like inflation or bouncing cosmologies), we are able to compute the curvature perturbations $\mathcal{R}$ and the gravity waves. These perturbations freeze out after they leave the Hubble radius, and only evolve again after they re-enter it at later times. If we want to measure these perturbations at late times, using CMB or the large scale structure, we need to take into account what is the relation of $\mathcal{R}$ with the measured quantity, and

the time evolution of $\mathcal{R}$ after the scale re-enters the Hubble radius. Given a perturbation measured at late times Q_k, we can relate that with $\mathcal{R}$, in a schematic way:

$$Q_k(\tau) = T_Q(k, \tau_{hc}, \tau)\, \mathcal{R}_k(\tau)\,, \tag{6.7}$$

where τ_{hc} is the time when the perturbations crossed the horizon and $T_k(k, \tau_{hc}, \tau)$ is the function connecting both Q an $\mathcal{R}$.

The large scale structure of our universe is formed when the dark matter clumps due to gravitational instability from an initial distribution given by the primordial perturbations. All the baryonic matter, like galaxies or gas in the universe, is going to be formed and fall into the high density regions of the dark matter distributions, tracing this distribution with a proportionality (that depends on the tracer and can depend on k) factor called bias. It is important, then, to know how to calculate the power spectrum for the dark matter fluctuations from the primordial power spectrum so we can understand the power spectrum we measure from observations of a given tracer (galaxies, 21-cm, ...). The matter power spectrum is defined as:

$$P_\delta(k, t) = \frac{4}{25}\left(\frac{k}{aH}\right)^4 T_\delta^2(k, \tau) P_{\mathcal{R}}(k)\,, \tag{6.8}$$

where $\delta = \delta\rho/\rho$ is the density contrast for dark matter. This is the quantity that the software of data analysis, CAMB [160] and CosmoMC [161], used in the works of Chapters 7 and 8, compute.

6.2.2 Cosmic Wave Background

The cosmological microwave background has been the main source of information for constraining the cosmological parameters, after the COBE, WMAP and *Planck* results. We wish to use the anisotropies in the CMB to probe the cosmological parameters of our model. These anisotropies are encoded in the photons of the CMB as a temperature fluctuation or polarization modes. We are only interested, in this work, in the temperature anisotropies, that can be expanded in a basis of spherical harmonics:

$$\Theta(\hat{n}) \equiv \frac{\delta T(\hat{n})}{T_0} = \sum_{lm} a_{lm} Y_{lm}(\hat{n})\,, \tag{6.9}$$

where $\hat{n}$ is the unit vector that gives you the direction in the sky, $T_0 = 2.75$ is the background black body temperature of the CMB, $Y_{lm}(\hat{n})$ is the spherical harmonics with $m = -l, ..., l$ and the coefficients are the multipole moment and can be written as:

$$a_{lm} = \int d\Omega Y^*_{lm}(\hat{n})\Theta(\hat{n})\,. \tag{6.10}$$

Given these perturbations, we want to evaluate the two point function, which is the angular power spectrum:

$$C_l^{TT} = \frac{1}{2l+1}\sum_m \langle a^*_{lm} a_{lm}\rangle\,. \tag{6.11}$$

This quantity is the one extracted from the observations of the CMB and it is related to the primordial power spectrum by:

$$C_l^{TT} = \frac{2}{\pi}\int k^2 dk P_{\mathcal{R}}(k)\,\Delta_{Tl}(k)\Delta_{Tl}(k)\,, \tag{6.12}$$

since the adiabatic scalar perturbations dominate. Here, $\Delta_{Tl}(k)$ are the transfer functions. This general formula is valid for other modes like the E and B (and correlations between all of these).

With that, the treatment given in [162] is that the data $\mathbf{m}X$ is modelled as being composed of the CMB signal ($\mathbf{s}^X$) and a instrumental noise that is assumed to be a nearly Gaussian distributed random field ($\mathbf{n}^X$): $\mathbf{m}^X = \mathbf{s}^X + \mathbf{s}^X$, with X being one of the modes T, E or B. Then, the low-l full likelihood is given by:

$$\mathcal{L}(C_l) = \mathcal{P}\left(\mathbf{m}|C_l\right) = \frac{1}{2\pi|M|^{1/2}}\exp\left(-\frac{1}{2}\mathbf{m}^T M^{-1}\mathbf{m}\right)\,, \tag{6.13}$$

where $M = S + N$ is the full data covariance. The high-multipole likelihood has further contributions from astrophysical foregrounds, so the noise is modeled in a more complicated fashion described in [163].

The data used in our analysis was the low-l ($2 \leq l < 50$) and high-l($50 \leq l \leq 2500$) multipole data from *Planck* 2013 TT (temperature) power spectrum [163, 164]. In order to break the degeneracy between reionization optical depth and the primordial amplitude, we include the WMAP low-l polarization power spectrum ($2 \leq l \leq 32$) [165].

6.2.3 Baryon Acoustic Oscillations

The BAO are acoustic oscillations imprinted in the CMB from sound waves coming from the primordial plasma. This imprinted spherical waves have a characteristic scale, given by the sound horizon at recombination. This scale known to 0.2% precision from CMB power spectrum ($147.4 \pm 0.3 Mpc$) [41]. BAOs are a (statistical) standard ruler. The change in the size of this scale can measure the expansion history of the universe, and is thus a good probe to constrain dark energy.

The early universe is permeated by many spherical acoustic waves, so the final density distribution is a linear superposition of the small-amplitude sound waves. Thus, the BAO can be inferred statistically through the two-point correlation function of the matter distribution of biased tracers like galaxies.

The BAO can be measured in the radial direction ($s_{||}$), where we can infer the expansion of the universe through the Hubble parameter, and in the angular direction ($s_{\perp}$), where we can infer the angular distance:

$$s_{||}(z) = \frac{c\Delta z}{H(z)}\,, \qquad s_{\perp}(z) = D_A(z)\,\Delta\theta(1+z)\,. \tag{6.14}$$

We can observe the preferred clustering scale set by the BAO at different redshifts to constrain the Hubble parameter and the angular diameter distance. This is exactly what it is measured by the SDSS-BOSS collaboration from the Lyman-α forest from high-redshift quasars.

Another quantity that can be inferred from the BAO measurement is the spherically-averaged two-point statistics, which is a combination of D_A and $H(z)$:

$$D_V(z) = \left[(1+z)^2 D_A^2 \frac{c\,z}{H(z)}\right]^1 /3\,. \tag{6.15}$$

This is usually used when the signal in the radial direction is small in comparison with cosmological distortions.

The data used in the analysis of Chapter 7 combines the value of $D_V(z)$ from the SDSS DR7 BAO measurement at $z = 0.35$ [166], the BOSS DR9 at $z = 0.57$ [167], and 6dF Galaxy Survey at $z = 0.106$ [168]. The data from Lyman-α forest from high-z quasars, consists in the pair $(D_A(z)/r_s, D_H(z)/r_s)$ from the autocorrelation [169] and from the crosscorrelation

with the Lyα data [170].

The value of D_V from these measurements is then included in the data analysis as a vector, and separately, the values of $(D_A(z)/r_s, D_H(z)/r_s)$ are included as a matrix. The likelihood is computed from the χ^2 statistics:

$$\chi^2_{BAO} = (\mathbf{x} - \mathbf{x}_{obs})^T \; C^{-1}_{BAO} \, (\mathbf{x} - \mathbf{x}_{obs}) \; , \tag{6.16}$$

where $\mathbf{x}$ is the theoretical prediction vector/matrix, $\mathbf{x}_{obs}$ is the observed vector/matrix, and C_{BAO} is the covariance matrix.

6.2.4 Type Ia Supernovae and the Hubble Parameter Measurements

Type Ia Supernovae are used as standard candles, and we can hence infer their distance from us, as we saw in Section (2.1.1). They were the objects observed when dark energy was discovery in 1998. They are still widely used to infer the expansion of the universe with, now, a much bigger and deeper sample. We use data from the Supernovae Cosmology Project (SCP) Union 2.1 compilation [171], that is composed of 508 objects.

The likelihood is also evaluated by using the χ^2 statistics:

$$\chi^2_{Sn} = \sum_{i=1}^{580} \frac{\left[\mu_B(\alpha, \beta, \delta, M_B) - \mu(z, \Omega_m, \Omega_d, \omega)\right]^2}{\sigma^2} \, , \tag{6.17}$$

where $\mu(z, \Omega_m, \Omega_d, \omega)$ is the theoretical distance modulus given by [172]:

$$\mu(z) = 5log_{10}\big[c(1+z)\int_0^z \frac{dz'}{H(z')/H_0}\big] + 25 - 5log_{10}H_0 \quad . \tag{6.18}$$

The distance modulus $\mu_B(\alpha, \beta, \delta, M_B)$ is a parametrization:

$$\mu_B(\alpha, \beta, \delta, M_B) = m_B^{max} + \alpha \, x_1 - \beta \, c + \delta \, P\left(m_\star^{true} < m_\star^{thr}\right) \; , \tag{6.19}$$

where m_B^{max} is the integrated B-band flux at maximum light and $P\left(m_\star^{true} < m_\star^{thr}\right)$ is the correlation of the mass of the host galaxy and the SnIa luminosity. This parametrization can be fitted using three nuisance parameters, and the absolute magnitude, M_B. The parameters α, β and δ are fixed in the CosmoMC Union 2.1 module.

For the local value of H_0, we use the value from the Hubble Space Telescope [42]: $H_0 =$

$73.8 \pm 2.4\,\mathrm{km\,s^{-1}\,Mpc^{-1}}$.

Chapter 7

Testing the Interaction between Dark Energy and Dark Matter with Planck Data

7.1 Introduction

The incredible amount of precise astronomical data released in the past few years provided great opportunities to answer problems in cosmology and astrophysics. Recently, the Planck team released their first data with higher precision and new full sky measurements of the Cosmic Microwave Background (CMB) temperature anisotropies in a wide range of multipoles ($l < 2500$) [162, 173, 174]. Such a precision allows us to test cosmological models and determine cosmological parameters with a high accuracy.

The Planck team analysis showed that the universe is flat and in full agreement with the ΛCDM cosmological model, especially for the high multipoles ($l > 40$). However, the value of the Hubble parameter today presents about 2.5σ tension in comparison with other low redshift probes, for example the direct measurement done by Hubble Space Telescope (HST) [42]. If this difference is not introduced by systematics, this can point out to an observational challenge for the standard ΛCDM model. The Planck determination of H_0 assumed a theoretical ΛCDM model, which can influence its value on H_0.

Theoretically the ΛCDM model itself is facing challenges, such as the cosmological constant problem [175] and the coincidence problem [176]. The first problem refers to the small

observed value of the cosmological constant incompatible with the vacuum energy description in field theory. The second problem refers to the fact that we have no natural explanation why the energy densities of dark matter and vacuum energy are of the same order today. These problems open the avenue for alternative models of dark energy to substitute the cosmological constant description. For example, the use of a component with dynamically varying equation of state parameter to describe the dark energy. However, although it can alleviate the coincidence problem, it suffers the fine tuning problem. Thus these models are not prevailing.

Another way to alleviate the coincidence problem, which embarrasses the standard ΛCDM cosmology is to consider an interaction between dark energy and dark matter. Considering that dark energy and dark matter contribute significant fractions of the contents of the universe, it is natural, in the framework of field theory, to consider an interaction between them. The appropriate interaction can accommodate an effective dark energy equation of state in the phantom region at the present time. The interaction between dark energy and dark matter will affect significantly the expansion history of the Universe and the evolution of density perturbations, changing their growth. The possibility of the interaction between dark sectors has been widely discussed in the literature [27, 29, 30, 177–207]. Determining the existence of dark matter and dark energy interactions is an observational endeavor that could provide an interesting insight into the nature of the dark sectors.

Since the physical properties of dark matter and dark energy at the present moment are unknown, we cannot derive the precise form of the interaction from first principles. For simplicity, most considerations of the interaction in the literature are from phenomenology. Attempts to describe the interaction from field theory have been proposed in [32, 33, 208]. In this chapter we will concentrate on a phenomenological model of the interaction between dark matter and dark energy, which is in a linear combination of energy densities of the dark sectors $Q_c = 3H(\xi_1\rho_c + \xi_2\rho_d)$ [26,29,200], where ξ_1 and ξ_2 are dimensionless parameters and assumed to be time independent for simplicity. This model was widely studied in [28, 29, 31, 190, 205, 209, 210]. It was disclosed that the interaction between dark matter and dark energy influences the CMB at low multipoles by the late integrated Sachs-Wolf (ISW) effect [197, 199] and at high multipoles through gravitational lensing [31, 211]. With the WMAP data [197, 199] together with galaxy clusters observations [205, 206] and also recent kinetic Sunyaev-Zel'dovich effect observations [212], it was found that this phenomenological interaction between dark energy and dark matter is viable and the coupling constant is

positive indicating that there is energy flow from dark energy to dark matter, which is required to alleviate the coincidence problem and to satisfy the second law of thermodynamics [188].

It is of great interest to employ the latest high precision Planck data to further constrain the phenomenological interaction model. This is the main motivation of the present work. We will compare the constraint from the Planck data with previous constraints from WMAP data [197, 199]. Especially, we want to examine whether, with the interaction between dark matter and dark energy, we can reduce the tension on the value of H_0 at present. We will combine the CMB data from Planck with other cosmological probes such as the Baryonic Acoustic Oscillations (BAO), Supernovas and the latest constraint on the Hubble constant [42]. We want to see how these different probes will influence the cosmological parameters and put tight constraints on the interaction between dark sectors.

This chapter is organized as follows: in Section 7.2 we will describe the phenomenological interaction model between dark sectors and present the linear perturbation equations. In Section 7.3 we will explain the methods used in the analysis. Section 7.4 will present the results of the analysis and discussions. In the last section we will summarize our results.

7.2 The phenomenological model on the interaction between dark sectors

The formalism describing the evolution of matter and dark energy density perturbations without [213,214] and with dark matter and dark energy interaction [200] is well established. If dark matter and dark energy are coupled with each other, the energy-momentum tensor $T^{\mu\nu}_{(\lambda)}$ of each individual component $\lambda = c, d$ is no longer conserved. Instead,

$$\nabla_\mu T^{\mu\nu}_{(\lambda)} = Q^\nu_{(\lambda)} \,, \tag{7.1}$$

where $Q^\nu_{(\lambda)}$ is the four vector governing the energy-momentum transfer between dark components and the subscript (λ) can refer to dark matter (c) and dark energy (d), respectively. With interaction between dark sectors, dark matter and dark energy components are not conserved separately, but the energy-momentum tensor of the whole dark sector is still conserved, thus, $Q^\nu_{(c)} = -Q^\nu_{(d)}$.

Assuming spatially flat Friedmann-Robertson-Walker background, from the energy con-

servation of the full energy-momentum tensor, we can derive the equations of evolution of the mean dark matter and dark energy densities

$$\begin{aligned} \dot{\rho}_c + 3\mathcal{H}\rho_c &= a^2 Q_c^0 = +aQ\,, \\ \dot{\rho}_d + 3\mathcal{H}\,(1+\omega)\,\rho_d &= a^2 Q_d^0 = -aQ\,, \end{aligned} \tag{7.2}$$

where the derivatives and the Hubble parameter $\mathcal{H}$ are in conformal time, ρ_c is the energy density for dark matter, $\omega = p_d/\rho_d$ is the equation of state of dark energy, a is the scale factor and Q was chosen to be the energy transfer in cosmic time coordinates. We emphasize that the homogeneity and isotropy of the background require the spatial components of $Q^{\nu}_{(\lambda)}$ to be zero.

We concentrate on the phenomenological interaction as a linear combination of energy densities of dark sectors with the form of $Q = 3H(\xi_1\rho_c + \xi_2\rho_d)$, which describes the energy transfer. In the above expression of the continuity equations, if $Q > 0$, we have the dark energy transfers energy to the dark matter while if it is negative, the transfer is in the opposite direction. In studying the curvature perturbation it has been made clear that when the interaction is proportional to the energy density of dark energy ($Q = 3H\xi_2\rho_d$), we get a stable curvature perturbation except for $\omega = -1$; however, when the interaction is proportional to the dark matter density ($Q = 3H\xi_1\rho_c$) or total dark sectors ($Q = 3H\xi(\rho_c + \rho_d)$), the curvature perturbation can only be stable when the constant dark energy equation of state satisfies $\omega < -1$ [29]. For the case of a time-dependent dark energy equation of state, the stability of curvature perturbations was discussed in [186, 187]. With the interaction, the effective background equations of state for the dark matter and dark energy change to

$$\omega_{c,eff} = -\frac{a^2 Q_c^0}{3\mathcal{H}\rho_c}\,, \qquad \omega_{d,eff} = \omega - \frac{a^2 Q_d^0}{3\mathcal{H}\rho_d}\,, \tag{7.3}$$

where ω is the equation of state of dark energy. We summarize different forms of the interaction with the effective background equation of state in Table 7.1 as done in [31], we label our models with Roman numbers.

In order to solve the coincidence problem, we require the ratio of the energy densities of dark matter and dark energy, $r = \rho_c/\rho_d$, to be a constant in the expansion history of our

universe. This leads to a quadratic equation,

$$\xi_1 r^2 + (\xi_1 + \xi_2 + \omega)\, r + \xi_2 = 0. \tag{7.4}$$

The solutions of this equation can lead to unphysical results, as negative energy density of cold DM in the past or complex roots. For different phenomenological models of the interaction between dark sectors, the conditions to obtain physical results, positive energy densities and real roots, were summarized in [31] as shown in Table 7.1. Fig.7.1 illustrates the behavior of r for the four interacting models. We observe that, for the interaction proportional to the energy density of dark energy, a positive interaction can help to alleviate the coincidence problem as there is a longer period for the energy densities of dark matter and dark energy to be comparable. In contrast, a negative interaction can not alleviate the coincidence problem. For the interaction proportional to the energy density of dark matter or to the sum of both energies, the ratio r presents a scaling behavior.

Table 7.1 In this table we present the different coupling models considered with its constraints, dark energy equation of state and the effective equation of state for both fluids.

Model	Q	DE EoS	$\omega_{c,eff}$	$\omega_{d,eff}$	Constraints
I	$3\xi_2 H\rho_d$	$-1 < \omega < 0$	$-\xi_2/r$	$\omega + \xi_2$	$\xi_2 < -2\omega\Omega_c$
II	$3\xi_2 H\rho_d$	$\omega < -1$	$-\xi_2/r$	$\omega + \xi_2$	$\xi_2 < -2\omega\Omega_c$
III	$3\xi_1 H\rho_c$	$\omega < -1$	$-\xi_1$	$\omega + \xi_1 r$	$0 < \xi_1 < -\omega/4$
IV	$3\xi H\,(\rho_d + \rho_c)$	$\omega < -1$	$-\xi\,(1 + 1/r)$	$\omega + \xi\,(r + 1)$	$0 < \xi < -\omega/4$

From the background dynamics we see that when we introduce the phenomenological interaction between dark sectors, it is possible to have the scaling solution of the ratio between dark matter and dark energy, which can help to alleviate the coincidence problem. However, in the background dynamics there appears an inevitable degeneracy between the coupling in dark sectors and the dark energy equation of state. In general this degeneracy cannot be broken by just investigating the dynamics of the background spacetime, except in the case when the coupling is proportional to the dark matter density (Model III) as was discussed in [31]. It is expected that the degeneracy between the coupling and other cosmological parameters can be solved in the perturbed spacetime by considering the evolution of the perturbations of dark energy and dark matter. The perturbed FRW space-time has a metric

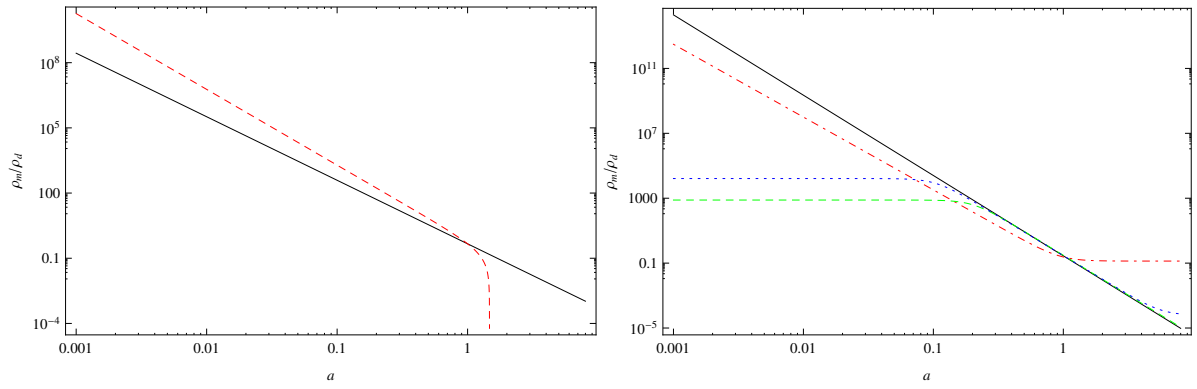

(a) (b)

Fig. 7.1 (Color online). Evolution of the dark energy/dark matter energy density ratio $r \equiv \rho_c/\rho_d$ in a model with $Q = 3H(\xi_1\rho_c + \xi_2\rho_d)$ for different coupling constants. (a) The red dashed line corresponds to Planck bestfit Model I, with $\xi_2 = -0.1881$ corresponding to the lowest value in the 68% C.L. as in Table 7.10. The black solid line has the same parameters but no interaction. (b) The black solid line corresponds to a non-interacting model with $w = -1.65$ and $\Omega_d = 0.78$. The red dot-dashed line describes Model II listed in the first column of Table 7.11 with $\xi_2 = 0.2$. The green dashed line corresponds to Planck bestfit Model III (see Table 7.12); and blue dotted line to Planck bestfit Model IV (see Table 7.13).

given by

$$ds^2 = a^2\left[-(1+2\psi)d\tau^2 + 2\partial_i B d\tau dx^i + (1+2\phi)\delta_{ij}dx^i dx^j + D_{ij}E dx^i dx^j\right], \tag{7.5}$$

where

$$D_{ij} = \left(\partial_i\partial_j - \frac{1}{3}\delta_{ij}\nabla^2\right). \tag{7.6}$$

The functions ψ, B, ϕ and E represent the scalar metric perturbations. In the synchronous gauge $\psi = B = 0$.

We will use an energy-momentum tensor of the form

$$T^{\mu\nu}(\tau, x, y, z) = (\rho + P)U^\mu U^\nu + Pg^{\mu\nu}, \tag{7.7}$$

where ρ, P are composed by a term depending only on time plus a small perturbation that depends on all coordinates. The four-velocity reads

$$U^\mu = a^{-1}(1 - \psi, \vec{v}_{(\lambda)}), \tag{7.8}$$

where $\vec{v}_{(\lambda)}$ can be written as minus the gradient of a peculiar velocity potential $v_{(\lambda)}$ plus a zero divergence vector. Only the first one contributes to scalar perturbations. In the Fourier space, we use the convention to divide the velocity potential by an additional factor of $k \equiv |\vec{k}|$ so that it has the same dimension as the vector part. Thus,

$$\theta \equiv \nabla \cdot \vec{v} = -\nabla^2 v = kv. \tag{7.9}$$

Following [185] we write the perturbed pressure of dark energy as

$$\delta P_d = c_e^2 \delta_d \rho_d + (c_e^2 - c_a^2) \left[\frac{3\mathcal{H}(1+\omega) v_d \rho_d}{k} - a^2 Q_d^0 \frac{v_d}{k} \right], \tag{7.10}$$

where $\delta = \delta\rho/\rho$ is the density contrast, c_e^2 is the effective sound speed of dark energy at its rest frame, which we set to one, and c_a^2 is the adiabatic sound speed. As discussed in [31], the perturbed four vector $\delta Q^\nu_{(\lambda)}$ can be decomposed into

$$\delta Q^0_{(\lambda)} = \pm \left(-\frac{\psi}{a} Q + \frac{1}{a} \delta Q \right), \qquad \delta Q_{p(\lambda)} = Q^I_{p(\lambda)}\big|_t + Q^0_{(\lambda)} v_t. \tag{7.11}$$

Here the $\pm$ sign refers to dark matter or dark energy respectively, and $\delta Q_{p(\lambda)}$ is the potential of the perturbed energy-momentum transfer $\delta Q^i_{(\lambda)}$. $Q^I_{p(\lambda)}\Big|_t$ is the external non-gravitational force density and v_t is the average velocity of the energy transfer. In this chapter we consider that there is no non-gravitational interaction between dark energy and dark matter, only inertial drag effect appears due to stationary energy transfer. Thus $Q^I_{p(\lambda)}\Big|_t$ and v_t vanish which implies that $\delta Q^i_{(\lambda)} = 0$.

In the synchronous gauge, the linear order perturbation equations for dark matter and

dark energy read [31]

$$\dot{\delta}_c = -(kv_c + \frac{\dot{h}}{2}) + 3\mathcal{H}\xi_2 \frac{1}{r}\left(\delta_d - \delta_c\right) , \tag{7.12}$$

$$\begin{aligned}\dot{\delta}_d = &-\left(1+\omega\right)\left(kv_d + \frac{\dot{h}}{2}\right) + 3\mathcal{H}(\omega - c_e^2)\delta_d + 3\mathcal{H}\xi_1 r\left(\delta_d - \delta_c\right) \\ &- 3\mathcal{H}\left(c_e^2 - c_a^2\right)\left[3\mathcal{H}\left(1+\omega\right) + 3\mathcal{H}\left(\xi_1 r + \xi_2\right)\right]\frac{v_d}{k} ,\end{aligned} \tag{7.13}$$

$$\dot{v}_c = -\mathcal{H}v_c - 3\mathcal{H}(\xi_1 + \frac{1}{r}\xi_2)v_c , \tag{7.14}$$

$$\dot{v}_d = -\mathcal{H}\left(1 - 3c_e^2\right)v_d + \frac{3\mathcal{H}}{1+\omega}\left(1 + c_e^2\right)\left(\xi_1 r + \xi_2\right)v_d + \frac{kc_e^2\delta_d}{1+\omega} , \tag{7.15}$$

where $h = 6\phi$ is the synchronous gauge metric perturbation and v_d is the peculiar velocity of the dark energy. The peculiar velocity of the dark matter v_c is considered to be null because we are working in a frame comoving with the matter fluid. To solve equations (7.12, 7.13, 7.14, 7.15) we set initial conditions according to [29]. In the linear perturbation formalism, the influence of the interaction between dark energy and dark matter on the CMB can be calculated by modifying the CAMB code [160]. This can be done by directly including equations (8.1, 7.12, 7.13, 7.14 and 7.15) in the code.

In [31], it was uncovered that in addition to modifying the CMB spectrum at small l, the coupling between dark sectors can shift the acoustic peaks at large multipoles. While the change of equation of state of dark energy can only modify the low l CMB power spectrum, it leaves the acoustic peaks basically unchanged. This provides the possibility to break the degeneracy between the coupling and the equation of state of dark energy in the linear perturbation theory. Furthermore, it was observed that the abundance of dark matter can influence the acoustic peaks in CMB, especially the first and the second ones. The degeneracy between the abundance of the dark matter and the coupling between dark sectors can be broken by examining the CMB spectrum at large scale, since only the coupling between dark sectors influences the large scale CMB spectrum. Theoretically it was observed that there are possible ways to break the degeneracy between the interaction, dark energy equation of state and the dark matter abundance in the perturbation theory [31]. This can help to get tight constraint on the interaction between dark energy and dark matter.

In the following we are going to extract the signature of the interaction and constraints on other cosmological parameters by using the Planck CMB data together with other ob-

servational data and compare with previous results obtained in [31] by employing WMAP data.

7.3 Method on data analysis

We compute the CMB power spectrum with the modified version of CAMB code [160], in which we have included both background and linear perturbation equations in the presence of a coupling between dark matter and dark energy. To compare theory with observations, we employ the Markov Chain Monte Carlo (MCMC) methodology and use the modified version of the program CosmoMC [161, 215], by setting the statistical convergence for Gelman and Rubin $R - 1 = 0.03$.

The Planck data set we use is a combination of the high-l TT likelihood, which includes measurements up to a maximum multipole number of $l_{max} = 2500$, combined with the low-l TT likelihood which includes measurements of $l = 2 - 49$ [162, 173, 174]. Together with the Planck data, we include the polarization measurements from the nine year Wilkinson Microwave Anisotropy Probe (WMAP) [165], the low-l ($l < 32$) TE, EE, BB likelihood.

In addition to the CMB data sets, we also consider Baryon Acoustic Oscillations (BAO) measurements. We combine the results from three data sets of BAO: the 6DF at redshift $z = 0.106$ [168], the DR7 at redshift $z = 0.35$ [166] and the DR9 at $z = 0.57$ [167].

Furthermore we examine the impact of the Supernova Cosmology Project (SCP) Union 2.1 compilation [171], which has 580 samples. Finally we also include the latest constraint on the Hubble constant [42]

$$H_0 = 73.8 \pm 2.4\,\mathrm{km\,s^{-1}Mpc^{-1}}. \tag{7.16}$$

In a recent paper [211], the authors examined the Model I of the interaction between dark sectors listed in Table 7.1 by confronting to observational data including the new measurements of the CMB anisotropies from the Planck satellite mission. They found that the Model I of coupled dark energy is compatible with the Planck measurements and can relax the tension on the Hubble constant by getting a consistent H_0 as the low redshift survey such as HST and SNIa measurements. In their analysis, they considered ranges for the priors of different cosmological parameters listed in Table 7.2 — ξ in Table 7.2 is the coupling constant defined in [211]. It relates to our definition ξ_2 in Model I by dividing

by 3. At the first sight, their prior of $\Omega_c h^2$ was set unreasonably small (see note in Table 7.2). It is interesting to check, if we allow an increase of $\Omega_c h^2$ prior, how the constraints of cosmological parameters for Model I behave. Besides, in [211], they fixed the dark energy equation of state to be $\omega = -0.999$. Actually there is no reason to fix the value of ω in the global fitting. It is more reasonable to inquire about the consequences of setting the equation of state of dark energy to be variable. The effect of letting ω free to vary under the condition $\omega > -1$ was also considered in [211] with the priors from Table 7.2. Furthermore, in [211], the authors fixed the relativistic number of degrees of freedom parameter to $N_{eff} = 3.046$, the helium abundance to $Y_p = 0.24$, the total neutrino mass to $\sum m_\nu = 0.06eV$, and the spectrum lensing normalization to $A_L = 1$. If we change the setting of these priors, we want to ask how the fitting results on the Model I change. Can Model I still be compatible with observational data? Can the constraint on the Hubble constant be relaxed as well? These questions are worthy of careful study.

Besides Model I of the interaction between dark sectors, in Table 7.1 we have listed other three interaction models. It would be of great interest to carry out global fitting of these models to the recent measurements of the CMB from the Planck satellite mission and other complementary observational data. In order to do so, in Table 7.3 we list the ranges for the priors of different cosmological parameters considered in our analysis. In our analysis we will use a big bang nucleosynthesis (BBN) consistent scenario to predict the primordial helium abundance Y_p as a function of the baryon density $\Omega_b h^2$ and number of extra radiation degrees of freedom ΔN. We will use interpolated results from the PArthENoPE code [216] to set Y_p, following [217].

Table 7.2 Initial parameters and priors used in the analysis in [211] for Model I.

Parameters	Prior
$\Omega_b h^2$	$[0.005, 0.1]$
$\Omega_c h^2$	$[0.005, 0.1]^1$
100θ	$[0.5, 10]$
τ	$[0.01, 0.8]$
n_s	$[0.9, 1.1]$
$log(10^{10} A_s)$	$[2.7, 4]$
$\xi_2 = \xi/3^2$	$[-0.333, 0]$

Table 7.3 The priors for cosmological parameters considered in the analysis for different interaction models.

Parameters	Prior			
$\Omega_b h^2$	$[0.005, 0.1]$			
$\Omega_c h^2$	$[0.001, 0.5]$			
100θ	$[0.5, 10]$			
τ	$[0.01, 0.8]$			
n_s	$[0.9, 1.1]$			
$log(10^{10} A_s)$	$[2.7, 4]$			
	Model I	Model II	Model III	Model IV
ω	$[-1, -0.1]$	$[-2.5, -1]$	$[-2.5, -1]$	$[-2.5, -1]$
ξ	$[-0.4, 0]$	$[0, 0.4]$	$[0, 0.01]$	$[0, 0.01]$

7.4 Fitting Results

We start with the Model I interacting model. We have initially performed two runs. In the first run we do not include the coupling, $\xi_2 = 0$, which corresponds to the ΛCDM case, and choose the priors of cosmological parameters listed in Table 7.2. In the second run, we follow [211] by setting the priors of different cosmological parameters as in Table 7.2, fixing the dark energy equation of state $\omega = -0.999$ and setting the helium abundance $Y_p = 0.24$, the total neutrino mass $\sum m_\nu = 0.06eV$, and the spectrum lensing normalization $A_L = 1$. We have let the coupling parameter ξ_2 to vary freely. Performing separately an analysis with Planck data alone, we show the result in Table 7.4.

Table 7.4 Best fit values and 68% c.l. constraints with the parameters in Table 7.2.

	ΛCDM Planck		Interacting Planck	
Parameter	Best fit	68% limits	Best fit	68% limits
$\Omega_b h^2$	0.0234	$0.0233^{+0.0003}_{-0.0003}$	0.0220	$0.0220^{+0.0003}_{-0.0003}$
$\Omega_c h^2$	0.099	> 0.099	0.044	unconstrained
H_0	76.9	$76.9^{+0.4}_{-0.4}$	73	72^{+2}_{-2}
w	—	—	—	—
ξ_2	—	—	-0.19	$-0.17^{+0.07}_{-0.07}$
τ	0.15	$0.13^{+0.02}_{-0.02}$	0.09	$0.09^{+0.01}_{-0.01}$
n_s	1.013	$1.008^{+0.005}_{-0.005}$	0.961	$0.957^{+0.007}_{-0.007}$
$\ln(10^{10} A_s)$	3.16	$3.13^{+0.03}_{-0.03}$	3.09	$3.08^{+0.02}_{-0.02}$

Our result for $\Omega_c h^2$ obeys the prior range as indicated in Table 7.2. If we look at the

Hubble constant value, in our fitting by obeying the prior of $\Omega_c h^2$ in Table 7.2, we get higher value of H_0, which shows that there is no more tension with the Hubble Space Telescope value. But if $\Omega_c h^2$ is above this prior range, the H_0 is much smaller. This gives us a hint that decreasing $\Omega_c h^2$ can lead to the effect of increasing H_0.

The presence of a dark coupling is perfectly compatible with the Planck data set. Our fitting result is consistent with that shown in Table 7.2 in [211] including the value of H_0 and the coupling ξ_2 (the relation between our coupling and theirs is $\xi_2 = \xi/3$). While the coupled dark Model I is compatible with most of the cosmological data, in Table 7.4 we see that the $\Omega_c h^2$ is unconstrained in the 1σ range although its best fitting value is still within the set prior. This is different from the result in Table 7.2 of [211].

We enlarge the prior to be $\Omega_c h^2 = [0.001, 0.99]$ and perform further two runs with Planck data alone for the ΛCDM model and the Model I of the interacting dark sectors. We show the results in Table 7.5. As expected, raising the upper range of prior for $\Omega_c h^2$ leads to the decrease of the values of H_0. This holds for both the ΛCDM and the coupling Model I. For the ΛCDM, our fitting result is consistent with Table 7.2 in [211]. For coupling Model I, we find that if we enlarge the prior of $\Omega_c h^2$, H_0 is decreased, although in Table 7.5 the fitting value of H_0 is still compatible with that of HST.

Table 7.5 Best fit values and 68% c.l. constraints with the parameters in Table 7.2, but with $\Omega_c h^2 = [0.001, 0.99]$

	ΛCDM Planck		Interacting Planck	
Parameter	Best fit	68% limits	Best fit	68% limits
$\Omega_b h^2$	0.0220	$0.0220^{+0.0003}_{-0.0003}$	0.0219	$0.0220^{+0.0003}_{-0.0003}$
$\Omega_c h^2$	0.120	$0.120^{+0.003}_{-0.003}$	0.12	$0.06^{+0.05}_{-0.03}$
H_0	67	67^{+1}_{-1}	67	71^{+3}_{-3}
w	—	—	—	—
ξ_2	—	—	-0.009	$-0.145^{+0.08}_{-0.10}$
τ	0.08	$0.09^{+0.01}_{-0.01}$	0.09	$0.09^{+0.01}_{-0.01}$
n_s	0.958	$0.957^{+0.007}_{-0.007}$	0.958	$0.957^{+0.007}_{-0.007}$
$\ln(10^{10} A_s)$	3.08	$3.08^{+0.02}_{-0.03}$	3.09	$3.08^{+0.02}_{-0.03}$

In the above fittings, we followed [211] to fix the equation of state of dark energy to be $\omega = -0.999$. In the global fitting, this condition is too strong. It is more reasonable to set the equation of state of dark energy to be free. We choose the prior of the equation of state of dark energy to be in the quintessence range $\omega = [-0.999, -0.1]$ and examine how this free

parameter affects the fitting result with Planck data alone. We show our results in Table 7.6. We find that in addition to enlarging the prior of $\Omega_c h^2$, setting ω to be free will further decrease the value of H_0 in the fitting. From the Planck data fitting, we see that the coupled dark sectors Model I is not of much help to relax the tension of H_0 with the Hubble Space Telescope value.

Table 7.6 Best fit values and 68% c.l. constraints with $w = [-0.999, -0.1]$.

	ωCDM Planck		Interacting Planck	
Parameter	Best fit	68% limits	Best fit	68% limits
$\Omega_b h^2$	0.0221	$0.0219^{+0.0003}_{-0.0003}$	0.0218	$0.0219^{+0.0003}_{-0.0003}$
$\Omega_c h^2$	0.118	$0.120^{+0.003}_{-0.003}$	0.10	$0.07^{+0.05}_{-0.02}$
H_0	66	63^{+4}_{-2}	65	67^{+5}_{-3}
w	-0.93	< -0.83	-0.91	< -0.85
ξ_2	—	—	-0.08	$-0.14^{+0.10}_{-0.08}$
τ	0.09	$0.09^{+0.01}_{-0.01}$	0.08	$0.09^{+0.01}_{-0.01}$
n_s	0.962	$0.957^{+0.007}_{-0.007}$	0.956	$0.957^{+0.007}_{-0.007}$
$\ln(10^{10} A_s)$	3.08	$3.09^{+0.02}_{-0.02}$	3.08	$3.08^{+0.02}_{-0.03}$

In Tables 7.7 and 7.8 we further show the fitting results with Planck data alone by fixing the helium abundance Y_p to the BBN prediction and assuming massless neutrinos, respectively. The fitting results are basically consistent with the result by fixing the helium abundance to $Y_p = 0.24$ and the total neutrino mass $\sum m_\nu = 0.06eV$, except that the constraint for the coupling is much tighter.

Table 7.7 Best fit values and 68% c.l. constraints in a BBN consistency scenario.

	ωCDM Planck		Interacting Planck	
Parameter	Best fit	68% limits	Best fit	68% limits
$\Omega_b h^2$	0.0220	$0.0220^{+0.0003}_{-0.0003}$	0.0222	$0.0220^{+0.0003}_{-0.0003}$
$\Omega_c h^2$	0.119	$0.120^{+0.003}_{-0.003}$	0.10	$0.07^{+0.05}_{-0.02}$
H_0	67	63^{+4}_{-2}	67	68^{+5}_{-4}
w	-0.98	< -0.82	-0.89	< -0.85
ξ_2	—	—	-0.07	$-0.13^{+0.13}_{-0.05}$
τ	0.09	$0.09^{+0.01}_{-0.01}$	0.09	$0.09^{+0.01}_{-0.01}$
n_s	0.960	$0.960^{+0.007}_{-0.007}$	0.969	$0.960^{+0.007}_{-0.007}$
$\ln(10^{10} A_s)$	3.10	$3.10^{+0.02}_{-0.03}$	3.08	$3.09^{+0.02}_{-0.03}$

Table 7.8 Best fit values and 68% c.l. constraints with $\sum m_\nu = 0eV$

	ωCDM Planck		Interacting Planck	
Parameter	Best fit	68% limits	Best fit	68% limits
$\Omega_b h^2$	0.02222	$0.02202^{+0.00028}_{-0.00028}$	0.02210	$0.02203^{+0.00028}_{-0.00028}$
$\Omega_c h^2$	0.1180	$0.1200^{+0.0027}_{-0.0026}$	0.1023	$0.07124^{+0.04748}_{-0.02382}$
H_0	66.56	$63.49^{+4.46}_{-2.26}$	68.10	$67.91^{+4.88}_{-3.52}$
w	-0.9306	< -0.8177	-0.9480	< -0.8487
ξ_2	—	—	-0.04789	> -0.17097
τ	0.09347	$0.08904^{+0.01245}_{-0.01442}$	0.08597	$0.08777^{+0.01269}_{-0.01399}$
n_s	0.9675	$0.9604^{+0.0072}_{-0.0073}$	0.9668	$0.9603^{+0.0073}_{-0.0073}$
$\ln(10^{10}A_s)$	3.094	$3.088^{+0.024}_{-0.027}$	3.082	$3.086^{+0.025}_{-0.025}$

We can also turn off the CMB lensing. We show the result of fitting with Planck data alone in Table 7.9. It is clear to see that turning off the CMB lensing will further reduce the Hubble constant at present and put tighter constraint on the interaction.

From the above analysis, we can conclude that although the coupled dark energy model I is fully compatible with the Planck measurements, it is not safe to argue that this model predicts the Hubble constant with less tension compared with the Hubble Space Telescope value.

Table 7.9 Best fit values and 68% c.l. constraints turning CMB lensing off.

	ωCDM Planck		Interacting Planck	
Parameter	Best fit	68% limits	Best fit	68% limits
$\Omega_b h^2$	0.0202	$0.0203^{+0.0003}_{-0.0003}$	0.0203	$0.0203^{+0.0003}_{-0.0003}$
$\Omega_c h^2$	0.126	$0.125^{+0.003}_{-0.003}$	0.11	$0.08^{+0.05}_{-0.02}$
H_0	63	59^{+5}_{-3}	63	64^{+5}_{-4}
w	-0.98	< -0.74	-0.89	< -0.81
ξ_2	—	—	-0.061	> -0.192
τ	0.07	$0.08^{+0.01}_{-0.01}$	0.06	$0.08^{+0.01}_{-0.01}$
n_s	0.936	$0.934^{+0.008}_{-0.008}$	0.932	$0.934^{+0.008}_{-0.008}$
$\ln(10^{10}A_s)$	3.06	$3.06^{+0.02}_{-0.02}$	3.04	$3.06^{+0.02}_{-0.03}$

Besides the interacting dark sector Model I, we would like to put constraints on other coupled dark energy models listed in Table 7.1 from the recent measurements of the Cosmic Microwave Background Anisotropies from the Planck satellite mission. We will also consider the combined constraints for the general phenomenological interacting models between dark

sectors from the Planck data plus the BAO measurements, SNIa and HST observational data. In our analysis, we will choose our priors of different cosmological parameters as listed in Table 7.3. We will allow the equation of state of dark energy to vary and choose the helium abundance Y_p from a BBN consistency scenario. We will take the relativistic number of degrees of freedom $N_{eff} = 3.046$, the total neutrino mass to $\sum m_\nu = 0.06eV$ and the spectrum lensing normalization to $A_L = 1$. After running the MCMC, we list our fitting results in Tables 7.10-7.13.

The constraints on the parameters and the best fit values for Model I are reported in Table 7.10. The 1-D posteriors for the parameters $\Omega_c h^2$, ω and ξ_2 are shown at the top row of Fig.7.2 and the main parameter degeneracies are shown in Fig.7.3. The presence of a dark coupling is perfectly compatible with the Planck data set. The marginalized value tells us $\xi_2 < 0$. With the combined constraint by including other observational data, the negative value of the coupling keeps, which shows that in this coupling model, there is a lower value of the cold dark matter density today, since there is energy flow from dark matter to dark energy. This direction of energy flow cannot alleviate the coincidence. As shown in Fig.7.1, there is even shorter period for the energy densities of dark matter and dark energy to be comparable. For the Hubble constant value, from the Planck data alone, H_0 is small in this interacting model, which is similar to that obtained in the ΛCDM case. This interaction model between dark sectors cannot be of much help to relax the tension on the Hubble parameter between Planck measurement and HST observation. After including other observational data at low redshift, we find that the tension between the Hubble constant measurements is alleviated.

Table 7.10 Cosmological parameters - Model I.

	Planck		Planck+BAO		Planck+BAO+SNIa+H0	
Parameter	Best fit	68% limits	Best fit	68% limits	Best fit	68% limits
$\Omega_b h^2$	0.0221	$0.0220^{+0.0003}_{-0.0003}$	0.0222	$0.0220^{+0.0003}_{-0.0003}$	0.0221	$0.0220^{+0.0002}_{-0.0002}$
$\Omega_c h^2$	0.12	$0.07^{+0.05}_{-0.02}$	0.11	$0.06^{+0.04}_{-0.03}$	0.07	$0.05^{+0.03}_{-0.03}$
H_0	67	68^{+5}_{-3}	68	69^{+2}_{-2}	71	71^{+1}_{-1}
w	-0.97	$-0.89^{+0.03}_{-0.12}$	-0.9934	$-0.91^{+0.02}_{-0.08}$	-0.99	$-0.94^{+0.02}_{-0.06}$
ξ_2	-0.00	$-0.13^{+0.13}_{-0.05}$	-0.02	$-0.15^{+0.07}_{-0.09}$	-0.14	$-0.18^{+0.05}_{-0.08}$
τ	0.09	$0.09^{+0.01}_{-0.01}$	0.10	$0.09^{+0.01}_{-0.01}$	0.09	$0.09^{+0.01}_{-0.01}$
n_s	0.960	$0.960^{+0.007}_{-0.007}$	0.964	$0.961^{+0.006}_{-0.006}$	0.964	$0.960^{+0.006}_{-0.006}$
$\ln(10^{10}A_s)$	3.09	$3.09^{+0.02}_{-0.03}$	3.11	$3.09^{+0.02}_{-0.03}$	3.10	$3.09^{+0.02}_{-0.03}$

Now we present the fitting result for the coupling Model II in Table 7.11, where the interaction between dark sectors is still proportional to the energy density of dark energy but with equation of state of dark energy smaller than -1. From the Planck data analysis alone, for this coupled dark energy model, using our cosmological parameters prior listed in Table 7.3, we obtain the Hubble constant value significantly larger than that in the standard ΛCDM case, $H_0 = 82.69^{+9.78}_{-11.9}$ km $\cdot$ s^{-1} $\cdot$ Mpc^{-1}. This is different from what we observed in the fitting result of Model I, where the H_0 is much smaller and consistent with the ΛCDM case. The lower fitting range of the H_0 in Model II is consistent with the observations in the low redshift. We have explored the degeneracy between the Hubble value and the equation of state of dark energy and found that smaller equation of state of dark energy leads to higher value of the Hubble parameter. The coupling constant ξ_2 is found to be positive, which shows that there is an energy flow from dark energy to dark matter. This is required to alleviate the coincidence problem, because with this interaction there is longer period for the energy densities of dark matter and dark energy to be comparable, which was illustrated in the Fig.7.1. Combined with other observational data, we show that a combined analysis provides significant evidence for this coupled dark energy with positive non-zero value of the coupling parameter, consistent Hubble constant and equation of state of dark energy. The 1-D posteriors for the parameters $\Omega_c h^2$, ω and ξ_2 are shown in the second row of Fig.7.2 and the main parameter degeneracies are shown in Fig.7.4.

Table 7.11 Cosmological parameters - Model II.

	Planck		Planck+BAO		Planck+BAO+SNIa+H0	
Parameter	Best fit	68% limits	Best fit	68% limits	Best fit	68% limits
$\Omega_b h^2$	0.0220	$0.0221^{+0.0003}_{-0.0003}$	0.0222	$0.0220^{+0.0003}_{-0.0003}$	0.0221	$0.0220^{+0.0002}_{-0.0002}$
$\Omega_c h^2$	0.131	$0.133^{+0.008}_{-0.012}$	0.132	$0.135^{+0.008}_{-0.011}$	0.143	$0.134^{+0.007}_{-0.012}$
H_0	89	83^{+10}_{-12}	71	71^{+2}_{-3}	70	71^{+1}_{-1}
w	-1.7	$-1.5^{+0.3}_{-0.3}$	-1.17	$-1.19^{+0.15}_{-0.07}$	-1.18	$-1.19^{+0.08}_{-0.07}$
ξ_2	0.03	$0.04^{+0.01}_{-0.04}$	0.03	$0.05^{+0.02}_{-0.04}$	0.08	$0.05^{+0.01}_{-0.05}$
τ	0.09	$0.09^{+0.01}_{-0.01}$	0.08	$0.09^{+0.01}_{-0.01}$	0.08	$0.09^{+0.01}_{-0.01}$
n_s	0.961	$0.960^{+0.007}_{-0.007}$	0.960	$0.958^{+0.006}_{-0.007}$	0.962	$0.959^{+0.006}_{-0.006}$
$\ln(10^{10}A_s)$	3.08	$3.09^{+0.02}_{-0.03}$	3.08	$3.09^{+0.02}_{-0.03}$	3.08	$3.09^{+0.02}_{-0.03}$

Now we turn our discussion to the coupled dark energy Model III, where the interaction is proportional to the energy density of dark matter. To ensure stability of the curvature perturbation, in this model if the equation of state of dark energy is constant, it has to be

smaller than -1 [29]. Looking at the new constraints on this coupled dark energy model from the recent measurements of CMB from the Planck satellite mission alone in Table 7.12, we find that the Hubble constant value is consistent with low redshift observations, but it is much higher than that of the ΛCDM result. The coupling constant is more tightly constrained in this coupled dark energy model than those in Models I and II, which is in agreement with the findings in the WMAP constraints [31, 197]. The value of the coupling parameter ξ_1 is small positive, which meets the requirement to alleviate the coincidence problem. The evolution of the ratio between energy densities of dark matter and dark energy with this small positive coupling was shown in the Fig.7.1, which has a longer period for the dark matter and dark energy energy densities to be comparable when ξ is positive and has the attractor solution with the ratio between dark energy and dark matter energy densities $r \sim constant$ in the past. We also consider the combined constraints from the Planck data plus other measurements. The results are listed in Table 7.12, which shows stronger evidence for this coupled dark energy model with small positive coupling. We plot the 1-D posteriors for the parameters $\Omega_c h^2$, ω and ξ in the third row of Fig.7.2 and show the main parameter degeneracies in Fig.7.5.

Table 7.12 Cosmological parameters - Model III.

	Planck		Planck+BAO		Planck+BAO+SNIa+H0	
Parameter	Best fit	68% limits	Best fit	68% limits	Best fit	68% limits
$\Omega_b h^2$	0.0222	$0.0226^{+0.0004}_{-0.0005}$	0.0225	$0.0224^{+0.0003}_{-0.0004}$	0.0223	$0.0223^{+0.0003}_{-0.0004}$
$\Omega_c h^2$	0.126	$0.129^{+0.005}_{-0.009}$	0.125	$0.125^{+0.003}_{-0.003}$	0.124	$0.123^{+0.002}_{-0.002}$
H_0	80	79^{+12}_{-12}	76	75^{+3}_{-5}	72	72^{+1}_{-1}
w	-1.6	$-1.8^{+0.5}_{-0.3}$	-1.5	$-1.4^{+0.3}_{-0.1}$	-1.30	$-1.25^{+0.09}_{-0.07}$
ξ_1	0.002	< 0.005	0.002	$0.002^{+0.001}_{-0.001}$	0.0018	$0.0014^{+0.0006}_{-0.0012}$
τ	0.08	$0.09^{+0.01}_{-0.01}$	0.09	$0.09^{+0.01}_{-0.01}$	0.08	$0.09^{+0.01}_{-0.01}$
n_s	0.958	$0.956^{+0.008}_{-0.008}$	0.960	$0.959^{+0.006}_{-0.007}$	0.963	$0.960^{+0.006}_{-0.006}$
$\ln(10^{10} A_s)$	3.07	$3.08^{+0.02}_{-0.03}$	3.095	$3.08^{+0.02}_{-0.03}$	3.07	$3.09^{+0.02}_{-0.03}$

Finally we present the fitting results for the coupled dark energy Model IV, where we consider the interaction between dark energy and dark matter is proportional to the energy density of the total dark sectors. In order to ensure the stability of the curvature perturbation, for the constant equation of state of dark energy, it has to be in the phantom range. This was disclosed in [29]. As observed in the WMAP fitting results, this type of interaction has very similar constraints to the Model III [31, 197]. Confronting the model to the Planck

data alone and the combined observational data, we list the constraints in Table 7.13. We show the 1-D posteriors for the parameters $\Omega_c h^2$, ω and ξ in the fourth row of Fig.7.2 and plot the main parameter degeneracies in Fig.7.6. From the Planck data alone, we again see that for this interacting dark energy model, the Hubble constant is much higher than that of the ΛCDM model. This is consistent with the observations from Model II and Model III. The coupling constant is more tightly constrained in Model IV to be very small but positive, what is needed to alleviate the coincidence problem with longer period for the dark energy and dark matter energy densities to be comparable in the expansion of the universe as shown in Fig.7.1. The Model IV has an attractor solution with $r \sim constant$ in the future. In the joint constraints, by including other observational data, we find that the coupled dark energy model IV is fully compatible with astronomical observations. It is a viable model.

Table 7.13 Cosmological parameters - Model IV.

	Planck		Planck+BAO		Planck+BAO+SNIa+H0	
Parameter	Best fit	68% limits	Best fit	68% limits	Best fit	68% limits
$\Omega_b h^2$	0.0205	$0.0204^{+0.0003}_{-0.0003}$	0.0204	$0.0204^{+0.0003}_{-0.0003}$	0.0205	$0.0206^{+0.0002}_{-0.0003}$
$\Omega_c h^2$	0.125	$0.127^{+0.003}_{-0.003}$	0.125	$0.126^{+0.002}_{-0.002}$	0.124	$0.124^{+0.002}_{-0.002}$
H_0	80	82^{+12}_{-10}	70	75^{+3}_{-5}	72	71^{+1}_{-1}
w	-1.6	$-1.8^{+0.4}_{-0.4}$	-1.3	$-1.5^{+0.2}_{-0.1}$	-1.30	$-1.29^{+0.08}_{-0.07}$
ξ_1	0.0001	< 0.0005	0.0000	< 0.0004	0.0001	< 0.0003
τ	0.09	$0.08^{+0.01}_{-0.01}$	0.07	$0.08^{+0.01}_{-0.01}$	0.07	$0.08^{+0.01}_{-0.01}$
n_s	0.930	$0.931^{+0.007}_{-0.007}$	0.929	$0.933^{+0.006}_{-0.006}$	0.934	$0.937^{+0.006}_{-0.006}$
$\ln(10^{10} A_s)$	3.09	$3.07^{+0.02}_{-0.02}$	3.04	$3.07^{+0.02}_{-0.02}$	3.06	$3.06^{+0.02}_{-0.02}$

7.5 Conclusions

In this chapter we have presented cosmological constraints on general phenomenological dark matter-dark energy interaction models from the new CMB measurements provided by the Planck experiment. We have found that a dark coupling interaction is compatible with Planck data. For Model I, the coupling parameter is weakly constrained to negative values by Planck measurements, while for the other three models the coupling constants are all positive from Planck data constraints. The positive coupling indicating that there is energy flow from dark energy to dark matter, as required to alleviate the coincidence problem and to satisfy the second law of thermodynamics [188]. Thus Model II, III and IV are very

reassuring in the light of the coincidence problem.

It was claimed that Model I gives a larger Hubble parameter compatible with the HST value [211]. However, this heavily depends on the prior of $\Omega_c h^2$, the fixed value of ω they chose and other factors. If we enlarge the prior of $\Omega_c h^2$ and allow ω to vary in the quintessence range, the H_0 constrained in Model I can be lower than the HST value and is consistent with the value in the ΛCDM case. Thus, the coupled dark energy Model I cannot be counted to resolve the tension between the Planck and the HST measurements of the Hubble parameter.

After examining the fitting results for the other phenomenological coupled dark energy models, we find that the dark interaction in Models II, III and IV can give a larger Hubble parameter. There is degeneracy between the Hubble parameter and the equation of state of dark energy. If future data can constrain ω closer to -1 from below, the fitting result of the Hubble parameter can be more consistent with the HST value. Thus Models II, III and IV have the possibility to relax the tension of the Hubble parameter between the Planck and the HST measurements.

We have also considered the combined constraints from the Planck data plus other observations. These analyzes have provided significant evidence that the phenomenological coupled dark energy models are viable. Taking into account all data sets, it appears in the data fittings that Model I shows the most significant departure from zero coupling, although it does not help to alleviate the coincidence problem.

The weak point of these models is the fact that the equation of state is fixed, not depending on time. In a more realistic model, we expect it to be time dependent (or else, redshift dependent). In order to probe such a statement we need a model grounded on cosmological fields rather than on simple phenomenology, e.g. coupled quintessence models [218]. This is currently under investigation.

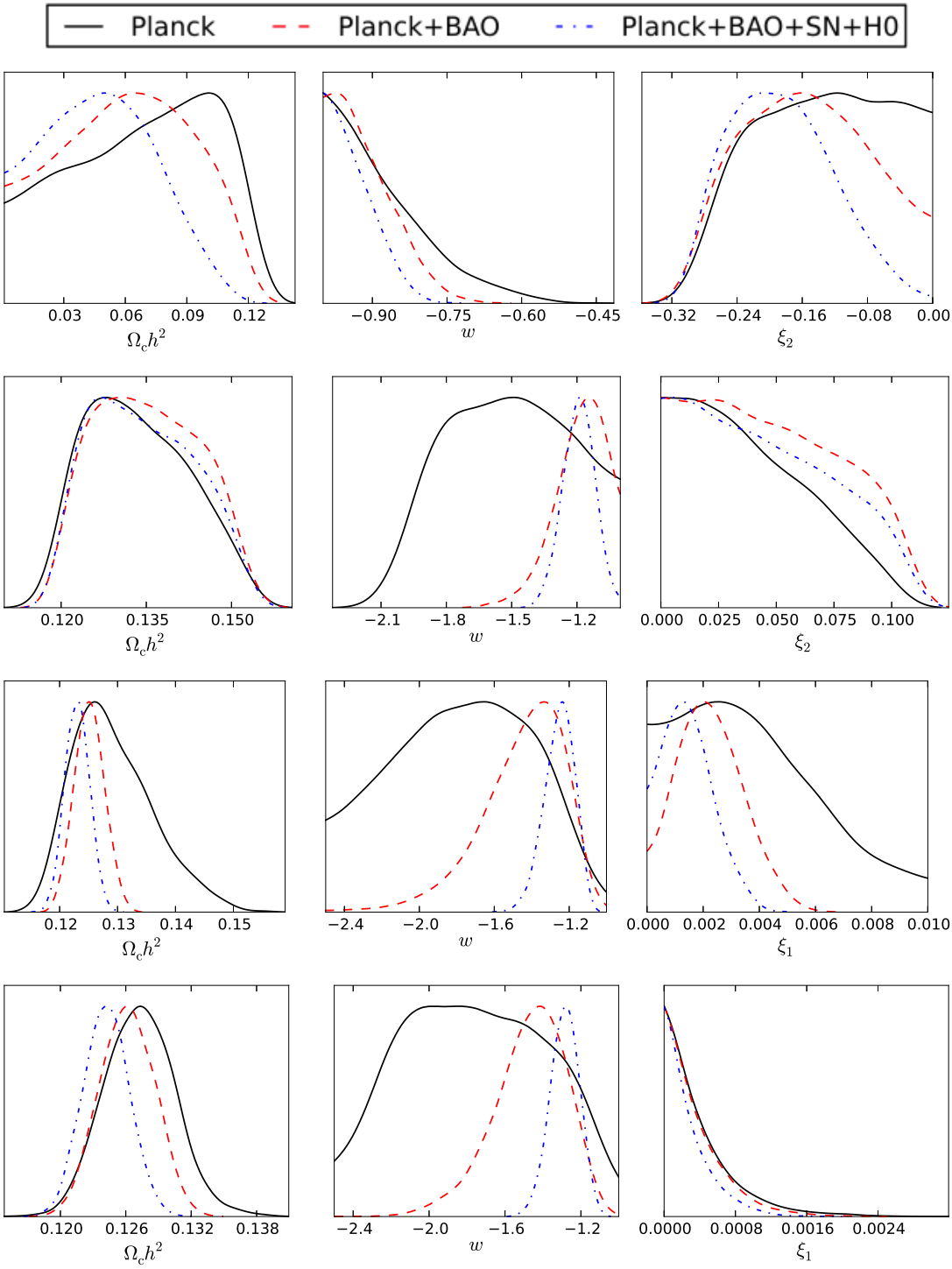

Fig. 7.2 The likelihood of cold dark matter abundance $\Omega_c h^2$, dark energy EoS ω and couplings ξ for the four models.

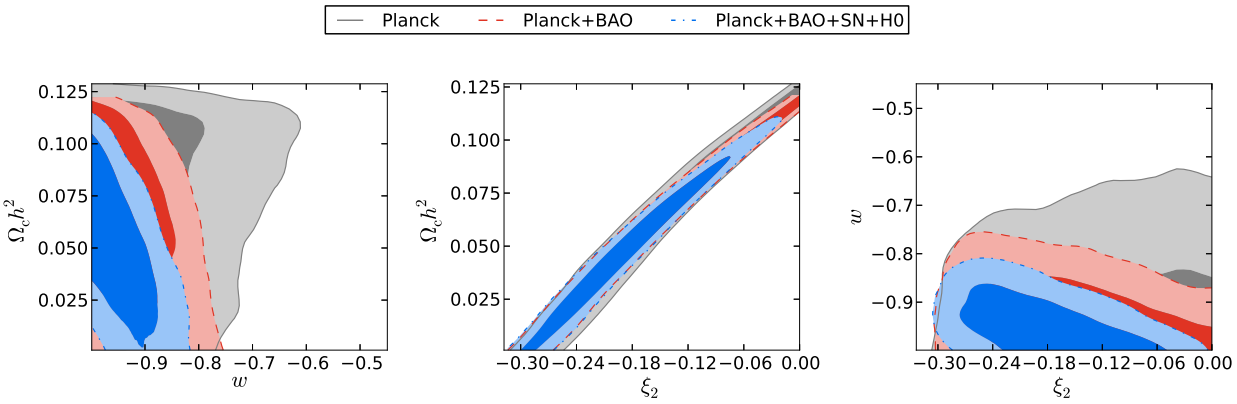

Fig. 7.3 2-D distribution for selected parameters - Model I.

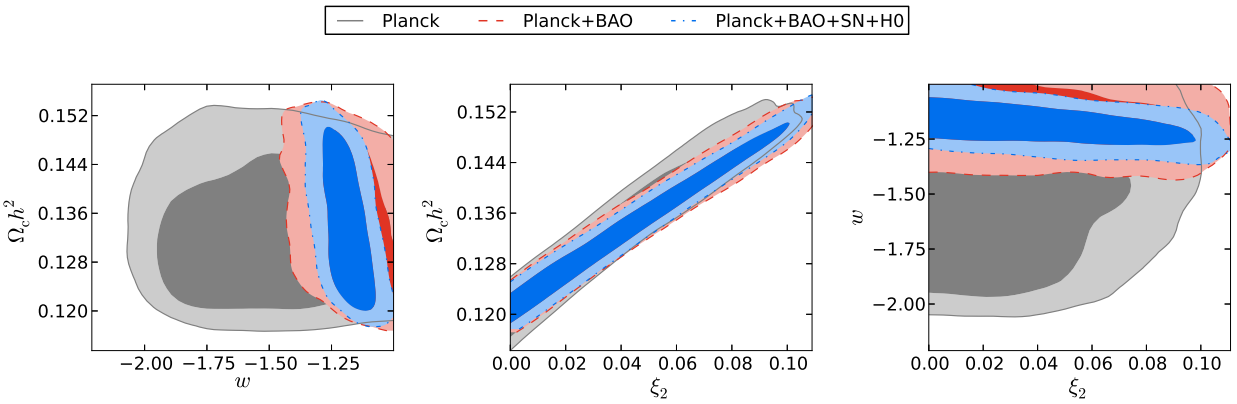

Fig. 7.4 2-D distribution for selected parameters - Model II.

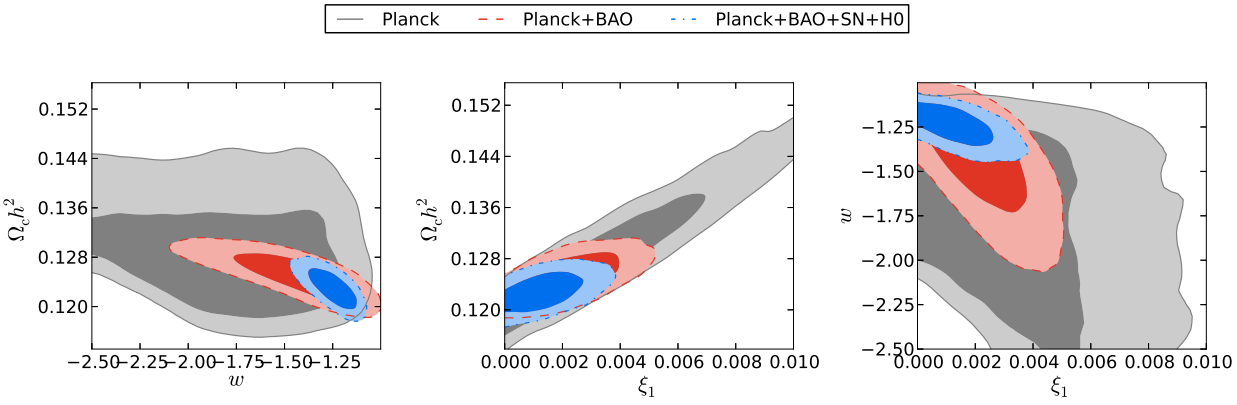

Fig. 7.5 2-D distribution for selected parameters - Model III.

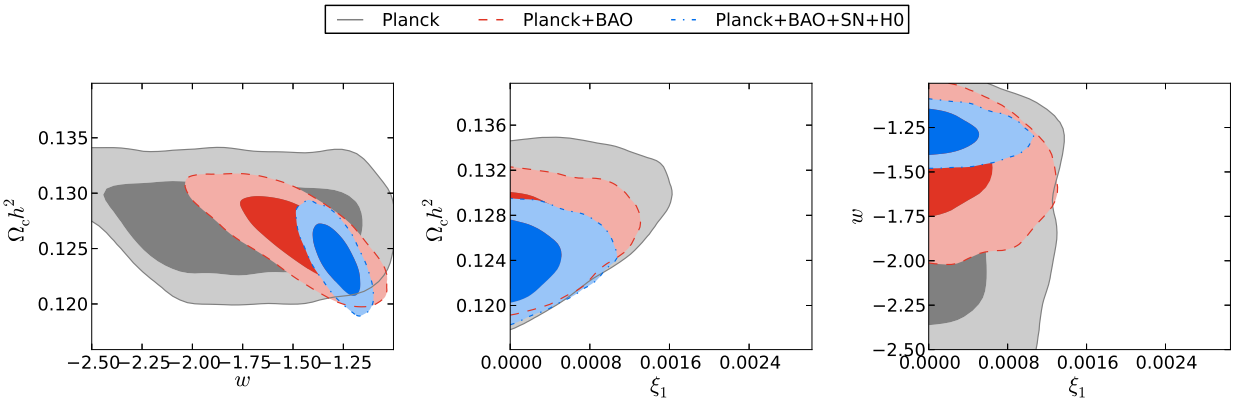

Fig. 7.6 2-D distribution for selected parameters - Model IV.

Chapter 8

Evidence for interacting dark energy from BOSS

8.1 Introduction

One of the biggest challenges in cosmology and astrophysics nowadays is to understand the nature of the two most abundant components of the Universe: dark energy and dark matter. These are usually described as two independent components where dark matter is responsible for most of the nonrelativistic matter in the Universe and where dark energy is responsible for the late time acceleration of our Universe, which is described by a cosmological constant in the Λ-cold-dark-matter (ΛCDM) model. This standard model is widely used to describe the cosmological evolution of the Universe [174], and it fits very well the current observational data. However, this model has some theoretical and observational challenges (see, e.g., Ref. [219]) that open the way for alternative models of dark energy.

Recently, the Baryon Oscillation Spectroscopic Survey (BOSS) experiment of the Sloan Digital Sky Survey (SDSS) Collaboration presented new evidence against the ΛCDM model [169] based on the measurements of the baryon acoustic oscillations (BAO) flux-correlation function of the Lyman-alpha (Ly-α) forest from $158,401$ quasars at high redshifts ($2.1 \leq z \leq 3.5$). Comparatively to previous experiments, they provide the line of sight and tangential BAO components, and this allows one to determine the angular distance and the Hubble distance independently. Their results indicate a deviation from ΛCDM of the Hubble parameter and of angular distance at an average redshift of 2.34 (roughly 2.5σ and 2.2σ

deviations from Planck+Wilkinson Microwave Anisotropy Probe (WMAP) polarization data and WMAP9+ACT+SPT, respectively). Assuming a ΛCDM Universe, this implies a negative energy density for the dark energy component, $\frac{\rho_{\rm DE}(z=2.34)}{\rho_{\rm DE}(0)} = -1.2 \pm 0.8$, which is 2.5σ away from the expected value. We point out that BOSS is not optimized to observe quasars at such high redshifts. However, if more data or other experiments show that this discrepancy stands, then it would indicate that ΛCDM needs to be revised. Its simplest generalization would consist in allowing for dynamical dark energy (see Ref. [21] for a review), but this would not be enough to fix this discrepancy. In dynamical dark energy models, all matter contents are individually conserved, and so, agreeing with the BOSS result for $H(z = 2.34)$ would require a negative energy density for dark energy [169]. This may lead one to study very exotic forms of dark energy.

A simpler solution is to consider interacting dark energy. Indeed, dark energy could couple to gravity, neutrinos, or dark matter since its effects have only been detected gravitationally. Interaction with baryonic matter (or radiation) has very tight constraints from observations [220] and must be very small or negligible. In this sense, we are interested in models in which dark energy interacts with the dark matter component. In a field theory description of those components, this interaction is allowed and even mandatory [33, 208]. However, the main motivation to introduce such an interaction is to alleviate the coincidence problem, which can be done given an appropriate interaction.

Since the nature of the dark sector is unknown, the study of these coupled dark energy models is challenging. Many different models of this interaction have been studied in the literature from the point of view of either interacting field theory or phenomenology (for a classification of those models, see Ref. [26]). As an example of phenomenological study, one can consider holographic dark energy or a quintessence field interacting with a dark matter fluid [27–31]. There are also attempts to develop Lagrangian models where one postulates an interaction between the scalar field, playing the role of dark energy, and a fermionic field, playing the role of dark matter [32–35] (see, however, Ref. [221]).

Recently, there have been studies of interacting dark energy models in light of new probes [222–225]. However, we note that there has been only little exploration of the consequences of the results from BOSS in the literature [226–228], and these studies do not explore the idea of interacting dark energy and dark matter. Thus, it would be interesting to see what the phenomenological implications from BOSS for interacting dark energy are. Since this model allows for one of the components to decay into the other, we claim that energy flow

from dark energy to dark matter implies a smaller amount of dark matter in the past, thus accommodating for the value of the Hubble parameter at $z = 2.34$ found by BOSS and still maintaining the cosmology today close to ΛCDM. For a first test, we perform a comparison by showing that the observational value of the Hubble parameter from quasars given by the BOSS Collaboration, $H(2.34) = 222 \pm 7$ km s^{-1} Mpc^{-1}, is consistent with the interacting model with a small positive coupling constant. This comparison serves to indicate that the interaction is able to accommodate the BOSS Collaboration result. After that, we perform a full Markov chain Monte Carlo (MCMC) analysis using the new BOSS data together with the Planck data for the interacting model. We show that the constraints on $H(z = 2.34)$ and $D_{\rm A}(z = 2.34)$ for the interacting model are compatible with the values obtained by the BOSS team, showing a slightly better concordance when compared to ΛCDM.

8.2 Model

8.2.1 Theoretical setup

Given the energy conservation of the full energy-momentum tensor, we can suppose that the fluid equations representing dark energy (DE) and dark matter (DM) are not conserved separately. In a Friedmann-Robertson-Walker Universe, we take

$$\begin{aligned} \dot{\rho}_{\rm DM} + 3H\rho_{\rm DM} &= Q_{\rm DM} = +Q\,, \\ \dot{\rho}_{\rm DE} + 3H\left(1+\omega_{\rm DE}\right)\rho_{\rm DE} &= Q_{\rm DE} = -Q\,, \end{aligned} \tag{8.1}$$

and all other components follow the standard conservation equations. In the above equations, $\rho_{\rm DM}$ and $\rho_{\rm DE}$ are the energy densities for dark matter and dark energy, respectively; $\omega_{\rm DE} = p_{\rm DE}/\rho_{\rm DE}$ is the equation of state (EoS) of dark energy, considered constant in this work; and Q indicates the interaction between dark energy and dark matter. One can take the Taylor expansion of the general interaction term $Q(\rho_{\rm DM}, \rho_{\rm DE})$, and thus, it can be represented phenomenologically as $Q \simeq 3H(\xi_1\rho_{\rm DM} + \xi_2\rho_{\rm DE})$, where the coefficients ξ_1 and ξ_2 are to be determined by observations [31, 194]. Following our definition, if $Q > 0$, then dark energy decays into dark matter, and for $Q < 0$, the energy flow is in the opposite direction. The first case is consistent with the requirement that the energy density for dark energy must be of the same order as the one for dark matter for a longer period of time in order to alleviate the coincidence problem.

The validity of the phenomenological interacting dark energy model was studied in Ref. [29], where it was found that the curvature perturbations can always be stable when the interaction is proportional to the energy density of dark energy, i.e. when $\xi_1 = 0$ while $\xi_2 \neq 0$, except when $\omega = -1$, which represents a central singularity in the cosmological perturbation equations. This is true for a constant EoS within the ranges $-1 < \omega_{\rm DE} < 0$ (we call this model I) and $\omega_{\rm DE} < -1$ (we call this model II). If the interaction term is proportional to the dark matter energy density, i.e. $\xi_1 \neq 0$ while $\xi_2 = 0$, then the curvature perturbations are only stable when $\omega_{\rm DE} < -1$ (we call this model III). The models are summarized in Table 8.1.

Table 8.1 Interacting dark energy models considered in this chapter.

Model	Q	DE EoS
I	$3\xi_2 H\rho_{\rm DE}$	$-1 < \omega < 0$
II	$3\xi_2 H\rho_{\rm DE}$	$\omega < -1$
III	$3\xi_1 H\rho_{\rm DM}$	$\omega < -1$

In this framework, the Friedmann equations can be written as

$$H^2(z) = \frac{8\pi G}{3}\left[\rho_{\rm DE}(z) + \rho_{\rm DM}(z) + \rho_{\rm b}(z)\right] , \tag{8.2}$$

$$\dot{H} = -4\pi G\left[\rho_{\rm DM}(z) + \rho_{\rm b}(z) + (1+\omega_{\rm DE})\rho_{\rm DE}(z)\right] , \tag{8.3}$$

where we are considering a Universe composed of only dark energy, dark matter, and baryons ($\rho_{\rm b}$). We will use these equations to construct the Hubble parameter for each of the interacting models and compare it with the Hubble parameter inferred from the BOSS quasar data in the next subsection.

For models I and II, the energy densities for dark energy and dark matter behave as [30]

$$\begin{aligned}\rho_{\rm DE} &= (1+z)^{3(1+\omega_{\rm DE}+\xi_2)}\rho^0_{\rm DE}\,,\\ \rho_{\rm DM} &= (1+z)^3\\ &\quad\times\left\{\frac{\xi_2\left[1-(1+z)^{3(\xi_2+\omega_{\rm DE})}\right]\rho^0_{\rm DE}}{\xi_2+\omega_{\rm DE}} + \rho^0_{\rm DM}\right\} ,\end{aligned} \tag{8.4}$$

where the superscript 0 indicates quantities measured today. The baryonic density is given by the standard expression, proportional to $(1+z)^3$. For model III, the evolution of the

energy densities is given by [30]

$$\rho_{\rm DE} = (1+z)^{3(1+\omega_{\rm DE})}\left(\rho^0_{\rm DE} + \frac{\xi_1\rho^0_{\rm DM}}{\xi_1+\omega_{\rm DE}}\right) - \frac{\xi_1}{\xi_1+\omega_{\rm DE}}(1+z)^{3(1-\xi_1)}\rho^0_{\rm DM}\,,$$
$$\rho_{\rm DM} = \rho^0_{\rm DM}(1+z)^{3-3\xi_1}\,. \tag{8.5}$$

One can see from these equations that if there is an energy flow from dark energy to dark matter (i.e., if the coupling constant is positive), then the energy density for dark matter is always smaller than what one would expect in the standard ΛCDM model. Since $\rho_{\rm DM}$ is the dominant contribution in the Friedmann equations at higher redshifts and since observations indicate that the Universe is well explained by the ΛCDM model at low redshifts (e.g., Ref. [174]), one can see from Eq. (8.3) that the interaction implies a smaller Hubble parameter in the past in comparison with ΛCDM, when H_0 is held fixed and for a positive coupling constant.

Furthermore, this mildly helps alleviate the coincidence problem (the fact that we do not understand why the energy densities of dark energy and dark matter are so close today). As it can be seen in Ref. [229], a positive coupling constant implies that the quantity $r \equiv \rho_{\rm DM}/\rho_{\rm DE}$ decreases at a slower rate in the interacting model than in the ΛCDM model. This makes the energy density of dark energy closer to that of dark matter in the past, giving us a better understanding of their closer values today.

8.2.2 Hubble parameter at $z = 2.34$

In order to gain some intuition before performing the proper statistical analysis, let us see whether the measured value of the Hubble parameter by the BOSS Collaboration, $H(2.34) = 222 \pm 7$ km s^{-1} Mpc^{-1}, can be accommodated by the phenomenological interacting models introduced above. From this perspective, we compare the Hubble parameter constructed theoretically with its observational value at $z = 2.34$.

In order to compute the value of the Hubble parameter from Eqs. (8.2), (8.4), and (8.5), one needs several cosmological parameters such as H_0, $\Omega^0_{\rm DE}$, $\Omega^0_{\rm DM}$, and $\Omega^0_{\rm b}$. The standard ΛCDM parameters found from the Planck analysis were used by the BOSS Collaboration

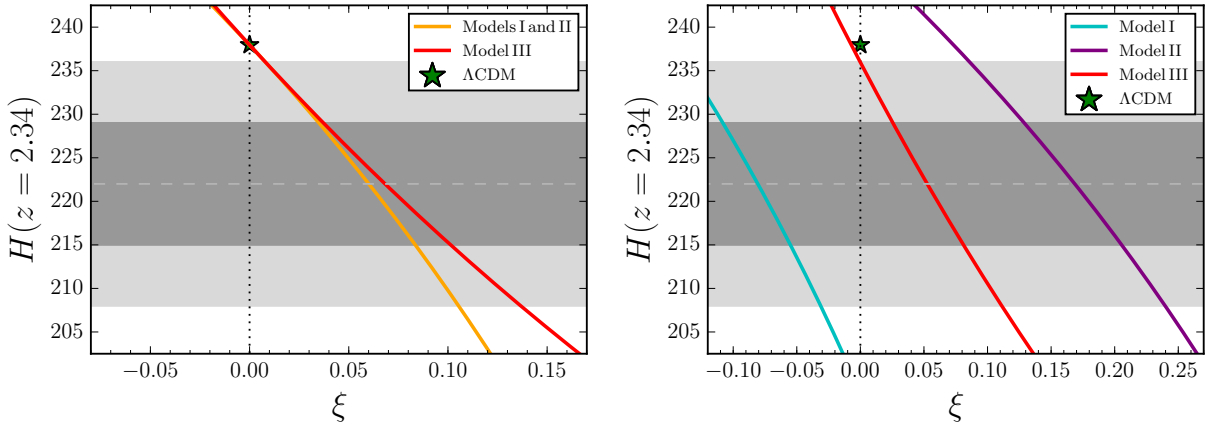

Fig. 8.1 We plot $H(z = 2.34)$ as a function of the coupling ξ (corresponding to ξ_2 for models I and II and to ξ_1 for model III). The interacting models correspond to the colored lines since they depend on the free parameter ξ, the coupling constant. The left panel represents the Hubble parameter calculated using the cosmological parameters from Table 8.2 and with $\omega_{\rm DE} = -1$. The right panel represents $H(2.34)$ using the parameters found in Ref. [38] (including $\omega_{\rm DE} \neq -1$; see Table X for model I, Table XI for model II, and Table XII for model III) obtained from Planck+BAO+SnIa+H_0. The dashed gray line is the BOSS measured value of $H(2.34) = 222 \pm 7$ km s^{-1} Mpc^{-1}, and the shaded areas represent 1σ and 2σ deviations from this average. For the sake of comparison, the green star represents $H(2.34) = 238$ km s^{-1} Mpc^{-1}, the value expected for ΛCDM given the cosmological parameters in Table 8.2.

(listed in Table 8.2). We first use these parameters and the dark energy EoS set to[1] $\omega_{\rm DE} = -1$ to construct $H(z)$, and we show the resulting Hubble parameter at $z = 2.34$ with respect to the coupling constant ξ in the left panel of Fig. 8.1. Alternatively, in the right panel of Fig. 8.1, we use the adjusted cosmological parameters found in Ref. [38] (including $\omega_{\rm DE} \neq -1$) from the analysis of the interacting models using Planck, BAO, type Ia supernovae (SnIa), and H_0 data. The goal of using different sets of cosmological parameters is to see if the parameters adjusted to the interacting models yield a different prediction than the parameters adjusted to ΛCDM.

We recall that the BOSS Collaboration measured $H(2.34) = 222 \pm 7$ km s^{-1} Mpc^{-1}, and this is indicated by the dashed gray line and by the 1σ and 2σ shaded areas in Fig. 8.1. In comparison, standard ΛCDM cosmology predicts $H(2.34) \approx 238$ km s^{-1} Mpc^{-1} when using the cosmological parameters of Table 8.2. This is represented by the green star in Fig. 8.1, which lies outside the 2σ measurement from BOSS. In the left panel of Fig. 8.1, all the

[1]The interacting models are not well defined at the perturbative level if $\omega_{\rm DE} = -1$, so we view $\omega_{\rm DE} = -1$ as a limit in this case.

Table 8.2 Cosmological parameters used by the BOSS Collaboration [169].

Parameter	Best fit	σ
h	0.706	0.032
$\Omega^0_{\rm DM}h^2$	0.143	0.003
$\Omega^0_{\rm DE}$	0.714	0.020
$\Omega^0_{\rm b}h^2$	0.02207	0.00033

curves that correspond to interacting dark energy pass through the green star at $\xi = 0$. This is because when the coupling constant vanishes there is no interaction left, and we recover ΛCDM (since we set $\omega_{\rm DE} = -1$). We also note that model I and model II correspond to the same curve, because in the limit where $\omega_{\rm DE} = -1$, they correspond to the same model (recall Table 8.1). In the right panel, we see that allowing for $\omega_{\rm DE}$ different than -1 can significantly alter the prediction for $H(z = 2.34)$. Yet, all the curves can be in accordance with the Hubble parameter inferred by BOSS given a nonzero coupling constant. Comparing the left and right panels for model I, we notice that different cosmological parameters require a different sign for the coupling constant ξ in order to match the BOSS result. This indicates that model I may not be fully robust at explaining the observed value of $H(z = 2.34)$ from BOSS. For models II and III, we see that the theory can easily be within the 1σ shaded area for a positive coupling constant in both panels. We notice that in order for the $H(2.34)$ theoretical value to match the BOSS measurement, the values of the coupling constant have to be larger in the right panel where the cosmological parameters were adjusted to Planck+BAO+SnIa+H_0 data using the interacting models.

At this point, Fig. 8.1 provides us with indications that a positive coupling constant allows one to explain in a very simple way a smaller value of the Hubble parameter in the past, which is not possible with ΛCDM or dynamical dark energy and without requiring a very exotic dark energy component. The fact that we obtain a positive coupling constant for some models is interesting, since it is precisely positive values that help alleviate the coincidence problem. Thus, this model gives a natural explanation for the energy densities of the dark components at low redshifts and also at high redshifts since they may explain the BOSS data.

This gives us evidence that the interacting dark energy model has the required features to be able to explain the different cosmological evolution shown by the BOSS Collaboration at higher redshifts. However, this difference from ΛCDM dynamics is also encoded in the

angular distances, as inferred by the BAO measurement. We now compare the results for these parameters by performing a global fit analysis of the interacting model with the currently available data.

8.3 Analysis

8.3.1 Methodology

Now that we see some evidence that the interacting dark energy models can explain the deviation from ΛCDM observed by BOSS, we perform a Bayesian statistical analysis of those models with the Planck and BOSS Ly-α quasar data. We wish to compare the interacting dark energy models presented here against ΛCDM and test their predictions with the addition of the new BOSS data. In order to achieve this, we perform a global fit by running the CosmoMC package [161], a publicly available code that performs an MCMC parameter sampling. To include the interaction between dark energy and dark matter, we modify the Boltzmann code CAMB [160] by adding the coupling constants ξ_2 for model II and ξ_1 for model III and by adding the constant dark energy EoS to the baseline ΛCDM parameters used by Planck [174]. From now on, we will omit model I from the analysis since this model showed us it was not very good to explain the new BOSS data. Also, this model does not help alleviate the coincidence problem. Model I will be explored in more detail in a follow-up paper.

The goal of this work is to compare the results of our global fit of the cosmic distances and expansion rates for the interacting models with the results obtained by the BOSS Collaboration. We also want to derive parameter constraints using cosmic microwave background (CMB) and BAO data, testing the sensitivity of the parameters and in the total goodness of fit when we include the new BAO data from higher redshifts. The novelty of this work is in the BAO data that we use. The BOSS Collaboration was the first team to measure the BAO from the autocorrelation of the quasar Ly-α forest for higher redshifts. We use the autocorrelation measurements from the DR11 catalog from the BOSS experiment of SDSS which contains $158,401$ quasars in the redshift range $2.1 \leq z \leq 3.5$ [169]. From the same volume, cross-correlation of quasars with the Ly-α absorption forest [170] was obtained for the same redshift range. We are able to use both sets of data, since those can be considered as independent, given that the fluctuations in the measurements are dominated by different

sources of systematics and not by cosmic variance. This analysis can be made by using the baofit software provided by the BOSS Collaboration and the χ^2 surfaces provided for each one of those measurements[2].

For our global fit of the interacting dark energy models, we used the Planck 2013 TT power spectrum in both the low-ℓ ($2 \leq \ell < 50$) and high-ℓ ($50 \leq \ell \leq 2500$) regimes. Together with the Planck data, we include the polarization measurements from the nine-year WMAP [165], the low-ℓ ($\ell < 32$) TE, EE, and BB likelihoods. In our first analysis, to illustrate the tension in the distance measurements between the BOSS measurement and our global fit using Planck data, we combine the autocorrelation and cross-correlation χ^2 surfaces provided by the BOSS Collaboration.

We also perform a joint analysis, where we include in the CosmoMC analysis the likelihood of the BOSS quasar Ly-α forest at $z = 2.34$. We can combine this new BAO data set with the CMB data sets since they are completely independent. This was made in a very conservative way by inserting the two sets of Gaussian likelihoods constructed with the best fit values of $(D_{\rm A}(z = 2.34)/r_{\rm d}, D_H(z = 2.34)/r_{\rm d})$ for the autocorrelation and cross-correlation given in Refs. [169, 170]. This appears to be a good choice, given that the study of BAO from Ly-α is a novel field[3].

We used flat priors within the Planck 2013 ranges for all the "vanilla" ΛCDM parameters [174]. The coupling constants[4] and dark energy EoS also received flat priors with $\xi_2 \in [0,\ 0.4[$ for model II, $\xi_1 \in [0,\ 0.01]$ for model III, and $\omega \in [-2.5,\ -1.001]$ for both models. We recall that we cannot allow for $\omega = -1$ since this represents a singularity in the perturbation equations. The priors are summarized in Table 8.3.

Table 8.3 Priors for the parameters of the interacting dark energy models. We recall that the definition of the different models is summarized in Table 8.1.

Model	Prior on ω	Prior on ξ
II	[-2.5 , -1.001]	[0 , 0.4[
III	[-2.5 , -1.001]	[0 , 0.01]

[2]Available at `http://github.com/deepzot/baofit/`.

[3]Although this is a novel field, Ref. [169] claims that the results are robust according to a consistency check using mock catalogs.

[4]The coupling constants are expected to be small and positive, for models II and III, from the previous analysis of Ref. [38]. This was also indicated by the analysis in Fig. 8.1. These results motivated our choice of priors for the interacting dark energy parameters.

8.3.2 Results

We wish to compare the constraints in $D_{\rm A}(z=2.34)/r_{\rm d} \times D_H(z=2.34)/r_{\rm d}$ found by the BOSS Collaboration with the global fits of the interacting dark energy models. We present these results in Fig. 8.2. The black contour curves show the combined contours from the BOSS data for the autocorrelation and cross-correlation[5], given that those data are independent.

First, we perform the analysis using only CMB data for the ΛCDM and interacting dark energy models. The constraints are shown by the blue contours in Fig. 8.2 for models II and III. We show for comparison the ΛCDM best fit values (green lines), where we obtain results compatible with Ref. [169], which confirms that ΛCDM differs from the BOSS combined contours by at least 2σ. When we test the interacting models (blue contours), this difference is reduced, and we can see that the contours overlap with the 2σ region of the BOSS combined data. Model II, for which we find[6] $D_H/r_{\rm d} = 8.72(8.73)^{0.09}_{0.05}$ and $D_{\rm A}/r_{\rm d} = 11.69(11.63) \pm 0.08$, shows the biggest overlap with the BOSS results (1.5σ and 1.7σ for $D_H/r_{\rm d}$ and $D_{\rm A}/r_{\rm d}$, respectively). The very elongated contours of model III imply that this conclusion is less strong in this case.

Although we show an apparent better concordance in comparison with the marginal overlap that ΛCDM presents for $D_{\rm A}(z=2.34)/r_{\rm d} \times D_H(z=2.34)/r_{\rm d}$, this does not represent an improvement in the fit, since the addition of extra parameters in the model can be the responsible for that. We can see the same type of not-statistically-significant improvement for ωCDM and other dynamical dark energy models in Ref. [226]. If you compare the constraints of our model II with the ones for ωCDM at $z = 2.34$ (see Fig. 7 of Ref. [226]), you can see that those contours almost overlap, showing a similar concordance with the new BOSS data.

Following that, we perform a joint analysis of the BOSS quasar Ly-α data together with the CMB data. We wish to compare the improvement of the fit when including the new BOSS data. Our results indicate that ΛCDM is not sensitive to the inclusion of this data set (BOSS quasar Ly-α data), and therefore it cannot accommodate the change in the Hubble parameter at high redshift. This shows a tension between those data sets.

The global fit of all the parameters of the interacting models reveals that the best fit values

[5] These contours are the same as the black contour curves that one can find in Fig. 13 of Ref. [169].
[6] Best fit values are presented inside brackets.

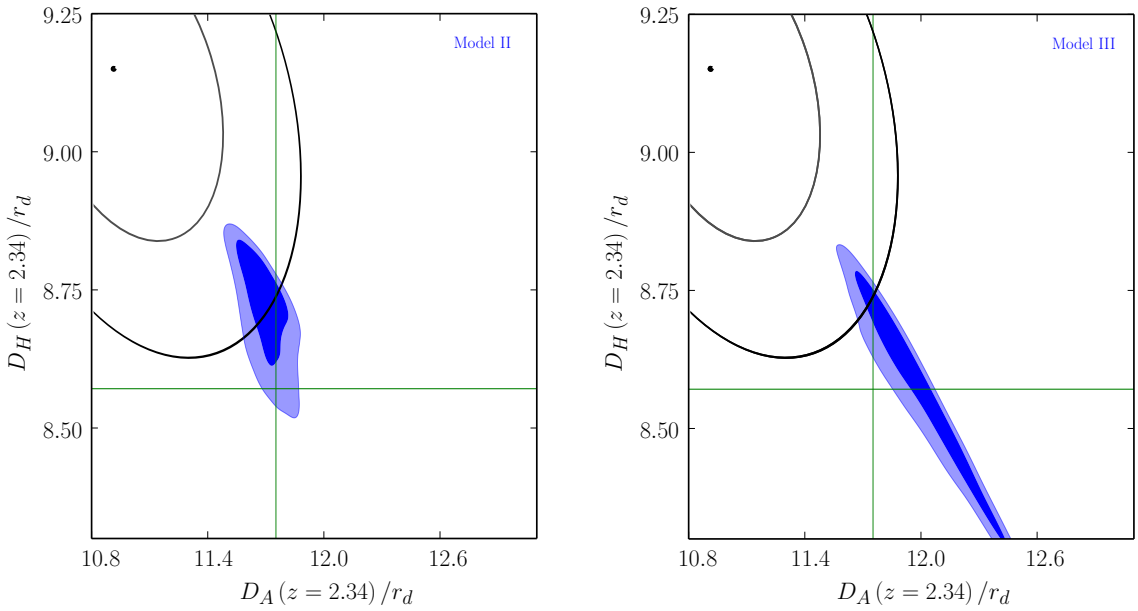

Fig. 8.2 Plot of the 68.3% and 95.5% likelihood contours in $D_{\rm A}(z=2.34)/r_{\rm d} \times D_H(z=2.34)/r_{\rm d}$ comparing the BOSS combined (autocorrelation and cross-correlation) contour in black with the results for the interacting models from the runs using Planck data in blue. Interacting model II is shown in the left panel and model III in the right panel. The green lines show the best fit values for ΛCDM.

of the six vanilla ΛCDM parameters are compatible with the ones obtained by Planck [174], except for model I, where the values for the density of matter show they are not in agreement with the Planck value. We use $\Delta\chi^2_{\rm eff}$ to quantify the improvement in the maximum likelihood of the interacting dark energy models using only Planck data in comparison to when we combine it with the likelihood from the BOSS team quasar data. We found $\Delta\chi^2_{\rm eff}$ to be -0.04, -2.88, and -1.85, for models I, II and III, respectively. Although these improvements are not statistically significant, they indicate that the interacting models, and especially model II, are mildly favored by the data. Another test that also shows that the improvement between the runs is not statistically significant is the reduced χ^2, computed for all models. This test takes into account that the interacting dark energy models have two extra degrees of freedom, in comparison with the ΛCDM model. The difference in the reduced χ^2 between the interacting models and ΛCDM is not significant; e.g., model II presents the biggest "improvement" of the order of 10^{-5}. However, one needs to be very careful when using an improvement diagnostic like $\Delta\chi^2_{\rm eff}$ since the best fit values in CosmoMC may not be fully

trustworthy and since this result could come from statistics overfitting the noisy data [230].

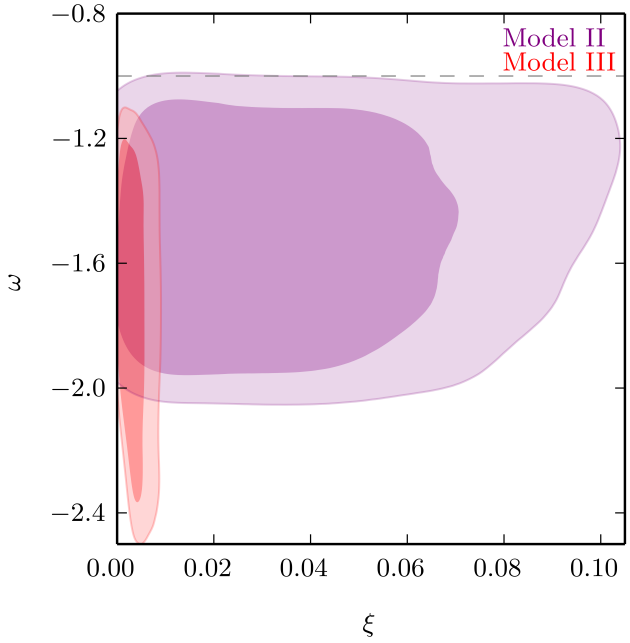

Fig. 8.3 Contour plot of the EoS for dark energy (ω) vs the coupling constant between dark energy and dark matter (ξ). In purple, we present the interacting model II, and in gray, we present the interacting model III fitted to the Planck data. The cosmological constant Λ of ΛCDM corresponds to $\omega = -1$, and it is depicted by the dashed black horizontal line.

In the MCMC analysis of the interacting models, we also obtained the adjusted values of the coupling constants. As was shown in Ref. [38], using only the Planck data is not sufficient to fully constrain the coupling constants. We note that we obtain the same result here, even with the inclusion of the BOSS quasar data: we find $\xi_2 < 0.045\,(0.048)$ for model II and $\xi_1 < 0.0016\,(0.0015)$ for model III. The upper bound on the coupling constant for model II is close to the ones predicted in Sec. II-B (see Fig. 8.1). Indeed, the corresponding Hubble parameters that result from the MCMC analysis are $H(2.34) = 232(231) \pm 2\,\mathrm{km/s/Mpc}$ for model II and $H(2.34) = 234(234)^{2}_{3}\,\mathrm{km/s/Mpc}$ for model III, a little bit more than 1σ away from the BOSS result[7], resulting in a reduced tension compared to ΛCDM. This indicates that the interacting models are good candidates to explain the observed deviation from ΛCDM from high-z BAO probes. The upper bound on the coupling constant for model III is

[7]We would like to stress that $H(z)$ is a model-dependent quantity, while D_H/r_d is not. It is in this context that we compare our results with BOSS. However, since we find that the fitted values for r_d are approximately equal to what one expects in ΛCDM (given the use of the Planck data), we can still compare the Hubble parameter values for the interacting models with the BOSS result.

much smaller than expected from Fig. 8.1. Still, it represents an improvement over ΛCDM in explaining the BOSS results as seen from Fig. 8.2, although to a smaller extent than model II.

The upper bounds found for the coupling constants are compatible with small positive values. Although we cannot exclude the possibility that the coupling constants are zero with the data set used, we can see from the constraints obtained for the EoS of dark energy that our models are not consistent with ΛCDM. The EoS for dark energy obtained in the MCMC analysis are the following: considering only Planck data, $\omega = -1.51(-1.55)^{+0.32}_{-0.30}$ for model II and $\omega = -1.75(-1.668)^{+0.46}_{-0.29}$ for model III. We can also see the constraints in the $\omega \times \xi$ plot, presented in Fig. 8.3. The dashed black horizontal line represents the value of the dark energy EoS for ΛCDM, $\omega = -1$. These contours show a small preference for $\omega < -1$ rather than $\omega = -1$ given the priors, $\omega = [-2.5\,,\,-1.001]$, with model II showing a slightly tighter constraint than the prior range. This result should be interpreted carefully since our prior is very close to -1 (but it is not including -1), and there can be boundary effects that might not be taken into account. Also, we have a large degeneracy between ω and ξ.

A more detailed analysis will be presented in a follow-up paper where we will combine this analysis with different cosmological probes, aiming at fully constraining the coupling constant of the interacting models.

8.4 Conclusions

In this chapter, we explored the consequences of interacting dark energy in light of the recent results by the BOSS experiment. The BOSS data indicate that the Hubble parameter at $z = 2.34$ is smaller than what one would expect from the standard ΛCDM model, something that cannot be explained by simple dynamical dark energy models such as quintessence. Our results suggest that interacting dark energy can naturally explain the BOSS data without introducing exotic forms of dark energy., although further studies are necessary.

We tested three different phenomenological models of interacting dark energy. First, we computed the theoretical value of the Hubble parameter at $z = 2.34$ for different sets of cosmological parameters. Models II and III showed they were in good agreement with the observations for a small positive coupling constant. Furthermore, such a positive coupling constant can help alleviate the coincidence problem. Model I was omitted from the analysis since it did not contribute to reducing the tension with the BOSS data, and also, in general,

it does not help relieve the coincidence problem.

We then performed a global fit of those models given the Planck 2013 and BOSS quasar Ly-α data. This showed that models II and III present a bigger overlap with the BOSS Collaboration results than what ΛCDM achieves. However, this improvement and also the improvement in the χ^2 when we made the joint analysis with CMB and BOSS likelihoods do not seem to justify the inclusion of extra parameters in the model as done by the interacting models. In this analysis, we can also see from the EoS obtained that those models are marginally different than ΛCDM. Yet, the results still suggest that the interacting dark energy models presented in this chapter can be used to explain the deviations from ΛCDM found in high-z BAO, and they represent a simpler solution than invoking exotic dark energy models.

In order to further constrain interacting dark energy models, one could refine the analysis done in this work by using more data sets and by combining the BOSS data with other observations. A more detailed analysis of the global fit of those models with the inclusion of BOSS data is the topic of a follow-up paper that is currently in preparation. We also need improvements in the BAO data at high redshifts. For models that allow the Hubble parameter to change with time such as interacting dark energy and other dynamical dark energy models (e.g., see Ref. [226]), we can see that the inclusion of the BAO data set changes considerably the results, indicating that this new data set is robust. However, with the use of only high-redshift BAO data, we are still not able to statistically differentiate between models of dark energy. New large scale structure surveys, like the JPAS telescope [36], will be able to reproduce and improve the BAO measurements at high redshifts since this instrument is supposed to be optimized to measure quasars at high redshifts compared to previous experiments [231]. Other large scale structure new windows of observation, like the 21 cm emission line from neutral hydrogen, will also contribute in the future for constraining dark energy [232]. Interacting dark energy models might also help alleviate the tension between other large-scale structure data sets and Planck such as, for example, cosmic shear probes from CFHTLenS [233, 234].

Chapter 9

Conclusion

This thesis presented works developed with the aim of solving some of the most outstanding problems in cosmology: the singularity problem and the dark energy mystery. We approached these problems by introducing novel theoretical frameworks, new models and by using cosmological observations.

The first problem we studied was the singularity problem, that plagues many of the bouncing models of the universe. Since our mathematical descriptions break down near the singularity, we do not know how to treat the evolution of perturbations when a singularity is present. This makes it hard to make precise predictions and to compare these with current observations. In the absence of a quantum theory of gravity, this problem is very challenging. We propose the use of a new tool that provides a non-perturbative description of string theory, the AdS/CFT correspondence, in order to resolve the singularity and evolve the perturbations in its presence.

In our first work we develop the formalism for the evolution of perturbations of a test scalar field in an AdS space-time that contains a space-like singularity. In the regions close to the singularity, we evolve the perturbations in the weakly coupled boundary field theory with a regularized coupling. We find that the momentum dependence of the perturbations after they cross the singularity remains unchanged. However, particle production occurs.

In our second work, we use this formalism to treat the curvature perturbation, which is the gauge invariant quantity that is related to the perturbations of density responsible for the formation of the large scale structure. This procedure is simplified by the choice of a convenient gauge, and the results for the curvature perturbations are similar to the ones for

a test scalar field.

Those works provide an initial framework for the research program of using the AdS/CFT correspondence to treat perturbations in a singular bouncing cosmology. This framework was already applied to different space-times, e.g. [235].

The second problem we discuss in this thesis is the nature of dark energy. Dark energy is proposed as a possible mechanism to explain the current accelerated expansion of the universe, but the properties of this component are still unknown. For that reason, there are in the literature a huge number of models that invoke different mechanisms devoted to explaining this period of accelerated expansion. An equally huge effort has been made by observational cosmologists in order to measure the properties of dark energy in the hopes of pinpointing the nature of the dark energy component. In the two works presented here we explore one of these models, the interacting dark energy/dark matter model, and test how well we can determine its parameters given the most recent and precise cosmological data available.

The interacting dark energy model imposes a phenomenological interaction between dark energy and dark matter, introducing two extra parameters to the standard ΛCDM model. In our work we find constraints on the two extra parameters, the coupling and the equation of state of dark energy, together with the 6 baseline ΛCDM parameters using data from CMB experiments (*Planck* and WMAP), BAO, type Ia supernovaes, and local measurements of H_0, for the first paper; and we add the new high redshift data from the Lyα emission from quasars from the BOSS (SDSS) collaboration, in the second paper.

In the first work, we can see that the interacting dark energy model presents a good agreement with observations, especially when we combine all the data sets. We change the priors adopted and conditions for neutrinos for each run to see how this impacts the cosmological parameters. We obtained a positive coupling constant for most of the tested models, which helps alleviate the coincidence problem. Although there is a degeneracy between the equation of state of dark energy and the Hubble parameter, in our analysis Models II, III and IV presented a possibility to relax the tension of the Hubble parameter between the Planck and the HST measurements.

If dark energy is a dynamical variable and not a cosmological constant, data from different redshifts is where the time dependence of dark energy will be manifest. However, such data is still not available, since higher-z objects are fainter and harder to see. The BOSS collaboration presented the first measurement of the Hubble parameter and the angular

distance for higher redshifts, $z = 2.34$. In this measurement they found a deviation from the ΛCDM prediction. Our second work aimed to see if the interacting dark energy model could be an alternate explanation for this measurement, since it has a dynamical dark energy component. We found that our models have values of $H(z - 2.34)$ and $D_A(z = 2.34)$ closer to the ones found by the BOSS team. Our model also presents a good fit to this new data set.

In general, the interacting DE models are a alternative to pure dark energy, since they yield a good agreement with cosmological data. However, as in all models in the literature, it does not present a better fit than ΛCDM with a good statistical significance, especially one that justifies the inclusion of two extra parameters. More observations are necessary to test this and all the other models of dark energy. We are living in a particularly good period for this study, since the large scale structure data from current and future experiments will revolutionize this search, measuring the properties of dark energy at the percent level. I am involved in two of those future probes, the Javalambre-Physics of the Accelerated Universe Astrophysical Survey [36] and the BINGO telescope [37].

Appendix A

Analysis in Terms of the Original Variables

The kinetic energy term of the gauge fields on the boundary is not of canonical form. This was the motivation for rescaling the gauge field. The rescaling factor, however, diverges at $t = 0$. Hence, we might worry that the divergence of the rescaled gauge field $\tilde{A}_\mu$ which we found is a result of this rescaling, and that the evolution in terms of the original variables A_μ might be better behaved.

In fact, the equation of motion for the fluctuation of the original variable is

$$\left(-\partial_t^2 + \frac{\sqrt{3}}{t}\partial_t + \partial_i\partial^i\right)A_j \;=\; 0\,, \tag{A.1}$$

which has Fourier mode solutions

$$A_j(kt) \;=\; t^{\nu_g}\left(c_+ J_{\nu_g}(kt) + c_- Y_{\nu_g}(kt)\right). \tag{A.2}$$

The first mode goes to zero at $t = 0$ whereas the second mode approaches a finite value. Hence, there is indeed no divergence in the solutions. However, the first mode has a branch cut at $t = 0$. Hence, matching conditions are still required in order to evolve the solutions from negative to positive values of t.

In the spirit of the AdS/CFT correspondence it would be nice not to have to impose any cutoffs in the matching calculation. This could have been expected since the gauge theory becomes free at $t = 0$. Indeed, there is a matching of the two modes at $t = 0$ for which there

is no particle production at all (in terms of the rescaled variables this matching corresponds to having the derivative of $\tilde{A}_{mu}$ match to its inverse between $t = \xi$ and $t = -\xi$). This matching, however, does not correspond to what is done in standard quantum mechanics problems and it misses the particle production which is expected on physical grounds.

Hence, it appears that a matching prescription is needed. An explicit calculation shows if the matching prescription is taken to be the same as the one we used for the rescaled variables, that then the matching calculation calculation in terms of the original variables leads to the same result as that obtained using the rescaled field.

References

[1] Alan H. Guth. The Inflationary Universe: A Possible Solution to the Horizon and Flatness Problems. *Phys. Rev.*, D23:347–356, 1981.

[2] R. Brout, F. Englert, and E. Gunzig. The Creation of the Universe as a Quantum Phenomenon. *Annals Phys.*, 115:78, 1978.

[3] Alexei A. Starobinsky. A New Type of Isotropic Cosmological Models Without Singularity. *Phys. Lett.*, B91:99–102, 1980.

[4] K. Sato. First Order Phase Transition of a Vacuum and Expansion of the Universe. *Mon. Not. Roy. Astron. Soc.*, 195:467–479, 1981.

[5] L. Z. Fang. Entropy Generation in the Early Universe by Dissipative Processes Near the Higgs' Phase Transitions. *Phys. Lett.*, B95:154–156, 1980.

[6] Robert H. Brandenberger. The Matter Bounce Alternative to Inflationary Cosmology. 2012.

[7] Steffen Gielen and Neil Turok. Quantum propagation across cosmological singularities. 2016.

[8] Sebastian F. Bramberger, Thomas Hertog, Jean-Luc Lehners, and Yannick Vreys. Quantum Transitions Through Cosmological Singularities. 2017.

[9] Juan Martin Maldacena. The Large N limit of superconformal field theories and supergravity. *Int. J. Theor. Phys.*, 38:1113–1133, 1999. [Adv. Theor. Math. Phys.2,231(1998)].

[10] Sumit R. Das, Jeremy Michelson, K. Narayan, and Sandip P. Trivedi. Time dependent cosmologies and their duals. *Phys. Rev.*, D74:026002, 2006.

[11] Adel Awad, Sumit R. Das, K. Narayan, and Sandip P. Trivedi. Gauge theory duals of cosmological backgrounds and their energy momentum tensors. *Phys. Rev.*, D77:046008, 2008.

[12] Adel Awad, Sumit R. Das, Suresh Nampuri, K. Narayan, and Sandip P. Trivedi. Gauge Theories with Time Dependent Couplings and their Cosmological Duals. *Phys. Rev.*, D79:046004, 2009.

[13] Adel Awad, Sumit R. Das, Archisman Ghosh, Jae-Hyuk Oh, and Sandip P. Trivedi. Slowly Varying Dilaton Cosmologies and their Field Theory Duals. *Phys. Rev.*, D80:126011, 2009.

[14] Chong-Sun Chu and Pei-Ming Ho. Time-dependent AdS/CFT duality and null singularity. *JHEP*, 04:013, 2006.

[15] Chong-Sun Chu and Pei-Ming Ho. Time-dependent AdS/CFT duality. II. Holographic reconstruction of bulk metric and possible resolution of singularity. *JHEP*, 02:058, 2008.

[16] Robert H. Brandenberger, Elisa G. M. Ferreira, Ian A. Morrison, Yi-Fu Cai, Sumit R. Das, and Yi Wang. Fluctuations in a cosmology with a spacelike singularity and their gauge theory dual description. *Phys. Rev.*, D94(8):083508, 2016.

[17] Elisa G. M. Ferreira and Robert Brandenberger. Holographic Curvature Perturbations in a Cosmology with a Space-Like Singularity. *JCAP*, 1607(07):030, 2016.

[18] S. Perlmutter et al. Measurements of Omega and Lambda from 42 high redshift supernovae. *Astrophys. J.*, 517:565–586, 1999.

[19] Adam G. Riess et al. Observational evidence from supernovae for an accelerating universe and a cosmological constant. *Astron. J.*, 116:1009–1038, 1998.

[20] Lauren Anderson et al. The clustering of galaxies in the SDSS-III Baryon Oscillation Spectroscopic Survey: baryon acoustic oscillations in the Data Releases 10 and 11 Galaxy samples. *Mon. Not. Roy. Astron. Soc.*, 441(1):24–62, 2014.

[21] Edmund J. Copeland, M. Sami, and Shinji Tsujikawa. Dynamics of dark energy. *Int. J. Mod. Phys.*, D15:1753–1936, 2006.

[22] Justin Khoury and Amanda Weltman. Chameleon fields: Awaiting surprises for tests of gravity in space. *Phys. Rev. Lett.*, 93:171104, 2004.

[23] Justin Khoury and Amanda Weltman. Chameleon cosmology. *Phys. Rev.*, D69:044026, 2004.

[24] Kurt Hinterbichler, Justin Khoury, Aaron Levy, and Andrew Matas. Symmetron Cosmology. *Phys. Rev.*, D84:103521, 2011.

[25] Philippe Brax, Carsten van de Bruck, Anne-Christine Davis, Baojiu Li, and Douglas J. Shaw. Nonlinear Structure Formation with the Environmentally Dependent Dilaton. *Phys. Rev.*, D83:104026, 2011.

[26] Kazuya Koyama, Roy Maartens, and Yong-Seon Song. Velocities as a probe of dark sector interactions. *JCAP*, 0910:017, 2009.

[27] Luca Amendola. Coupled quintessence. *Phys. Rev.*, D62:043511, 2000.

[28] Bin Wang, Yun-gui Gong, and Elcio Abdalla. Transition of the dark energy equation of state in an interacting holographic dark energy model. *Phys. Lett.*, B624:141–146, 2005.

[29] Jian-Hua He, Bin Wang, and Elcio Abdalla. Stability of the curvature perturbation in dark sectors' mutual interacting models. *Phys. Lett.*, B671:139–145, 2009.

[30] Jian-Hua He and Bin Wang. Effects of the interaction between dark energy and dark matter on cosmological parameters. *JCAP*, 0806:010, 2008.

[31] Jian-Hua He, Bin Wang, and Elcio Abdalla. Testing the interaction between dark energy and dark matter via latest observations. *Phys. Rev.*, D83:063515, 2011.

[32] A. B. Pavan, Elisa G. M. Ferreira, S. Micheletti, J. C. C. de Souza, and E. Abdalla. Exact cosmological solutions of models with an interacting dark sector. *Phys. Rev.*, D86:103521, 2012.

[33] Sandro Micheletti, Elcio Abdalla, and Bin Wang. A Field Theory Model for Dark Matter and Dark Energy in Interaction. *Phys. Rev.*, D79:123506, 2009.

[34] Elcio Abdalla, L. L. Graef, and Bin Wang. A Model for Dark Energy decay. *Phys. Lett.*, B726:786–790, 2013.

[35] Andr A. Costa, Lucas C. Olivari, and E. Abdalla. Quintessence with Yukawa Interaction. *Phys. Rev.*, D92(10):103501, 2015.

[36] N. Benitez et al. J-PAS: The Javalambre-Physics of the Accelerated Universe Astrophysical Survey. 2014.

[37] Richard Battye et al. Update on the BINGO 21cm intensity mapping experiment. 2016.

[38] Andr A. Costa, Xiao-Dong Xu, Bin Wang, Elisa G. M. Ferreira, and E. Abdalla. Testing the Interaction between Dark Energy and Dark Matter with Planck Data. *Phys. Rev.*, D89(10):103531, 2014.

[39] Elisa G. M. Ferreira and Robert Brandenberger. The Trans-Planckian Problem in the Healthy Extension of Horava-Lifshitz Gravity. *Phys. Rev.*, D86:043514, 2012.

[40] Edwin Hubble. A relation between distance and radial velocity among extra-galactic nebulae. *Proc. Nat. Acad. Sci.*, 15:168–173, 1929.

[41] P. A. R. Ade et al. Planck 2015 results. XIII. Cosmological parameters. *Astron. Astrophys.*, 594:A13, 2016.

[42] Adam G. Riess, Lucas Macri, Stefano Casertano, Hubert Lampeitl, Henry C. Ferguson, et al. A 3Space Telescope and Wide Field Camera 3. *Astrophys.J.*, 730:119, 2011.

[43] Hubert Goenner. *Weyl's contributions to cosmology*, pages 105–137. Birkhäuser Basel, Basel, 2001.

[44] D. N. Spergel et al. Wilkinson Microwave Anisotropy Probe (WMAP) three year results: implications for cosmology. *Astrophys. J. Suppl.*, 170:377, 2007.

[45] V. Mukhanov. *Physical Foundations of Cosmology*. Cambridge University Press, Oxford, 2005.

[46] Viatcheslav F. Mukhanov, H. A. Feldman, and Robert H. Brandenberger. Theory of cosmological perturbations. Part 1. Classical perturbations. Part 2. Quantum theory of perturbations. Part 3. Extensions. *Phys. Rept.*, 215:203–333, 1992.

[47] Robert H. Brandenberger. Lectures on the theory of cosmological perturbations. *Lect. Notes Phys.*, 646:127–167, 2004. [,127(2003)].

[48] James M. Bardeen. Gauge Invariant Cosmological Perturbations. *Phys. Rev.*, D22:1882–1905, 1980.

[49] D. H. Lyth. Large Scale Energy Density Perturbations and Inflation. *Phys. Rev.*, D31:1792–1798, 1985.

[50] Richard L. Arnowitt, Stanley Deser, and Charles W. Misner. The Dynamics of general relativity. *Gen. Rel. Grav.*, 40:1997–2027, 2008.

[51] Leonard Susskind. The World as a hologram. *J. Math. Phys.*, 36:6377–6396, 1995.

[52] Gerard 't Hooft. Dimensional reduction in quantum gravity. In *Salamfest 1993:0284-296*, pages 0284–296, 1993.

[53] SHIRAZ MINWALLA. Applications of the ads/cft correspondence. *Pramana*, 79(5):1075–1090, 2012.

[54] Joseph Polchinski. Introduction to Gauge/Gravity Duality. In *Proceedings, Theoretical Advanced Study Institute in Elementary Particle Physics (TASI 2010). String Theory and Its Applications: From meV to the Planck Scale: Boulder, Colorado, USA, June 1-25, 2010*, pages 3–46, 2010.

[55] Horatiu Nastase. AdS-CFT and the RHIC fireball. *Prog. Theor. Phys. Suppl.*, 174:274–285, 2008.

[56] Edward Witten. Anti-de Sitter space and holography. *Adv. Theor. Math. Phys.*, 2:253–291, 1998.

[57] S. S. Gubser, Igor R. Klebanov, and Alexander M. Polyakov. Gauge theory correlators from noncritical string theory. *Phys. Lett.*, B428:105–114, 1998.

[58] Vijay Balasubramanian, Per Kraus, and Albion E. Lawrence. Bulk versus boundary dynamics in anti-de Sitter space-time. *Phys. Rev.*, D59:046003, 1999.

[59] Eric D'Hoker and Daniel Z. Freedman. Supersymmetric gauge theories and the AdS / CFT correspondence. In *Strings, Branes and Extra Dimensions: TASI 2001: Proceedings*, pages 3–158, 2002.

[60] Peter Breitenlohner and Daniel Z. Freedman. Positive Energy in anti-De Sitter Backgrounds and Gauged Extended Supergravity. *Phys. Lett.*, B115:197–201, 1982.

[61] Thomas Hertog and Gary T. Horowitz. Holographic description of AdS cosmologies. *JHEP*, 04:005, 2005.

[62] Neil Turok, Ben Craps, and Thomas Hertog. From big crunch to big bang with AdS/CFT. 2007.

[63] Ben Craps, Thomas Hertog, and Neil Turok. On the Quantum Resolution of Cosmological Singularities using AdS/CFT. *Phys. Rev.*, D86:043513, 2012.

[64] Ben Heidenreich, Matthew Reece, and Tom Rudelius. Weak Gravity Strongly Constrains Large-Field Axion Inflation. *JHEP*, 12:108, 2015.

[65] Jon Brown, William Cottrell, Gary Shiu, and Pablo Soler. On Axionic Field Ranges, Loopholes and the Weak Gravity Conjecture. *JHEP*, 04:017, 2016.

[66] Jon Brown, William Cottrell, Gary Shiu, and Pablo Soler. Fencing in the Swampland: Quantum Gravity Constraints on Large Field Inflation. *JHEP*, 10:023, 2015.

[67] Tom Rudelius. Constraints on Axion Inflation from the Weak Gravity Conjecture. *JCAP*, 1509(09):020, 2015.

[68] Tom Rudelius. On the Possibility of Large Axion Moduli Spaces. *JCAP*, 1504(04):049, 2015.

[69] Robert Brandenberger. Initial conditions for inflation A short review. *Int. J. Mod. Phys.*, D26(01):1740002, 2016.

[70] Nima Arkani-Hamed, Lubos Motl, Alberto Nicolis, and Cumrun Vafa. The String landscape, black holes and gravity as the weakest force. *JHEP*, 06:060, 2007.

[71] David Wands. Duality invariance of cosmological perturbation spectra. *Phys. Rev.*, D60:023507, 1999.

[72] Fabio Finelli and Robert Brandenberger. On the generation of a scale invariant spectrum of adiabatic fluctuations in cosmological models with a contracting phase. *Phys. Rev.*, D65:103522, 2002.

[73] Yi-Fu Cai and Edward Wilson-Ewing. A ΛCDM bounce scenario. *JCAP*, 1503(03):006, 2015.

[74] Chunshan Lin, Robert H. Brandenberger, and Laurence Perreault Levasseur. A Matter Bounce By Means of Ghost Condensation. *JCAP*, 1104:019, 2011.

[75] Damien A. Easson, Ignacy Sawicki, and Alexander Vikman. G-Bounce. *JCAP*, 1111:021, 2011.

[76] Taotao Qiu, Jarah Evslin, Yi-Fu Cai, Mingzhe Li, and Xinmin Zhang. Bouncing Galileon Cosmologies. *JCAP*, 1110:036, 2011.

[77] Robert Brandenberger. Matter Bounce in Horava-Lifshitz Cosmology. *Phys. Rev.*, D80:043516, 2009.

[78] Robert H. Brandenberger and C. Vafa. Superstrings in the Early Universe. *Nucl. Phys.*, B316:391–410, 1989.

[79] Ali Nayeri, Robert H. Brandenberger, and Cumrun Vafa. Producing a scale-invariant spectrum of perturbations in a Hagedorn phase of string cosmology. *Phys. Rev. Lett.*, 97:021302, 2006.

[80] Robert H. Brandenberger, Ali Nayeri, Subodh P. Patil, and Cumrun Vafa. String gas cosmology and structure formation. *Int. J. Mod. Phys.*, A22:3621–3642, 2007.

[81] Costas Kounnas, Herve Partouche, and Nicolaos Toumbas. S-brane to thermal non-singular string cosmology. *Class. Quant. Grav.*, 29:095014, 2012.

[82] Costas Kounnas, Herve Partouche, and Nicolaos Toumbas. Thermal duality and non-singular cosmology in d-dimensional superstrings. *Nucl. Phys.*, B855:280–307, 2012.

[83] Robert H. Brandenberger, Costas Kounnas, Hervé Partouche, Subodh P. Patil, and N. Toumbas. Cosmological Perturbations Across an S-brane. *JCAP*, 1403:015, 2014.

[84] J. L. F. Barbon and E. Rabinovici. AdS Crunches, CFT Falls And Cosmological Complementarity. *JHEP*, 04:044, 2011.

[85] Ben Craps, Frederik De Roo, and Oleg Evnin. Quantum evolution across singularities: The Case of geometrical resolutions. *JHEP*, 04:036, 2008.

[86] Ben Craps, Thomas Hertog, and Neil Turok. Multitrace deformation of the aharony-bergman-jafferis-maldacena theory. *Phys. Rev. D*, 80:086007, Oct 2009.

[87] Michael Smolkin and Neil Turok. Dual description of a 4d cosmology. 2012.

[88] Netta Engelhardt, Thomas Hertog, and Gary T. Horowitz. Holographic Signatures of Cosmological Singularities. *Phys. Rev. Lett.*, 113:121602, 2014.

[89] Netta Engelhardt, Thomas Hertog, and Gary T. Horowitz. Further Holographic Investigations of Big Bang Singularities. *JHEP*, 07:044, 2015.

[90] Netta Engelhardt and Gary T. Horowitz. Holographic Consequences of a No Transmission Principle. *Phys. Rev.*, D93(2):026005, 2016.

[91] Sebastian Fischetti, David Kastor, and Jennie Traschen. Non-Vacuum AdS Cosmologies and the Approach to Equilibrium of Entanglement Entropy. *Class. Quant. Grav.*, 31(23):235007, 2014.

[92] Souvik Banerjee, Samrat Bhowmick, Soumyabrata Chatterjee, and Sudipta Mukherji. A note on AdS cosmology and gauge theory correlator. *JHEP*, 06:043, 2015.

[93] Jose L. F. Barbon and Eliezer Rabinovici. Holographic complexity and spacetime singularities. *JHEP*, 01:084, 2016.

[94] S. Prem Kumar and Vladislav Vaganov. Probing crunching AdS cosmologies. *JHEP*, 02:026, 2016.

[95] S. Prem Kumar and Vladislav Vaganov. Quasinormal modes and holographic correlators in a crunching AdS geometry. *JHEP*, 02:065, 2016.

[96] Adam Bzowski, Thomas Hertog, and Marjorie Schillo. Cosmological singularities encoded in IR boundary correlations. *JHEP*, 05:168, 2016.

[97] Justin Khoury, Burt A. Ovrut, Paul J. Steinhardt, and Neil Turok. The Ekpyrotic universe: Colliding branes and the origin of the hot big bang. *Phys. Rev.*, D64:123522, 2001.

[98] A. Notari and A. Riotto. Isocurvature perturbations in the ekpyrotic universe. *Nucl. Phys.*, B644:371–382, 2002.

[99] F. Finelli. A contracting universe driven by two scalar fields. *Physics Letters B*, 545:1–7, October 2002.

[100] Jean-Luc Lehners, Paul McFadden, Neil Turok, and Paul J. Steinhardt. Generating ekpyrotic curvature perturbations before the big bang. *Phys. Rev.*, D76:103501, 2007.

[101] Evgeny I. Buchbinder, Justin Khoury, and Burt A. Ovrut. New Ekpyrotic cosmology. *Phys. Rev.*, D76:123503, 2007.

[102] Paolo Creminelli and Leonardo Senatore. A Smooth bouncing cosmology with scale invariant spectrum. *JCAP*, 0711:010, 2007.

[103] Ruth Durrer and Filippo Vernizzi. Adiabatic perturbations in pre - big bang models: Matching conditions and scale invariance. *Phys. Rev.*, D66:083503, 2002.

[104] Yi-Fu Cai, Taotao Qiu, Robert Brandenberger, Yun-Song Piao, and Xinmin Zhang. On Perturbations of Quintom Bounce. *JCAP*, 0803:013, 2008.

[105] Yi-Fu Cai, Tao-tao Qiu, Robert Brandenberger, and Xin-min Zhang. A Nonsingular Cosmology with a Scale-Invariant Spectrum of Cosmological Perturbations from Lee-Wick Theory. *Phys. Rev.*, D80:023511, 2009.

[106] Xian Gao, Yi Wang, Wei Xue, and Robert Brandenberger. Fluctuations in a Horava-Lifshitz Bouncing Cosmology. *JCAP*, 1002:020, 2010.

[107] Yi-Fu Cai, Evan McDonough, Francis Duplessis, and Robert H. Brandenberger. Two Field Matter Bounce Cosmology. *JCAP*, 1310:024, 2013.

[108] Lorenzo Battarra, Michael Koehn, Jean-Luc Lehners, and Burt A. Ovrut. Cosmological Perturbations Through a Non-Singular Ghost-Condensate/Galileon Bounce. *JCAP*, 1407:007, 2014.

[109] Alex Hamilton, Daniel N. Kabat, Gilad Lifschytz, and David A. Lowe. Local bulk operators in AdS/CFT: A Boundary view of horizons and locality. *Phys. Rev.*, D73:086003, 2006.

[110] Alex Hamilton, Daniel N. Kabat, Gilad Lifschytz, and David A. Lowe. Holographic representation of local bulk operators. *Phys. Rev.*, D74:066009, 2006.

[111] Daniel Kabat, Gilad Lifschytz, and David A. Lowe. Constructing local bulk observables in interacting AdS/CFT. *Phys. Rev.*, D83:106009, 2011.

[112] Ian A. Morrison. Boundary-to-bulk maps for AdS causal wedges and the Reeh-Schlieder property in holography. *JHEP*, 05:053, 2014.

[113] Alberto Enciso and Niky Kamran. Causality and the conformal boundary of AdS in real-time holography. *Phys. Rev.*, D85:106016, 2012.

[114] A. Enciso and N. Kamran. A singular initial-boundary value problem for nonlinear wave equations and holography in asymptotically anti-de Sitter spaces. *ArXiv e-prints*, October 2013.

[115] Alberto Enciso and Niky Kamran. Determining an asymptotically AdS Einstein spacetime from data on its conformal boundary. *Gen. Rel. Grav.*, 47(12):147, 2015.

[116] N. D. Birrell and P. C. W. Davies. *Quantum Fields in Curved Space*. Cambridge Monographs on Mathematical Physics. Cambridge Univ. Press, Cambridge, UK, 1984.

[117] Vijay Balasubramanian, Per Kraus, and Albion E. Lawrence. Bulk versus boundary dynamics in anti-de Sitter space-time. *Phys. Rev.*, D59:046003, 1999.

[118] Vijay Balasubramanian, Per Kraus, Albion E. Lawrence, and Sandip P. Trivedi. Holographic probes of anti-de Sitter space-times. *Phys. Rev.*, D59:104021, 1999.

[119] R. Brout, F. Englert, and E. Gunzig. THE CAUSAL UNIVERSE. *Gen. Rel. Grav.*, 10:1–6, 1979.

[120] D. Kazanas. Dynamics of the Universe and Spontaneous Symmetry Breaking. *Astrophys. J.*, 241:L59–L63, 1980.

[121] S. W. Hawking and R. Penrose. The Singularities of gravitational collapse and cosmology. *Proc. Roy. Soc. Lond.*, A314:529–548, 1970.

[122] Arvind Borde and Alexander Vilenkin. Eternal inflation and the initial singularity. *Phys. Rev. Lett.*, 72:3305–3309, 1994.

[123] Yi-Fu Cai, Taotao Qiu, Yun-Song Piao, Mingzhe Li, and Xinmin Zhang. Bouncing universe with quintom matter. *JHEP*, 10:071, 2007.

[124] V. Mukhanov and R. Brandenberger. A nonsingular universe. *Phys. Rev. Lett.*, 68:1969–1972, Mar 1992.

[125] Robert H. Brandenberger, Viatcheslav F. Mukhanov, and A. Sornborger. A Cosmological theory without singularities. *Phys. Rev.*, D48:1629–1642, 1993.

[126] Tirthabir Biswas, Anupam Mazumdar, and Warren Siegel. Bouncing universes in string-inspired gravity. *JCAP*, 0603:009, 2006.

[127] Tirthabir Biswas, Robert Brandenberger, Anupam Mazumdar, and Warren Siegel. Non-perturbative Gravity, Hagedorn Bounce & CMB. *JCAP*, 0712:011, 2007.

[128] Allan Adams, Nima Arkani-Hamed, Sergei Dubovsky, Alberto Nicolis, and Riccardo Rattazzi. Causality, analyticity and an IR obstruction to UV completion. *JHEP*, 10:014, 2006.

[129] Ofer Aharony, Steven S. Gubser, Juan Martin Maldacena, Hirosi Ooguri, and Yaron Oz. Large N field theories, string theory and gravity. *Phys. Rept.*, 323:183–386, 2000.

[130] M. Gasperini and G. Veneziano. Pre - big bang in string cosmology. *Astropart. Phys.*, 1:317–339, 1993.

[131] Edmund J. Copeland, Richard Easther, and David Wands. Vacuum fluctuations in axion - dilaton cosmologies. *Phys. Rev.*, D56:874–888, 1997.

[132] Edmund J. Copeland, James E. Lidsey, and David Wands. S duality invariant perturbations in string cosmology. *Nucl. Phys.*, B506:407–420, 1997.

[133] Jai-chan Hwang and Ethan T. Vishniac. Gauge-invariant joining conditions for cosmological perturbations. *Astrophys. J.*, 382:363–368, 1991.

[134] Nathalie Deruelle and Viatcheslav F. Mukhanov. On matching conditions for cosmological perturbations. *Phys. Rev.*, D52:5549–5555, 1995.

[135] Robert H. Brandenberger. Lectures on the theory of cosmological perturbations. *Lect. Notes Phys.*, 646:127–167, 2004. [,127(2003)].

[136] James M. Bardeen, Paul J. Steinhardt, and Michael S. Turner. Spontaneous Creation of Almost Scale - Free Density Perturbations in an Inflationary Universe. *Phys. Rev.*, D28:679, 1983.

[137] Robert H. Brandenberger and Ronald Kahn. COSMOLOGICAL PERTURBATIONS IN INFLATIONARY UNIVERSE MODELS. *Phys. Rev.*, D29:2172, 1984.

[138] Niayesh Afshordi and Robert H. Brandenberger. Super Hubble nonlinear perturbations during inflation. *Phys. Rev.*, D63:123505, 2001.

[139] David Langlois and Filippo Vernizzi. Evolution of non-linear cosmological perturbations. *Phys. Rev. Lett.*, 95:091303, 2005.

[140] David Langlois and Filippo Vernizzi. Conserved non-linear quantities in cosmology. *Phys. Rev.*, D72:103501, 2005.

[141] C. Fefferman and C. R. Graham. The ambient metric. *ArXiv e-prints*, October 2007.

[142] Charles Fefferman and C. Robin Graham. Conformal invariants. *Astérisque*, (Numéro Hors Série):95–116, 1985. The mathematical heritage of Élie Cartan (Lyon, 1984).

[143] Kostas Skenderis. Asymptotically Anti-de Sitter space-times and their stress energy tensor. *Int. J. Mod. Phys.*, A16:740–749, 2001. [,394(2000)].

[144] Shinji Mukohyama. Gauge invariant gravitational perturbations of maximally symmetric space-times. *Phys. Rev.*, D62:084015, 2000.

[145] David Langlois. Brane cosmological perturbations. *Phys. Rev.*, D62:126012, 2000.

[146] Carsten van de Bruck, Miquel Dorca, Robert H. Brandenberger, and Andre Lukas. Cosmological perturbations in brane world theories: Formalism. *Phys. Rev.*, D62:123515, 2000.

[147] Carlo Angelantonj, Costas Kounnas, Herve Partouche, and Nicolaos Toumbas. Resolution of Hagedorn singularity in superstrings with gravito-magnetic fluxes. *Nucl. Phys.*, B809:291–307, 2009.

[148] Yeuk-Kwan E. Cheung, Xue Song, Shuyi Li, Yunxuan Li, and Yiqing Zhu. The CST Bounce Universe model – a parametric study. 2016.

[149] R. Hagedorn. Statistical thermodynamics of strong interactions at high-energies. *Nuovo Cim. Suppl.*, 3:147–186, 1965.

[150] Robert H. Brandenberger, Ali Nayeri, Subodh P. Patil, and Cumrun Vafa. Tensor Modes from a Primordial Hagedorn Phase of String Cosmology. *Phys. Rev. Lett.*, 98:231302, 2007.

[151] Robert H. Brandenberger, Ali Nayeri, and Subodh P. Patil. Closed String Thermodynamics and a Blue Tensor Spectrum. *Phys. Rev.*, D90(6):067301, 2014.

[152] Yi Wang and Wei Xue. Inflation and Alternatives with Blue Tensor Spectra. *JCAP*, 1410(10):075, 2014.

[153] Jean-Luc Lehners and Edward Wilson-Ewing. Running of the scalar spectral index in bouncing cosmologies. *JCAP*, 1510(10):038, 2015.

[154] Yi-Fu Cai, Wei Xue, Robert Brandenberger, and Xinmin Zhang. Non-Gaussianity in a Matter Bounce. *JCAP*, 0905:011, 2009.

[155] Bin Chen, Yi Wang, Wei Xue, and Robert Brandenberger. String Gas Cosmology and Non-Gaussianities. *The Universe*, 3(3):2–10, 2015.

[156] Licia Verde. A practical guide to Basic Statistical Techniques for Data Analysis in Cosmology. 2007.

[157] Licia Verde. Statistical methods in cosmology. *Lect. Notes Phys.*, 800:147–177, 2010.

[158] Alan Heavens. Statistical techniques in cosmology. 2009.

[159] Roberto Trotta. Bayesian Methods in Cosmology. 2017.

[160] Antony Lewis, Anthony Challinor, and Anthony Lasenby. Efficient computation of CMB anisotropies in closed FRW models. *Astrophys. J.*, 538:473–476, 2000.

[161] Antony Lewis and Sarah Bridle. Cosmological parameters from CMB and other data: A Monte Carlo approach. *Phys. Rev.*, D66:103511, 2002.

[162] P.A.R. Ade et al. Planck 2013 results. XV. CMB power spectra and likelihood. 2013.

[163] P. A. R. Ade et al. Planck 2013 results. I. Overview of products and scientific results. *Astron. Astrophys.*, 571:A1, 2014.

[164] P. A. R. Ade et al. Planck 2013 results. XV. CMB power spectra and likelihood. *Astron. Astrophys.*, 571:A15, 2014.

[165] C. L. Bennett et al. Nine-Year Wilkinson Microwave Anisotropy Probe (WMAP) Observations: Final Maps and Results. *Astrophys. J. Suppl.*, 208:20, 2013.

[166] Nikhil Padmanabhan, Xiaoying Xu, Daniel J. Eisenstein, Richard Scalzo, Antonio J. Cuesta, et al. A 2 per cent distance to z=0.35 by reconstructing baryon acoustic oscillations - I. Methods and application to the Sloan Digital Sky Survey. *Mon.Not.Roy.Astron.Soc.*, 427(3):2132–2145, 2012.

[167] Lauren Anderson, Eric Aubourg, Stephen Bailey, Dmitry Bizyaev, Michael Blanton, et al. The clustering of galaxies in the SDSS-III Baryon Oscillation Spectroscopic Survey: Baryon Acoustic Oscillations in the Data Release 9 Spectroscopic Galaxy Sample. *Mon.Not.Roy.Astron.Soc.*, 427(4):3435–3467, 2013.

[168] Florian Beutler, Chris Blake, Matthew Colless, D. Heath Jones, Lister Staveley-Smith, et al. The 6dF Galaxy Survey: Baryon Acoustic Oscillations and the Local Hubble Constant. *Mon.Not.Roy.Astron.Soc.*, 416:3017–3032, 2011.

[169] Timothe Delubac et al. Baryon acoustic oscillations in the Ly forest of BOSS DR11 quasars. *Astron. Astrophys.*, 574:A59, 2015.

[170] Andreu Font-Ribera et al. Quasar-Lyman α Forest Cross-Correlation from BOSS DR11 : Baryon Acoustic Oscillations. *JCAP*, 1405:027, 2014.

[171] N. Suzuki, D. Rubin, C. Lidman, G. Aldering, R. Amanullah, et al. The Hubble Space Telescope Cluster Supernova Survey: V. Improving the Dark Energy Constraints Above $z > 1$ and Building an Early-Type-Hosted Supernova Sample. *Astrophys.J.*, 746:85, 2012.

[172] Scott Dodelson. *Modern Cosmology*. Academic Press, Amsterdam, 2003.

[173] P.A.R. Ade et al. Planck 2013 results. I. Overview of products and scientific results. 2013.

[174] P.A.R. Ade et al. Planck 2013 results. XVI. Cosmological parameters. 2013.

[175] Steven Weinberg. The Cosmological Constant Problem. *Rev.Mod.Phys.*, 61:1–23, 1989.

[176] Luis P. Chimento, Alejandro S. Jakubi, Diego Pavon, and Winfried Zimdahl. Interacting quintessence solution to the coincidence problem. *Phys.Rev.*, D67:083513, 2003.

[177] Luca Amendola and Claudia Quercellini. Tracking and coupled dark energy as seen by WMAP. *Phys.Rev.*, D68:023514, 2003.

[178] Luca Amendola, Shinji Tsujikawa, and M. Sami. Phantom damping of matter perturbations. *Phys.Lett.*, B632:155–158, 2006.

[179] Diego Pavon and Winfried Zimdahl. Holographic dark energy and cosmic coincidence. *Phys.Lett.*, B628:206–210, 2005.

[180] Sergio del Campo, Ramon Herrera, and Diego Pavon. Toward a solution of the coincidence problem. *Phys.Rev.*, D78:021302, 2008.

[181] Christian G. Boehmer, Gabriela Caldera-Cabral, Ruth Lazkoz, and Roy Maartens. Dynamics of dark energy with a coupling to dark matter. *Phys.Rev.*, D78:023505, 2008.

[182] Songbai Chen, Bin Wang, and Jiliang Jing. Dynamics of interacting dark energy model in Einstein and Loop Quantum Cosmology. *Phys.Rev.*, D78:123503, 2008.

[183] German Olivares, Fernando Atrio-Barandela, and Diego Pavon. Observational constraints on interacting quintessence models. *Phys.Rev.*, D71:063523, 2005.

[184] German Olivares, Fernado Atrio-Barandela, and Diego Pavon. Dynamics of Interacting Quintessence Models: Observational Constraints. *Phys.Rev.*, D77:063513, 2008.

[185] Jussi Valiviita, Elisabetta Majerotto, and Roy Maartens. Instability in interacting dark energy and dark matter fluids. *JCAP*, 0807:020, 2008.

[186] Pier Stefano Corasaniti. Slow-Roll Suppression of Adiabatic Instabilities in Coupled Scalar Field-Dark Matter Models. *Phys.Rev.*, D78:083538, 2008.

[187] Brendan M. Jackson, Andy Taylor, and Arjun Berera. On the large-scale instability in interacting dark energy and dark matter fluids. *Phys.Rev.*, D79:043526, 2009.

[188] Diego Pavon and Bin Wang. Le Chatelier-Braun principle in cosmological physics. *Gen.Rel.Grav.*, 41:1–5, 2009.

[189] Bin Wang, Chi-Yong Lin, Diego Pavon, and Elcio Abdalla. Thermodynamical description of the interaction between dark energy and dark matter. *Phys.Lett.*, B662:1–6, 2008.

[190] Bin Wang, Jiadong Zang, Chi-Yong Lin, Elcio Abdalla, and S. Micheletti. Interacting Dark Energy and Dark Matter: Observational Constraints from Cosmological Parameters. *Nucl.Phys.*, B778:69–84, 2007.

[191] Fergus Simpson, Brendan M. Jackson, and John A. Peacock. Unmodified Gravity. MNRAS:411 (2): 1053–1058, 2011.

[192] Winfried Zimdahl. Interacting dark energy and cosmological equations of state. *Int.J.Mod.Phys.*, D14:2319–2326, 2005.

[193] Zong-Kuan Guo, Nobuyoshi Ohta, and Shinji Tsujikawa. Probing the Coupling between Dark Components of the Universe. *Phys.Rev.*, D76:023508, 2007.

[194] Chang Feng, Bin Wang, Elcio Abdalla, and Ru-Keng Su. Observational constraints on the dark energy and dark matter mutual coupling. *Phys. Lett.*, B665:111–119, 2008.

[195] Jussi Valiviita, Roy Maartens, and Elisabetta Majerotto. Observational constraints on an interacting dark energy model. *Mon.Not.Roy.Astron.Soc.*, 402:2355–2368, 2010.

[196] Jun-Qing Xia. Constraint on coupled dark energy models from observations. *Phys.Rev.*, D80:103514, 2009.

[197] Jian-Hua He, Bin Wang, and Pengjie Zhang. The Imprint of the interaction between dark sectors in large scale cosmic microwave background anisotropies. *Phys.Rev.*, D80:063530, 2009.

[198] Matteo Martinelli, Laura Lopez Honorez, Alessandro Melchiorri, and Olga Mena. Future CMB cosmological constraints in a dark coupled universe. *Phys.Rev.*, D81:103534, 2010.

[199] Laura Lopez Honorez, Beth A. Reid, Olga Mena, Licia Verde, and Raul Jimenez. Coupled dark matter-dark energy in light of near Universe observations. *JCAP*, 1009:029, 2010.

[200] Jian-Hua He, Bin Wang, and Y.P. Jing. Effects of dark sectors' mutual interaction on the growth of structures. *JCAP*, 0907:030, 2009.

[201] Gabriela Caldera-Cabral, Roy Maartens, and Bjoern Malte Schaefer. The Growth of Structure in Interacting Dark Energy Models. *JCAP*, 0907:027, 2009.

[202] Jian-Hua He, Bin Wang, Elcio Abdalla, and Diego Pavon. The Imprint of the interaction between dark sectors in galaxy clusters. *JCAP*, 1012:022, 2010.

[203] Orfeu Bertolami, F. Gil Pedro, and M. Le Delliou. Dark Energy-Dark Matter Interaction and the Violation of the Equivalence Principle from the Abell Cluster A586. *Phys.Lett.*, B654:165–169, 2007.

[204] O. Bertolami, F. Gil Pedro, and M. Le Delliou. The Abell Cluster A586 and the Equivalence Principle. *Gen.Rel.Grav.*, 41:2839–2846, 2009.

[205] E. Abdalla, L. Raul W. Abramo, Jr. Sodre, L., and B. Wang. Signature of the interaction between dark energy and dark matter in galaxy clusters. *Phys.Lett.*, B673:107–110, 2009.

[206] Elcio Abdalla, L. Raul Abramo, and Jose C. C. de Souza. Signature of the interaction between dark energy and dark matter in observations. *Phys.Rev.*, D82:023508, 2010.

[207] C. E. Pellicer, Elisa G. M. Ferreira, Daniel C. Guariento, Andre A. Costa, Leila L. Graef, et al. The role of Dark Matter interaction in galaxy clusters. *Mod.Phys.Lett.*, A27:1250144, 2012.

[208] Sandro M. R. Micheletti. Observational constraints on holographic tachyonic dark energy in interaction with dark matter. *JCAP*, 1005:009, 2010.

[209] Jia Zhou, Bin Wang, Diego Pavon, and Elcio Abdalla. A Preliminary analysis of the energy transfer between the dark sectors of the Universe. *Mod.Phys.Lett.*, A24:1689–1698, 2009.

[210] Bin Wang, Chi-Yong Lin, and Elcio Abdalla. Constraints on the interacting holographic dark energy model. *Phys.Lett.*, B637:357–361, 2006.

[211] Valentina Salvatelli, Andrea Marchini, Laura Lopez-Honorez, and Olga Mena. New constraints on Coupled Dark Energy from the Planck satellite experiment. *Phys.Rev.*, D88:023531, 2013.

[212] Xiao-Dong Xu, Bin Wang, Pengjie Zhang, and Fernando Atrio-Barandela. The effect of Dark Matter and Dark Energy interactions on the peculiar velocity field and the kinetic Sunyaev-Zel'dovich effect. 2013.

[213] Hideo Kodama and Misao Sasaki. Cosmological Perturbation Theory. *Prog.Theor.Phys.Suppl.*, 78:1–166, 1984.

[214] Chung-Pei Ma and Edmund Bertschinger. Cosmological perturbation theory in the synchronous and conformal Newtonian gauges. *Astrophys.J.*, 455:7–25, 1995.

[215] Antony Lewis. Efficient sampling of fast and slow cosmological parameters. *Phys.Rev.*, D87:103529, 2013.

[216] O. Pisanti, A. Cirillo, S. Esposito, F. Iocco, G. Mangano, et al. PArthENoPE: Public Algorithm Evaluating the Nucleosynthesis of Primordial Elements. *Comput.Phys.Commun.*, 178:956–971, 2008.

[217] Jan Hamann, Steen Hannestad, Georg G. Raffelt, and Yvonne Y.Y. Wong. Sterile neutrinos with eV masses in cosmology: How disfavoured exactly? *JCAP*, 1109:034, 2011.

[218] Valeria Pettorino. Testing modified gravity with Planck: the case of coupled dark energy. *Phys. Rev. D 88,*, 063519, 2013.

[219] Philip Bull et al. Beyond ΛCDM: Problems, solutions, and the road ahead. *Phys. Dark Univ.*, 12:56–99, 2016.

[220] T. Damour, G. W. Gibbons, and C. Gundlach. Dark Matter, Time Varying G, and a Dilaton Field. *Phys. Rev. Lett.*, 64:123–126, 1990.

[221] Valerio Faraoni, James B. Dent, and Emmanuel N. Saridakis. Covariantizing the interaction between dark energy and dark matter. *Phys. Rev.*, D90(6):063510, 2014.

[222] Valentina Salvatelli, Najla Said, Marco Bruni, Alessandro Melchiorri, and David Wands. Indications of a late-time interaction in the dark sector. *Phys. Rev. Lett.*, 113(18):181301, 2014.

[223] Rafael C. Nunes, Supriya Pan, and Emmanuel N. Saridakis. New constraints on interacting dark energy from cosmic chronometers. *Phys. Rev.*, D94(2):023508, 2016.

[224] Andr A. Costa, Xiao-Dong Xu, Bin Wang, and E. Abdalla. Constraints on interacting dark energy models from Planck 2015 and redshift-space distortion data. *JCAP*, 1701(01):028, 2017.

[225] Rafael J. F. Marcondes, Ricardo C. G. Landim, Andr A. Costa, Bin Wang, and Elcio Abdalla. Analytic study of the effect of dark energy-dark matter interaction on the growth of structures. *JCAP*, 1612(12):009, 2016.

[226] ric Aubourg et al. Cosmological implications of baryon acoustic oscillation measurements. *Phys. Rev.*, D92(12):123516, 2015.

[227] Victor H. Cardenas. Exploring hints for dark energy density evolution in light of recent data. *Phys. Lett.*, B750:128–134, 2015.

[228] Varun Sahni, Arman Shafieloo, and Alexei A. Starobinsky. Model independent evidence for dark energy evolution from Baryon Acoustic Oscillations. *Astrophys. J.*, 793(2):L40, 2014.

[229] Pedro C. Ferreira, Diego Pavn, and Joel C. Carvalho. On detecting interactions in the dark sector with H(z) data. *Phys. Rev.*, D88:083503, 2013.

[230] P. A. R. Ade et al. Planck 2013 results. XXII. Constraints on inflation. *Astron. Astrophys.*, 571:A22, 2014.

[231] L. Raul Abramo, Michael A. Strauss, Marcos Lima, Carlos Hernandez-Monteagudo, Ruth Lazkoz, Mariano Moles, Claudia M. de Oliveira, Irene Sendra, Laerte Sodre, Jr, and Thaisa Storchi-Bergmann. Measuring large-scale structure with quasars in narrow-band filter surveys. *Mon. Not. Roy. Astron. Soc.*, 423(4):3251–3267, 2012.

[232] R. A. Battye, I. W. A. Browne, C. Dickinson, G. Heron, B. Maffei, and A. Pourtsidou. HI intensity mapping : a single dish approach. *Mon. Not. Roy. Astron. Soc.*, 434:1239–1256, 2013.

[233] Shahab Joudaki et al. CFHTLenS revisited: assessing concordance with Planck including astrophysical systematics. *Mon. Not. Roy. Astron. Soc.*, 465(2):2033–2052, 2017.

[234] Niall MacCrann, Joe Zuntz, Sarah Bridle, Bhuvnesh Jain, and Matthew R. Becker. Cosmic Discordance: Are Planck CMB and CFHTLenS weak lensing measurements out of tune? *Mon. Not. Roy. Astron. Soc.*, 451(3):2877–2888, 2015.

[235] Lei Ming, Taifan Zheng, and Yeuk-Kwan E. Cheung. Following the density perturbations through a bounce with AdS/CFT Correspondence. 2017.